PUBLICATIONS OF THE ASTRONOMICAL SOCIETY OF THE PACIFIC, **113**:1449–1485, 2001 December


***Invited Review***

# The Dust Opacity of Star-forming Galaxies

DANIELA CALZETTI

Space Telescope Science Institute, 3700 San Martin Drive, Baltimore, MD 21218; calzetti@stsci.edu

*Received 2001 August 31; accepted 2001 August 31*

**ABSTRACT.** The presence of dust in galaxies removes one-half or more of the stellar energy from the UV-optical budget of the universe and has a profound impact on our understanding of how galaxies evolve. Measures of opacity in local galaxies are reviewed together with widely used theoretical and empirical methods for quantifying its effects. Existing evidence shows that the dust content of nearby galaxies depends not only on their morphology but also on their luminosity and activity level. A digression is devoted to starbursts in view of their potential relevance for measures of opacity in distant galaxies. Scarcity of coherent multiwavelength data sets hampers our ability to derive reliable obscuration estimates in intermediate- and high-redshift galaxies. This, in turn, limits the reliability of inferred physical quantities, such as star formation rates, stellar population ages, galaxy luminosity functions, and others.

## 1. INTRODUCTION

After *IRAS* showed that most galaxies in the nearby universe contain at least some dust (Soifer, Houck, & Neugebauer 1987), the main question moved from "whether" to "when, where, and how much." "When" did galaxies start to be enriched in metals and dust, and how did their dust content evolve as a function of redshift? "Where" is the dust located within a galaxy, and how is it distributed among Hubble types? "How much" dust is there in galaxies, how much stellar light is absorbed by dust, and how is it reemitted?

More than one-third of the bolometric luminosity of local galaxies is processed by dust into the infrared. The fraction of stellar radiation reprocessed into the *IRAS* 8–120 $\mu$m window is ~25%–30% (Soifer & Neugebauer 1991); this implies an infrared energy fraction around 35%–40% of the total bolometric energy within the local ~100 Mpc, once bolometric corrections from the *IRAS* window to the full infrared range are included (Désert, Boulanger, & Puget 1990; Xu & Buat 1995; Calzetti et al. 2000). This average value comes with a large variation between galaxies, depending on luminosity, morphological type, and activity level (see § 3).

The cosmic infrared background (CIB) observed by *COBE* (Puget et al. 1996; Fixsen et al. 1998; Hauser et al. 1998) sets equally stringent limits on the total amount of stellar energy reprocessed by dust into the infrared at *all* redshifts. About one-half, and possibly more, of the background radiation between 0.1 and 1000 $\mu$m is emerging at wavelengths $\lambda > 40$ $\mu$m (Hauser & Dwek 2001). This implies that at some epoch(s) in the past galaxies have been infrared luminous at least as much as, and possibly more than, today to produce the observed balance between UV/optical and infrared energy in the cosmic background. Infrared-bright sources are also found to be about 2 orders of magnitude more numerous in the past than today (§ 5.2 and Barger, Cowie, & Richards 2000). The infrared luminosity of a galaxy is related to both its dust content and nuclear/star formation activity. The lower metal content of distant galaxies does not necessarily make them more transparent systems than galaxies today. The dust content of galaxies is, in fact, proportional to both metallicity and gas content; as stellar populations evolve in time and more gas is locked into stars, the metallicity of a galaxy increases while its gas content decreases. The two trends go in opposite directions, and the dust content reaches a peak sometime during the evolution of the galaxy. Models predict that galaxies at $z \sim 1$–2 have about twice the dust opacity of local galaxies (Wang 1991; Edmunds & Phillips 1997; Calzetti & Heckman 1999; Pei, Fall, & Hauser 1999). High-redshift, star-forming galaxies are indirectly observed to have large gas column densities; the average *SFR* (*star formation rate*) *per unit galactic area* increases by more than 1 order of magnitude between redshift 0 and 3 (Giavalisco et al. 1996a; Meurer et al. 1997; Lanzetta et al. 1999), which is an indication of a similar increase in the average gas column density via the global Schmidt law (Kennicutt 1998).

The presence of dust in galaxies limits our ability to interpret the local and distant universe because dust extinction dims and reddens the galaxy light in the traditional UV–to–near-IR windows, where the vast majority of the data have been obtained. Dust effects hamper the interpretation of galaxies' spectral energy distributions (SEDs) in terms of their fundamental parameters, such as age, stellar population mix, SFRs, and stellar initial mass function (IMF). Since young stellar populations are on average more deeply embedded in dust clouds than older stars, dust opacity variations within a galaxy impact the derivation of a galaxy's star formation history, by altering the census of the populations in the different age bins. Heavy dust extinction

in nearby starburst galaxies still prevents establishing whether the stellar IMF in these systems is different from that of more quiescent environments (Rieke et al. 1980, 1993; Alonso-Herrero et al. 2001). The increase of dust content with luminosity in spirals may be responsible for the nonlinear behavior of the Tully-Fisher relation, and this translates into biased distance estimates (Giovanelli et al. 1995). Determinations of luminosity functions, mass-to-light ratios, and number counts, especially at short wavelengths, suffer from both the presence of dust and the variations of dust content from galaxy to galaxy. Light dimming by dust biases measurements of galaxies' SFRs, both locally (Bell & Kennicutt 2001; Sullivan et al. 2000) and at high redshift (Glazebrook et al. 1999; Madau et al. 1996; Steidel et al. 1999), and is the cause of uncertain cross-calibrations between different indicators. The evolution with redshift of the SFR of galaxies per unit comoving volume is still debated: unclear is whether it has a peak around $z \sim 1$–3 (Madau et al. 1996; Blain et al. 1999b) or is mostly flat between $z \sim 1$ and $z \sim 4$ (Steidel et al. 1999; Barger et al. 2000). Answering this question, which requires understanding the dust opacity characteristics and the nature of high-redshift galaxies, can discriminate between different flavors of galaxy formation scenarios (White & Frenk 1991; Ortolani et al. 1995; Baugh et al. 1998). Finally, measuring the fraction of metals locked into dust at different epochs is a crucial ingredient for tracing the chemical evolution of galaxies.

The quantification of the dust opacity of galaxies of all types and at all redshifts as a function of wavelength has required the collective effort of many investigators over the last ~10–15 years and is still, in many aspects, an ongoing process. This review attempts to capture the main results obtained so far; it concentrates on star-forming galaxies because of their key role for interpreting the star formation history and evolution of galaxies. The topic has acquired with time large breadth, and numerous publications have appeared in the field; despite the effort to include as many relevant results as possible, some important contributions may have been inadvertently overlooked.

After *IRAS*, the *Infrared Space Observatory* (*ISO*) continued to shed light on the dust emission properties of galaxies, and comprehensive reviews are given in Genzel & Cesarsky (2000) and in the proceedings of the 1998 Paris conference "The Universe as Seen by *ISO*" (Cox & Kessler 1999). The status of the topic before *ISO* is reported in the proceedings of the 1994 Cardiff (UK) conference "The Opacity of Spiral Disks" (Davies & Burstein 1995) and of the 1996 Johannesburg (South Africa) conference "New Extragalactic Perspectives in the New South Africa" (Block & Greenberg 1996).

Throughout the following, the adopted cosmology is a flat universe with $\Omega_\Lambda = 0$ and Hubble constant $H_0 = 65$ km s$^{-1}$ Mpc$^{-1}$. "Local universe" refers to a sphere of 100–200 Mpc radius centered on the Milky Way.

## 2. THE RADIATIVE TRANSFER OF DUST IN GALAXIES

The transfer of radiation through dust is governed by the well-known equation (e.g., Chandrasekhar 1960; Sobolev 1963)

$$\frac{dI_\lambda}{ds} = -\kappa_\lambda I_\lambda(s, \theta, \phi) + \epsilon_\lambda(s, \theta, \phi) + \kappa_\lambda \frac{\omega_\lambda}{4\pi} \int_\Omega I_\lambda(s, \theta', \phi')\Phi_\lambda(\cos\Theta)d\Omega', \quad (1)$$

where $I_\lambda(s, \theta, \phi)$ is the radiation intensity, $ds$ is the element of linear distance along the direction of propagation, $d\Omega'$ is the element of solid angle as seen by the dust grain, $\kappa_\lambda$ is the opacity (absorption plus scattering) of the dust per unit separation $s$, $\epsilon_\lambda(s, \theta, \phi)$ is the emissivity of the sources along the direction of propagation, $\omega_\lambda$ is the albedo, i.e., the fraction of the opacity due to scattering, and $\Phi_\lambda(\cos\Theta)$ is the phase function of the dust grains expressed as a function of $\Theta$, the angle between the directions determined by the incident radiation $(\theta, \phi)$ and the scattered radiation $(\theta', \phi')$. One commonly used expression of the scattering phase function, the Henyey-Greenstein function (Henyey & Greenstein 1941), is characterized by a single parameter, the asymmetry parameter $g_\lambda = \langle\cos\Theta\rangle$, which is the average of the cosine of the scattering angle.

Determining the dust opacity and recovering the intrinsic physical properties of complex systems like galaxies typically requires the full treatment of the transfer of radiation through dust (eq. [1]). The efforts to solve the integrodifferential equation (1) in the case of galactic environments have generated increasingly sophisticated radiative transfer models and codes to deal with the complexity of both the dust physical properties and the dust/emitter geometry. A representative, although nonexhaustive, list of models and their salient characteristics is given in Table 1. A detailed description and comparison between these models and codes is beyond the scope of the present review, and the interested reader is referred to the papers listed in the table. Although the simplifying assumptions implemented in many cases often appear to yield as good a solution as more complex treatments (see, e.g., Misiriotis et al. 2000), the large number of free parameters is a fundamental shortcoming of radiative transfer models. Workarounds to this shortcoming range from assembling large, coherent sets of independent observational data on just one or a small number of objects to making oversimplistic assumption on the age and metallicity mix of the galaxy stellar populations, and often both. This clearly bears deeply on the generality and applicability of any result and may account to an extent for the wide variety of conclusions on the opacity of galaxies reached by different authors.

TABLE 1
PROPERTIES OF RADIATIVE TRANSFER MODELS

| Dust Geometry[a] | Medium Structure[b] | Stellar Distribution[c] | Reference | Extinction Curves[d] | Comments |
|---|---|---|---|---|---|
| Spherical ..... | Homogeneous | Central/spherical | Witt et al. (1992) | MW | Multiple density profiles, multiple scale lengths |
| | | | Rowan-Robinson & Efstathiou (1993) | | Starburst/IR modeling, central source only |
| | | | Wise & Silva (1996) | | Multiple scale lengths |
| | | | Városi & Dwek (1999) | | Also external source |
| | | | Ferrara et al. (1999a) | MW, SMC | Multiple dust/star density profiles |
| | | | Efstathiou et al. (2000) | | Starburst/IR modeling, multiple spheres, central source only |
| | | | Witt & Gordon (2000) | MW, SMC | Updated albedo/phase function values |
| Spherical ..... | Clumpy | Central/spherical | Witt & Gordon (1996) | MW | Central source only |
| | | | Városi & Dwek (1999) | | Also external source |
| | | | Witt & Gordon (2000) | MW, SMC | Updated albedo/phase function values |
| Plane-parallel ..... | Homogeneous | Plane-parallel | Bruzual et al. (1988) | MW, LMC | Multiple scale heights |
| | | | Disney et al. (1989) | | No scattering |
| | | | Di Bartolomeo, Barbaro, & Perinotto (1995) | MW | Multiple scale heights |
| | | | Xu & Buat (1995) | | Multiple scale heights |
| Exponential ..... | Homogeneous | Exponential | Kylafis & Bahcall (1987) | MW | Edge-on only, isothermal vertical distribution |
| | | | Disney et al. (1989) | | No scattering |
| | | | Byun et al. (1994) | MW | Stellar bulge, multiple scale lengths/heights |
| | | | Corradi, Beckman, & Simonneau (1996) | MW | Face-on only |
| | | | Kuchinski et al. (1998) | MW | Stellar bulge |
| | | | Ferrara et al. (1999a) | MW, SMC | Stellar bulge, multiple scale lengths/heights |
| Exponential ..... | Clumpy | Exponential | Kuchinski et al. (1998) | MW | Stellar bulge |
| | | | Silva et al. (1998) | MW | Stellar bulge, IR modeling |
| | | | Bianchi et al. (2000) | MW | Clumping of stars as well |
| Arbitrary ..... | Homogeneous/clumpy | Arbitrary | Trewhella, Madore, & Kuchinski (1999) | | Multiphase clumpy medium and emitters |
| | | | Gordon et al. (2001); Misselt et al. (2001) | All | Multiphase clumpy medium and emitters, polarization, IR modeling |

[a] The dust geometrical distribution: spherical, plane-parallel slab, double exponential, or arbitrary.
[b] The structure of the dust, i.e., homogeneous or clumpy (clumpy media can be two phase or multiphase).
[c] The distribution of the stellar population: central to the dust distribution, diffuse through the spherical dust distribution (with variable scale length), plane-parallel, double exponential, or arbitrary. In most cases, a single SED is assumed and multiple stellar populations are not included.
[d] The adopted extinction curve(s): MW = Milky Way; LMC = Large Magellanic Cloud; SMC = Small Magellanic Cloud; All = MW, LMC, SMC.

### 2.1. Point Sources and the Interstellar Extinction

A pointlike source (a star or an active galactic nucleus [AGN]) behind a screen of dust is the simplest source/dust geometry, and equation (1) has the solution

$$I_a(\lambda) = I_o(\lambda)e^{-\tau(\lambda)} = I_o(\lambda)10^{-0.4A_\lambda^o}, \quad (2)$$

where $I_a(\lambda)$ and $I_o(\lambda)$ are the attenuated (observed) and intrinsic radiation intensity, and $\tau(\lambda) = \int \kappa_\lambda\, ds = 0.921A_\lambda^o$ is the optical depth of the dust screen.[1] The total-to-selective extinction, i.e., the part of the optical depth that depends only on the physics of the dust grains and, therefore, only on the wavelength, is often expressed as $k(\lambda) = A_\lambda^o/E(B-V)$. The color excess $E(B-V)$ is defined as $A^o(B) - A^o(V)$, hence $k(B) - k(V) = 1$.

Although many studies traditionally employ a "mean Galactic extinction curve" to correct Galactic and extragalactic sources

[1] See Appendix A for the distinction between $A_\lambda^o$ and $A_\lambda$ that will be used later.

for the effects of dust obscuration, the well-studied Milky Way interstellar extinction has been shown to be spatially variable and highly dependent on the dust grain environment along the line of sight (see reviews of Mathis 1990 and Fitzpatrick 1999). Cardelli, Clayton, & Mathis (1989) demonstrated that the variations can be effectively parameterized by the total-to-selective extinction at $V$, $R(V) = A_V^o/E(B-V)$. Both the steepness of the far-UV ($\lambda \lesssim 0.3$ $\mu$m) rise of the extinction curve and the strength of the 0.2175 $\mu$m absorption feature decrease for increasing $R(V)$, as schematically shown in Figure 1 (Cardelli et al. 1989). Most sight lines have $R(V) \approx 2$–6, with the low values corresponding to the diffuse ISM [for which $R(V) = 3.1$ is a reasonable average value; e.g., Rieke & Lebofsky 1985] and the high values pertaining to dense clouds. The large values of $R(V)$ in dense clouds, usually accompanied by a gray extinction curve, are consistent with dust grains having systematically larger sizes than in the diffuse medium (Cardelli et al. 1989).

The only galaxies external to the Milky Way for which some measurements of the UV extinction curves exist are the Magellanic Clouds (Fig. 1; Koornneef & Code 1981; Nandy et al. 1981; Bouchet et al. 1985; Fitzpatrick 1986; Gordon & Clayton 1998; Misselt, Clayton, & Gordon 1999), although tentative measurements in M31 have been made (Bianchi et al. 1996). Despite the large variation of extinction properties found within each of the Magellanic Clouds (e.g., Fitzpatrick 1986; Lequeux et al. 1982; Misselt et al. 1999), the *average* curves of the Clouds appear to have some intrinsic differences from the average Milky Way curve, including a smaller $R(V)$ [$R(V) \simeq 2.4$–2.9; Gordon & Clayton 1998; Misselt et al. 1999]. This has been interpreted as an effect of the lower metallicity in the Clouds, which causes the molecular clouds to be more diffuse (Pak et al. 1998) and, possibly, to produce on average smaller dust grains (Misselt et al. 1999). The weak or absent UV absorption "bump" at 0.2175 $\mu$m in the extinction curves of the LMC 30 Doradus region and of the SMC bar, respectively (Fig. 1), could be related to local processes in these regions, possibly to the ongoing star formation activity (Fitzpatrick 1986; Gordon & Clayton 1998; Misselt et al. 1999; Reach et al. 2000). Although the bump carriers have not been positively identified yet (e.g., Reach et al. 2000), mid- and far-infrared studies of star-forming regions in the Milky Way have provided evidence that the environmental UV energy density level affects the dust properties, such as the grain size distribution, via destruction or coagulation, and/or the dust physical characteristics, via ionization state changes (Boulanger et al. 1988; Cesarsky et al. 1996). Thus, the environmental UV energy density appears to play as important a role as the metallicity in shaping the extinction curve. If confirmed by further observations, this hypothesis may explain the general absence of a 0.2175 $\mu$m absorption bump in the extinction curve of starburst galaxies (§ 4.1) and may partially account for its weakness in QSOs (e.g., Jura 1977; Sprayberry & Foltz 1992; Yamamoto & Vansevicius 1999).

In addition to absorbing stellar light, dust manifests itself through emission and absorption features and continuum emission at $\lambda > 1$ $\mu$m. Features in the near/mid-IR include, among others, the silicate absorption at 9.7 and 18 $\mu$m, $H_2O$ and $CO_2$ ice absorption at 3.0 and 4.3 $\mu$m (see Lutz et al. 1996 and Schutte et al. 1998) for a list of other absorption features), and the emission bands at 3.3, 6.2, 7.7, 8.6, and 11.3 $\mu$m (Sellgren 1994, 2001). The continuum emission beyond a few microns and up to ~40–70 $\mu$m is considered to be mainly due to discrete photon heating of very small dust grains, the smallest among which are transiently heated up to ≈1000 K (e.g., Sellgren 1984; Draine & Anderson 1985; Li & Draine 2001); dust heated by massive stars to temperatures greater than 70 K also contributes to the flux in the wavelength region below ~50 $\mu$m, albeit with decreasing filling factor for increasing temperature (Natta & Panagia 1976). Beyond 40–70 $\mu$m, the emission is mainly due to dust grains in nearly steady balance with the average heating by starlight; the transition wavelength between predominance of discrete photon heating versus that of nearly steady state depends on the average color temperature of the dust and, thus,

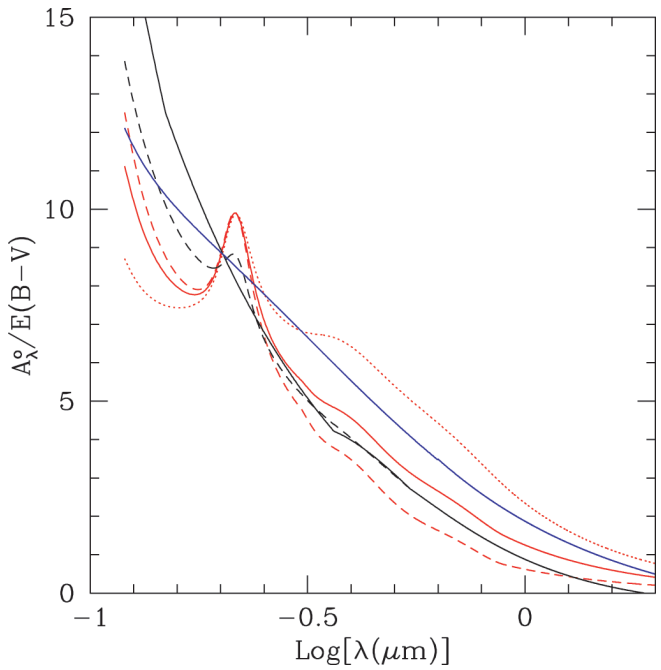


FIG. 1.—Examples of extinction curves in local galaxies. The MW extinction curve is shown for three different values of $R(V)$, 3.1 (*solid red line*), 5.0 (*dashed red line*), and 2.0 (*dotted red line*) (Cardelli et al. 1989; Fitzpatrick 1999). The extinction curves of the Large Magellanic Cloud's 30 Doradus region (*dashed black line*) and of the Small Magellanic Cloud's bar (*solid black line*) are reported for $R(V) = 2.7$ (Gordon & Clayton 1998; Misselt et al. 1999). The starburst obscuration curve (§ 4; *blue line*) is shown here for a purely illustrative comparison. The comparison should not be taken at face value because the dust obscuration of galaxies is conceptually different from the dust extinction of stars. The latter measures strictly the optical depth of the dust between the observer and the star, while the former expresses a more general attenuation, in that it folds in one expression the effects of extinction, scattering, and the geometrical distribution of the dust relative to the emitters (§ 4).

on the mean UV energy density level of the galaxy (Mezger, Mathis, & Panagia 1982; Mathis, Mezger, & Panagia 1983; Helou 1986; Chini, Krügel, & Kreysa 1986; Lonsdale-Persson & Helou 1987; Rowan-Robinson & Crawford 1989; Désert et al. 1990).

The original dust model of bare graphite and silicate grains (Mathis, Rumpl, & Nordsieck 1977; Draine & Lee 1984) has evolved over time by including more complex grain compositions and extended grain size distributions, to accommodate all the details of the absorption and emission, and the variability of the environment, while at the same time accounting for the constraints imposed by the heavy elements' overall abundance (e.g., Mathis 1996). Polycyclic aromatic hydrocarbons (PAHs; Léger & Puget 1984; Désert et al. 1990; Weingartner & Draine 2001; Sellgren 2001), hydrogenated amorphous carbons (Duley, Jones, & Williams 1989; Furton, Laiho, & Witt 1999), icy and organic refractory mantles (Greenberg 1984, 1989; Tielens 1989; Jenniskens 1993; Greenberg et al. 2000), and composite and/or porous grains (Mathis & Whiffen 1989; Mathis 1996; Wolff, Clayton, & Gibson 1998; Voshchinnikov & Mathis 1999), as well as grain size distributions that significantly depart from the original power-law model (Kim, Martin, & Hendry 1994; Weingartner & Draine 2001), have all been suggested as possible alternatives/complements to the graphite/silicate model.

### 2.2. Extended Emitting Sources

In the late 1980s, Disney, Davies, & Phillips (1989) and Valentijn (1990) revived the decade-long debate on whether galaxy disks are mainly transparent or opaque to dust. Using multiwavelength information and surface brightness versus inclination tests, respectively, the two groups of authors reached the similar conclusion that the disks of galaxies are fairly opaque, with total face-on extinctions in the $B$ band $A_{B,f} \gtrsim 1$ mag.[2] These results countered earlier findings, also based on the surface brightness versus inclination tests, that galaxy disks are mostly transparent with face-on extinctions at $B$ of less than 1 mag (Holmberg 1958; de Vaucouleurs 1959a).

The reason why similar approaches can produce very different results can be found in the complexity of the absolute and relative distribution of stars and dust inside galaxies. When there is a significant departure from the simplest geometry of a point source (a star) behind a homogeneous screen of dust, the dust distribution, rather than the optical depth of the dust layer, becomes the dominant factor in determining the obscuration suffered by the stellar radiation (Natta & Panagia 1984; Witt, Thronson, & Capuano 1992; Calzetti, Kinney, & Storchi-Bergmann 1994). In particular, differential optical depth effects come into play. If, for instance, the stars are homogeneously mixed with the dust, the shorter the wavelength of the radiation, the smaller the optical depth of the dust layer from which it can emerge; thus, an observer will detect blue light only from the closest outer "skin" of the mixed distribution, while redder light will come from deeper layers. An extreme case is that of infinitely optically thick clumps in front of an extended light distribution: the stellar emission will come only from those lines of sight that do not intersect clumps, and the net result will be an unreddened, albeit dimmer than the original, SED. The scattering component of the extinction curve will also modify the general characteristics of the dust obscuration, as light will be scattered *into the line of sight* as well as out of it. The net result of all these effects is a general blueing of the emerging SED relative to the foreground homogeneous dust screen case, or, in other words, an often much grayer "effective extinction," even in the presence of large dust optical depths[3] (Bruzual, Magris, & Calvet 1988; Witt et al. 1992).

For illustrative purposes, Figures 2 and 3 show how photometric and spectroscopic quantities are affected by the dust geometry for five "toy models." The models represent plane-parallel geometries of dust and stars (details are given in Natta & Panagia 1984; Calzetti et al. 1994; Wang & Heckman 1996) for (1) the simple case of a homogeneous, nonscattering dust screen foreground to the light source; (2) a homogeneous, scattering dust screen foreground to the light source (e.g., a screen in close proximity to the source, so that scattering into the line of sight becomes an important effect); (3) a Poissonian distribution of clumps in front of the light source, with average number $\mathcal{N} = 10$; (4) a homogeneous mixture of dust and emitters; and (5) a homogeneous dust/emitter distribution averaged over all inclination angles, with the UV and ionized gas emission having the same scale height of the dust while the scale height of the optical light gradually increases to twice that of the dust at $V$ and beyond. Models 2–5 include scattering in the calculations.[4] In all cases, the light source is assumed to be extended and to be represented by a 300 Myr old stellar population undergoing constant star formation, with solar metallicity and a Salpeter IMF in the mass range 0.1–100 $M_\odot$ (Leitherer et al. 1999).

The "blueing" effect of geometries more complex than a foreground dust screen is evident from the comparison of the five models. At fixed optical depth $\tau_V$ (fixed amount of dust), the reddening of the $V-I$ color of a stellar population induced

[2] See Appendix A for the definition of $A_{\lambda,f}$.

[3] See Appendix A for the relation between optical depth, extinction, and effective extinction.

[4] For the models, the compilation of albedo and asymmetry parameter values of Witt & Gordon (2000) is used. In this compilation, the data are mainly from studies of reflection nebulae, and the 0.2175 $\mu$m feature is due to pure absorption (no scattering) (Calzetti et al. 1995a). These $a$ and $g$ values are assumed here to be representative of dust properties, although the following caveats need to be kept in mind: some values, especially for the albedo, are still unsettled (Burgh 2001); the generalization of the reflection nebulae results [$R(V) > 3.1$] to the diffuse dust is not immediate (Witt, Friedmann, & Sasseen 1997; Kim et al. 1994; Weingartner & Draine 2001); and the UV $a$ and $g$ values could be lower in the Magellanic Clouds than in the MW (Weingartner & Draine 2001).

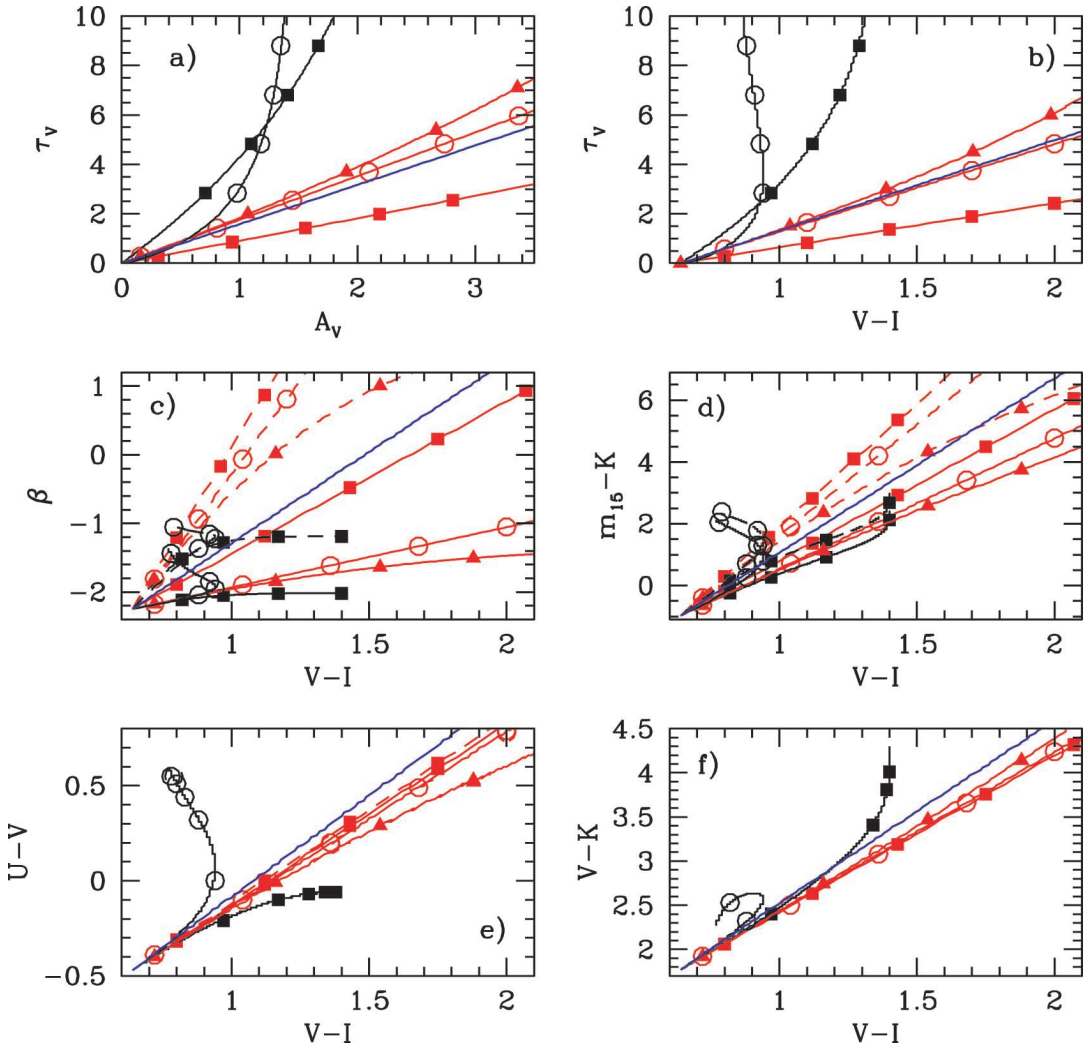


FIG. 2.—Predicted reddening and attenuation values for five simple models of plane-parallel dust/emitter distributions (§ 2.2 and Natta & Panagia 1984; Calzetti et al. 1994; Wang & Heckman 1996): a homogeneous, nonscattering dust screen foreground to the light source (*red squares*); a homogeneous, scattering dust screen foreground to the light source (*red circles*); a Poissonian distribution of clumps in front of the light source, with average number $\mathcal{N} = 10$ (*red triangles*); a homogeneous mixture of dust and emitters (*black squares*); and a homogeneous distribution averaged over all inclination angles, with increasing star-to-dust scale height ratio from UV (and ionized gas emission) to *K* (*black circles*). Both the MW extinction curve for diffuse ISM (*solid lines*) and the SMC bar extinction curve (*dashed lines*) are used in the models. The reddening and attenuation given by the starburst obscuration curve (§ 4; *blue line*) are also shown for comparison. The quantity $\tau_V$ is the front-to-back optical depth of the dust layer. (*a*, *b*): Relation between $\tau_V$ and the effective extinction $A_V$ and color $V-I$. (*c*–*f*): Effects of dust reddening on the UV, optical, and near-IR colors of a stellar population. The default population is a 300 Myr constant star formation one. *U*, *V*, *I* are standard Johnson magnitudes; *K* has central wavelength 2.163 $\mu$m and zero point −26. The quantity $m_{0.15}$ is defined as $-2.5 \log [ f(0.15)] - 21.1$, where $f(0.15)$ is the flux density at 0.15 $\mu$m.

by a generic geometry of stars and dust will be less, and the effective extinction $A_V$ lower, than that induced by a foreground screen (Figs. 2*a* and 2*b*). The same will be true for colors at other wavelengths (Fig. 2), where, again, the foreground nonscattering screen will provide the maximum reddening. For mixtures of dust and stars (models 4 and 5), reddening of colors and effective extinction reach asymptotic values; beyond certain values of the optical depth, an increase in $\tau_V$ corresponds to small or negligible changes in colors and $A_V$. This is due to the fact that the shortest wavelength emission is contributed only by the dust layers closest to the observer. One common consequence of the grayer "effective extinction" caused by complex dust/emitter geometries is that a limited number of diagnostics over a small wavelength range will lead to underestimates of the true galaxy opacity, especially if the actual dust geometry is not known and is a priori assumed to be foreground (Witt et al. 1992).

To aid the comparison with data on local starbursts and high-redshift star-forming galaxies (§§ 4 and 5), the models shown in Figure 3 are a function of the ratio of the attenuated-to-

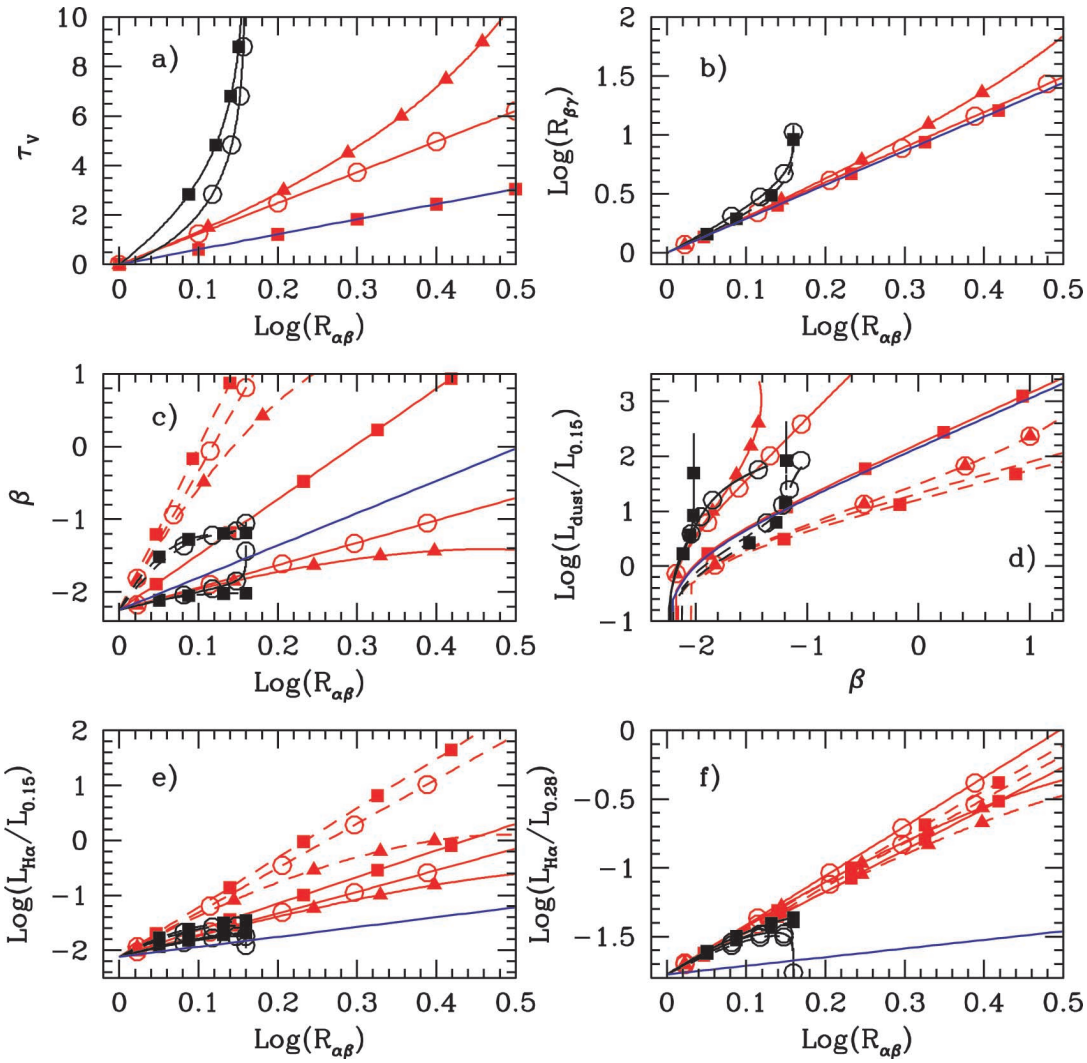


FIG. 3.—Same models as in Fig. 2 for additional spectroscopic and photometric quantities. The dust optical depth $\tau_V$ is defined in the previous figure. $R_{\alpha\beta}$ and $R_{\beta\gamma}$ are the attenuated-to-intrinsic H$\alpha$/H$\beta$ and H$\beta$/Br$\gamma$ ratios, respectively (eq. [3] and Table 2). The UV spectral slope $\beta$ is defined in Appendix B. $L_{dust}$ is the dust luminosity, corresponding to the stellar light removed (absorbed and scattered) by dust from the line of sight. This is generally larger than the dust infrared luminosity, which includes only the *absorbed* fraction of the energy, unless scattering in and out of the line of sight compensate each other. The latter can be often safely adopted for large samples of galaxies with random inclinations (exemplified by the fifth model). $L_{H\alpha}$ is the luminosity of the nebular emission at H$\alpha$. Continuum luminosities at 0.15 and 0.28 $\mu$m are given as $L_\lambda = 4\pi D^2 \lambda f(\lambda)$, where $D$ is the galaxy distance and $f(\lambda)$ is the flux density at wavelength $\lambda$; the reference wavelengths are chosen to span the UV spectrum while avoiding prominent absorption lines (including the broad 0.2175 $\mu$m bump in the MW extinction curve). The large deviation of the starburst reddening curve from the other models in the last two panels is due to the differential obscuration between ionized gas and stellar continuum (§ 4).

intrinsic Balmer line ratio

$$R_{\alpha\beta} = \frac{(L_{H\alpha}/L_{H\beta})_a}{(L_{H\alpha}/L_{H\beta})_o}, \quad (3)$$

and of the UV spectral slope[5] $\beta$. The luminosity ratios of nebular hydrogen lines, such as H$\beta$, H$\alpha$, Pa$\beta$, Br$\gamma$, etc., are rather insensitive to the details of the underlying stellar population and of the IMF, being affected at the ~5%–10% level by variations of the gas physical conditions (e.g., Osterbrock 1989); they represent, therefore, accurate probes of dust reddening and geometry. Table 2 lists the commonly used hydrogen emission line ratios and the differential extinction between each pair. When multiple line ratios widely separated in wavelength are available, they can constrain the dust geometry in the sampled wavelength range. The two drawbacks of using nebular lines are that (1) they are produced by ionizing photons; therefore, an ionizing stellar population needs to be present in the galaxy;

[5] See Appendix B for the definition of $\beta$.

TABLE 2
REDDENING BETWEEN HYDROGEN EMISSION LINES

| Line Ratio (1) | $\lambda_1$, $\lambda_2$ ($\mu$m) (2) | $L_{\lambda_1}/L_{\lambda_2}$ [a] (3) | $k(\lambda_2) - k(\lambda_1)$ (4) |
|---|---|---|---|
| H$\alpha$, H$\beta$ ..... | 0.6563, 0.4861 | 2.87 | 1.163 |
| H$\alpha$, H$\gamma$ ..... | 0.6563, 0.4340 | 6.16 | 1.628 |
| Br$\gamma$, H$\beta$ ..... | 2.166, 0.4861 | 0.0302 | 3.352 |
| Br$\gamma$, Pa$\beta$ ..... | 2.166, 1.282 | 0.175 | 0.457 |
| Pa$\alpha$, H$\alpha$ ..... | 1.876, 0.6563 | 0.123 | 2.104 |

NOTES.—Col. (1): the pair of hydrogen emission lines; col. (2): the vacuum wavelengths of the two lines; col. (3): their intrinsic luminosity ratio for temperature $T = 10{,}000$ K and case B recombination (Osterbrock 1989); col. (4): the differential extinction between the two wavelengths, for a foreground nonscattering dust screen and an MW extinction curve for diffuse ISM (Cardelli et al. 1989). Note that $k(V) = 3.1$ and $k(\mathrm{H}\alpha) = 2.468$.

[a] Variations in the ratio due to variations in the gas temperature between 5000 and 20,000 K amount to ~5%–10% (Osterbrock 1989).

and (2) they probe the attenuation of only the *ionized gas*, and such attenuation may or may not be directly related to that of the stellar population (§ 4). The explicit expression of $R_{\alpha\beta}$ depends on the dust geometry; in the simple case of a foreground, nonscattering screen,

$$R_{\alpha\beta} = 10^{0.4E(B-V)[k(\mathrm{H}\beta)-k(\mathrm{H}\alpha)]}, \quad (4)$$

where the values of $k(\mathrm{H}\alpha)$ and $k(\mathrm{H}\beta)$ are given in Table 2.

Degeneracies between the reddening induced by dust and that induced by variations in the age, metallicity, and IMF of the stellar populations play a nonnegligible role in opacity determinations of galaxies. These effects are especially important when only broadband colors or low-resolution spectroscopy are available and age-sensitive or IMF-sensitive stellar features are not identifiable (e.g., discussion in Papovich, Dickinson, & Ferguson 2001). For the age-dust degeneracy, an example is given in Figure 4; here, the broadband colors and magnitudes of a dust-free, aging stellar population produced by an instantaneous burst of star formation are compared with the analogous

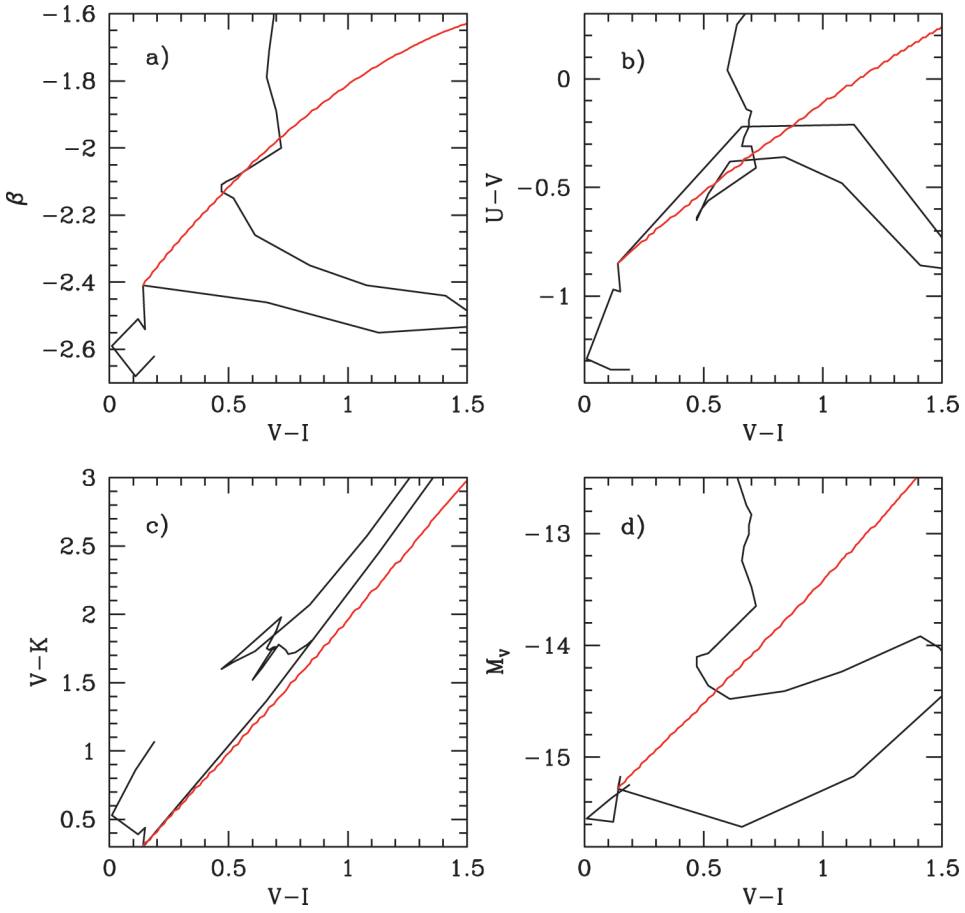


FIG. 4.—Comparison of colors and absolute magnitude between an aging instantaneous burst of star formation in the range 1–80 Myr (*black line*) and a fixed-age (6 Myr) stellar population subject to increasing dust obscuration (*red line*). The model used for the dust obscuration is a foreground clumpy distribution, with optical depth range $\tau_V = 0$–6.3.

quantities of an increasingly extincted 6 Myr old stellar population. A clumpy dust distribution with $\tau_V \sim 2$ in front of the young population reddens and attenuates it enough that its broadband UV, optical, and near-IR colors closely resemble those of a 20 Myr old, dust-free population (corresponding to the color $V-I \sim 0.6$ in Fig. 4). Thus, the dusty, young population can be mistaken for a dust-free population a factor of ~3 older. This example is just one of a large range of possibilities in the multidimensional dust/age/IMF/metallicity parameter space.

In summary, the gray effective extinction produced by dust geometry and scattering and the age-IMF-metallicity-dust degeneracy, together with uncertainties on the appropriate extinction curve to be applied to different galaxies (§ 2.1) and the absence of strong emission and absorption features below ~1 $\mu$m (apart from the ~0.22 Å absorption bump that is not universal), all contribute to make dust obscuration measurements very difficult in galaxies.

## 3. MEASUREMENTS OF DUST OPACITY IN LOCAL GALAXIES

### 3.1. Spiral Disks

Efforts to determine the dust opacity of local galaxies have spawned the development of a number of independent techniques that have been applied to a large array of samples. The most widely used methods in the case of galaxy disks are tests of the dependence of the surface brightness on inclination, multiwavelength comparisons, and statistical analysis of the color and number count variations induced by a foreground galaxy onto background sources. Each method has its strengths and weaknesses, as briefly detailed below.

As Burstein, Haynes, & Faber (1991), Choloniewski (1991), and Davies et al. (1993) pointed out, probing galaxy dust opacity by measuring the surface brightness dependence of galaxy disks on inclination can suffer from drastic selection biases. For increasing inclination, an apparent magnitude–limited catalog will mimic the condition for transparent galaxies, with mildly increasing surface brightnesses, increasing diameters, and constant total luminosities. Conversely, an apparent diameter–limited catalog will mimic the conditions for opaque disks, with roughly constant surface brightnesses, increasing magnitudes, and constant diameters as a function of increasing inclination (Burstein et al. 1991). Selection effects can, however, be controlled by combining different samples and by using galaxy redshifts/distances to discriminate among the different biases, and analysis of large samples of late-type (mainly Sbc and Sc) spirals (Huizinga & van Albada 1992; Peletier & Willner 1992; Giovanelli et al. 1994, 1995; Jones, Davies, & Trewhella 1996; Moriondo, Giovanelli, & Haynes 1998) has shown that the central regions of disk galaxies are opaque while the external regions beyond 2–3 scale lengths are almost completely transparent; there is also a trend for luminous galaxies to be more opaque than less luminous galaxies (Giovanelli et al. 1995). In bright, $M_I < -21$ disk galaxies, the observed magnitude correction from edge-on to face-on, $\Delta m_I \sim 1$ mag, corresponds to a face-on central optical depth[6] $\tau_V(0) \gtrsim 5$; this implies effective face-on extinctions $A_{B,f} \sim 0.4$–$0.5$ mag, $A_{I,f} \sim 0.2$ mag, and $A_{H,f} \sim 0.1$ mag (Peletier & Willner 1992) for a double exponential distribution of dust and stars and for practically transparent external galaxy regions (Byun, Freeman, & Kylafis 1994). Less luminous galaxies are progressively less opaque in their central regions, with an edge-on to face-on correction of $\Delta m_I \sim 0.5$ mag at $M_I > -18$, corresponding to effective face-on extinctions $A_{B,f} < 0.1$ mag (Giovanelli et al. 1995).

Qualitative results similar to those above have been obtained by Bosma et al. (1992) and Byun (1993) for a small number of edge-on late-type spirals using multiwavelength kinematic information. The method, proposed by Goad & Roberts (1981), consists of comparing rotation curves of an edge-on galaxy at widely different wavelengths. If the edge-on galaxy is optically thick at a given wavelength, say, H$\alpha$, the rotation curve measured at this wavelength shows apparent solid-body rotation throughout the entire disk because the H$\alpha$ emission is coming only from the external regions of the galaxy. A comparison with a mostly unextincted rotation curve measured at a longer wavelength, such as H I, can then establish whether optical thickness at H$\alpha$ exists. This method, although fairly direct in principle, may suffer from two limitations: first, dust in galaxies tends to be patchy and the H$\alpha$ emission may be detected along the least extincted sight lines even in the presence of considerable opacity; second, the method implicitly assumes that H$\alpha$-emitting regions are uniformly distributed across the disk.

The multiwavelength comparison method provides an independent approach to the problem of determining the dust opacity of galaxies. In broad terms, the technique consists of using multiwavelength data to solve simultaneously for the intrinsic colors of the stellar populations and for the reddening/attenuation induced by the dust. Generally, broadband images covering as large as possible a wavelength baseline, often from *B* to *K* band, are used to determine the opacity of the disks by exploiting the differential extinction property of dust (Rix & Rieke 1993; Block et al. 1994; Peletier et al. 1995; Emsellem 1995; Beckman et al. 1996; Kuchinski et al. 1998; Xilouris et al. 1999). Indeed, in face-on quiescent galaxies, *K*-band emission appears negligibly affected by dust obscuration, with $\lesssim$10% of the light lost to dust absorption and scattering (Rix & Rieke 1993). The multiwavelength technique is the most widely adopted for measuring dust opacity in galaxies because it employs easily accessible information on diverse galaxy types and enables detailed modeling of optical depths as a function of galactic region. There are, however, three main weaknesses to the method: first, this technique needs as wide a wavelength coverage as possible, often difficult to obtain, to yield unam-

[6] The face-on central optical depth $\tau(0)$ is the optical depth of the dust at the geometrical center of the tridimensional dust distribution for a face-on disk galaxy.

biguous results; second, if the dust optical depth exceeds unity at some wavelength, different volumes of the galaxy will be sampled at different wavelengths; third, the need for large data sets and detailed modeling makes obtaining results on large samples relatively cumbersome. Results vary from author to author because of the different sample selections, galaxy and dust distribution models, and measurement techniques applied. Optical and near-IR image analysis gives typical central optical depths $\tau_V(0)$ in the range 0.3–2.5 for types Sab–Sc (Peletier et al. 1995; Kuchinski et al. 1998; Xilouris et al. 1999), although higher values have been obtained by Block et al. (1994). For exponential stellar and dust profiles, these values of $\tau_V(0)$ result in optical depths $\langle\tau_V\rangle \lesssim 1$ averaged over the inner 2–3 scale lengths (Rix & Rieke 1993; Beckman et al. 1996; Kuchinski et al. 1998) and $A_{B,f} \sim 0.3$–0.4 mag and $A_{I,f} \lesssim 0.15$ mag over the same area. Much lower values of the optical depth are found for late-type, low surface brightness galaxies, with face-on, central values $\tau_V(0) \sim 0.15$ (Matthews & Wood 2001). In galaxy disks, arm regions tend to be opaque, with $\tau_V \sim 1.4$–5.5 ($A_{I,f} \sim 0.2$–0.7 mag) and peak values at $\tau_V \sim 10$–12, while interarm regions are generally transparent, with $\tau_V \sim 0.3$–1.1 ($A_{I,f} \sim 0.05$–0.15 mag; Elmegreen 1980; Rix & Rieke 1993; Beckman et al. 1996; but see the higher interarm extinction values found by Trewhella 1998).

Energy balance estimates between dust absorption and emission can also be classified as a "multiwavelength technique," but it is conceptually different from the one above. This technique employs direct measurements of the dust emission in the infrared to derive an estimate of the total stellar energy absorbed by dust and then derive opacities at shorter wavelengths; whenever possible, the wavelength baseline is extended to the UV to probe the direct light from massive stellar populations and constrain bolometric quantities (Xu & Buat 1995; Xu & Helou 1996; Buat & Xu 1996; Wang & Heckman 1996; Trewhella et al. 1997; Trewhella 1998). By combining UV and infrared (*IRAS*) data, Xu & Buat (1995), Wang & Heckman (1996), and Buat & Xu (1996) find typically lower $\langle\tau_V\rangle$ values than those derived from optical/near-IR images. This is not incompatible with those results, since the models of Xu & Buat (1995) and Wang & Heckman (1996) assume plane-parallel dust and stars, instead of exponential profiles, and thus the opaque inner regions are averaged with the nearly transparent outer regions (Peletier et al. 1995; Kuchinski et al. 1998). Still, the UV selection of the samples may bias the conclusions toward lower optical depths, and the use of *IRAS* data leaves some uncertainty as to the bolometric correction of the dust emission. The use of *ISO* data, which extend the infrared wavelength coverage out to 200 $\mu$m, appears indeed to favor higher values of the effective extinction (Trewhella 1998). Wang & Heckman (1996) find that opacity in disk galaxies is a function of luminosity (Fig. 5), in agreement with Giovanelli et al. (1995). These authors parameterize the opacity as $\langle\tau_V\rangle = \langle\tau_{V,*}\rangle(L_V/L_{V,*})^{0.5}$, with $\langle\tau_{V,*}\rangle = 0.6$ and $L_{V,*}$ the visible luminosity of an $L^*$ galaxy in the local universe. Similarly, Buat & Xu (1996) note that Sb–Scd galaxies have $\langle\tau_V\rangle \sim 0.8$ and are on average 1.5 times more opaque than Sa–Sab and ~3 times more opaque than Sd–Irr galaxies, with effective face-on extinctions $A_{B,f} \sim 0.3$ mag, $A_{B,f} \sim 0.15$ mag, and $A_{B,f} < 0.1$ mag for Sb–Scd, Sa–Sab, and Sd–Irr, respectively.

All methods described so far use the stellar radiation of the galaxy itself as the light source for the dust, with the complication that intrinsic colors, age and metallicity gradients of the stellar populations, and the relative distributions of dust and stars need to be disentangled from the extinction proper. A technique that overcomes these problems is the one that uses background sources as "light bulbs" for the dust in foreground galaxies. In this case, the dust opacity is measured across the full thickness of the foreground galaxy. There are basically two approaches to the technique. In the first approach the foreground galaxy is partially projected onto a nearby background galaxy (Keel 1983; White & Keel 1992; White, Keel, & Conselice 2000; Keel & White 2001a, 2001b; Berlind et al. 1997; Pizagno & Rix 1998). In general, the background galaxy needs to present a smooth light profile; thus, early types and preferably elliptical galaxies are required (see, however, Keel & White 2001b); the dimming and color changes induced by the foreground galaxy dust onto the isophotes of the background source provide a measurement of dust opacity. The drawbacks of this approach are twofold: (1) there are very few known pairs of galaxies that fulfill all the requirements and (2) the method is limited by the degree of symmetry of both galaxies (White, Keel, & Conselice 2000). The second approach uses distant galaxies as background light sources. Statistical variations in number counts and colors of the background galaxies relative to control fields provide a handle on the total dust optical depth of the foreground galaxy (González et al. 1998). This method overcomes most of the limitations of the first one, but it presents some of its own: (1) high angular resolution images (e.g., from the *Hubble Space Telescope* [*HST*]) are needed in order to identify background galaxies; (2) even with such images it is often difficult to discriminate background sources from extended regions within the foreground galaxy (e.g., H II regions), especially in crowded areas. Because of these limitations, the second method may also tend to avoid crowded and/or heavily extincted areas, thus biasing the results toward less dusty galactic regions. Results from various authors indicate that the spiral arms of galaxies tend to be opaque with $A_B^o \sim 0.5$–2 mag and $A_I^o \sim 0.3$–1.5 mag at any radius, while the opacity of interarm regions decreases with increasing distance from the galaxy center, starting at $A_I^o \approx 0.7$ mag within $0.3R_{25}$ and decreasing to practically zero at $R_{25}$ (González et al. 1998; White et al. 2000; Keel & White 2001b). The dust masses inferred from these extinction measures agree within a factor of ~2 with masses derived from the infrared/submillimeter (*ISO* and Submillimeter Common User Bolometer Array [SCUBA]) dust emission (Domingue et al. 1999). One common trend generally found is the grayer than Galactic reddening in the arm regions (see, however, Keel & White 2001b). The clumpiness

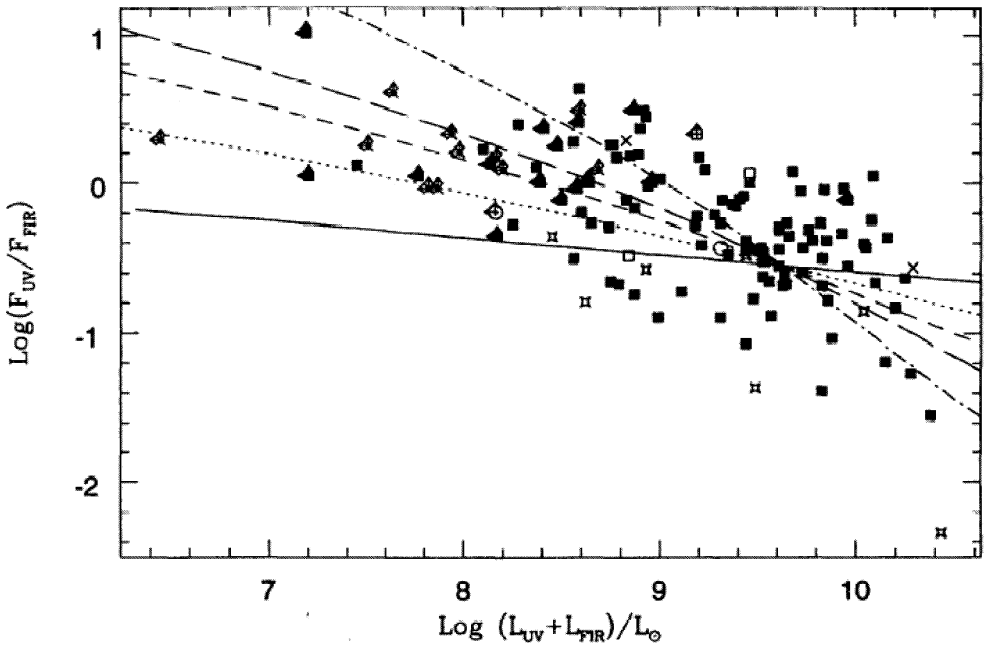


FIG. 5.—UV-to-IR flux ratio as a function of the sum of the UV and IR luminosities for star-forming galaxies (reproduction of Fig. 4 of Wang & Heckman 1996). The UV flux is centered at 0.20 $\mu$m and is defined as $F_{\rm UV} = \lambda f(\lambda)$. The IR emission in this figure (called "FIR") is the integrated emission in the 40–120 $\mu$m *IRAS* window, which contains roughly between 35% and 60% of the dust bolometric emission (Dale et al. 2001). The ratio UV/IR is a measure of the total opacity of a star-forming galaxy (see also § 4). The plot shows that more luminous galaxies are more opaque. The symbols indicate spirals (*filled squares*), irregulars (*crosses*), elliptical/lenticulars (*open squares*), amorphous (*stars*), and unknown (*circles*). The lines show predictions for a range of parameters from the model described in Wang & Heckman (1996). Figure reproduced with permission from the author and the *Astrophysical Journal*.

of the dust within each resolution bin has been suggested to be responsible for the gray reddening (Berlind et al. 1997; González et al. 1998; White et al. 2000; Keel & White 2001a). Less agreement exists on the shape of the reddening curve in the interarm regions, because of the larger uncertainties resulting from the lower extinction values. The measured extinctions are front to back, i.e., represent the optical depth of the intervening dust between the observer and the background sources. To relate these numbers to those derived from the inclination and multiwavelength tests, one has to make assumptions as to the distribution of stars relative to the dust in the foreground galaxy; for a mixed geometry of stars and small dusty clumps, the measured optical depths correspond to effective $I$ extinctions of $A_{I,f} \sim 0.3$–$0.4$ mag and $A_{I,f} \lesssim 0.2$ mag for the arms and the interarm regions, respectively.

### 3.2. Beyond the Optical Disks

Multiwavelength optical and near-IR imaging of edge-on or nearly edge-on systems indicates that the scale length of the dust is about 40% larger than the scale length of the stars (Xilouris et al. 1999), while the dust/stars scale height ratio is in the range 0.25–0.75, with a mean value of 0.5 (Kylafis & Bahcall 1987; Xilouris et al. 1997, 1999), for late-type spirals (Sb and later) and appears to have a ratio of ~1 in early-type spirals (Wainscoat, Hyland, & Freeman 1990). *IRAS* 100 $\mu$m (Nelson, Zaritsky, & Cutri 1998) and *ISO* long-wavelength maps (Alton et al. 1998; Davies et al. 1999; Trewhella et al. 2000; Radovich, Kahanpää, & Lemke 2001) confirm that cold dust emission extends beyond the limits of the optical disks along the radial direction, with scales that are ~40% larger than those of the *B*-band–emitting stars, but still well within the H I disks (e.g., Martin 1998). Using statistical measurements of color variations between background galaxies and control fields, Zaritsky (1994) gives a $\gtrsim 2\ \sigma$ detection of $A_I^o \approx 0.04$ in galaxy halos, at a distance of about 60 kpc from the galaxy centers, along the optical major axis.

### 3.3. Irregular Galaxies

Spiral and irregular galaxies follow a global metallicity-luminosity (and metallicity-mass) relation, where the oxygen abundance increases by a factor of ~100 for an increase of $\sim 10^4$ in absolute blue luminosity (Skillman, Kennicutt, & Hodge 1989; Zaritsky, Kennicutt, & Huchra 1994). Irregulars occupy the low-metallicity locus of the relation, with ≈10 times on average lower oxygen abundance than spirals. Since the H I masses per unit $L_B$ in irregulars are a factor of ≈3 larger than in spirals (Roberts & Haynes 1994; Zaritsky et al. 1994), the mass in interstellar metals per unit $L_B$ is ≈3 times smaller. Adding the $H_2$ gas into the balance does not change this conclusion, since the $H_2$/H I mass ratio in irregulars appears to be

no larger than that in spirals, even accounting for the uncertainties in the CO-to-$H_2$ conversion factor (Verter & Hodge 1995; Arimoto, Sofue, & Tsujimoto 1996; Wilson, Walker, & Thornley 1997). Measurements give the $H_2$ mass as 25%–50% of the H I mass in late spirals and as ≈20% of the H I mass in irregulars (Young & Scoville 1991; Hunter & Sage 1993; Hunter & Thronson 1996; Hunter 1997; Meier et al. 2001). Smaller metal masses for the irregulars translate into smaller dust masses per unit $L_B$, for standard values of the metal-to-dust ratio (van den Bergh 1974; Lequeux et al. 1984), and into the expectation that irregular galaxies are at least 3 times more transparent at $B$ than spiral galaxies, for similar dust/star geometries.

The analysis of the blue, H$\alpha$, and *IRAS*-detected infrared emission confirms that irregular galaxies are relatively transparent systems (Hunter et al. 1986, 1989). In a study of the Magellanic Clouds using background galaxies, Dutra et al. (2001) find that the central regions have $A_B^o \gtrsim 0.25$ in the LMC and $A_B^o \gtrsim 0.16$ in the SMC. In their UV-selected samples, Wang & Heckman (1996) find that a 0.1 $L^*$ galaxy has a mean optical depth about $\frac{1}{3}$ of the optical depth of an $L^*$ galaxy, and Buat & Xu (1996) reach a similar conclusion by comparing Sb–Scd galaxies with Sd–Irr. Thus, if the typical face-on effective extinction for an Sc galaxy is $A_{B,f} \sim 0.4$–$0.5$ mag, the analogous quantities for an irregular are $A_{B,f} \sim 0.15$ and $A_{I,f} \sim 0.05$–$0.10$.

### 3.4. Early Hubble Types

Although early Hubble type galaxies (elliptical galaxies and S0s) do not generally fall under the category of "star-forming" galaxies, they occupy a niche in terms of dust opacity properties that is at the same time opposite and complementary to that of other galaxies. Elliptical galaxies and S0s are at the opposite end of the Hubble classification relative to irregulars, but they appear to be no more opaque than those late systems.

Early-type galaxies cover a metallicity range similar to that of late-type spirals (Brodie & Huchra 1991; Zaritsky et al. 1994) but have total (H I + $H_2$) gas fractions per unit optical luminosity that are ∼3 times or more smaller (Young & Scoville 1991; Roberts & Haynes 1994). Thus, for standard interstellar metal-to-dust ratios, early-type galaxies are expected to be more transparent than disk galaxies.

The *IRAS* survey has shown that between 10% and 50% of all nearby early-type systems (45% of elliptical galaxies and 68% of S0s) contain dust (Jura et al. 1987; Knapp et al. 1989; Bregman et al. 1998), although the involved masses are generally modest, typically in the range $10^5$–$10^6$ $M_\odot$ or $M_{\rm dust}/L_B \approx 10^{-5}$–$10^{-4}$ $M_\odot$ $L_\odot^{-1}$ (Roberts et al. 1991; Goudfrooij & de Jong 1995; Wise & Silva 1996; Bregman et al. 1998). The exact fraction of dusty systems appears to depend on the adopted detection threshold (Bregman et al. 1998), but it is likely a lower bound to the actual value, given the limits in the *IRAS* sensitivity. The 50% figure seems in agreement with the results of optical surveys: at least 40% of the local elliptical galaxies and S0s show the presence of disks, lanes, and/or patchy distributions of dust in visual images (Ebneter & Balick 1985; Sadler & Gerhard 1985; Ebneter, Djorgovski, & Davis 1988; Goudfrooij et al. 1994). About 40%–50%, and possibly as many as 80%, of elliptical galaxies also show evidence for circumnuclear dust on scales less than 100 pc, as seen in *HST* images; the small-scale dust is mostly associated with nuclear radio activity (van Dokkum & Franx 1995; Lauer et al. 1995; Forbes, Franx, & Illingworth 1995; Carollo et al. 1997; Tran et al. 2001).

Despite the abundance of evidence for dust, optical extinction determinations of dust features in elliptical galaxies generally account for only ∼1/10–∼1/5 of the dust mass measured from the infrared (*IRAS*) emission; the remaining 80%–90% of the dust mass is probably associated with a component smoothly distributed across the galaxy and thus difficult to detect with standard techniques (Goudfrooij & de Jong 1995; Wise & Silva 1996; Bregman et al. 1998; Merluzzi 1998). Limited data from *ISO* in the wavelength range 120–200 $\mu$m confirm these findings (Haas 1998). Using the elliptical galaxy model of Witt et al. (1992), Goudfrooij & de Jong (1995) determine that the observed infrared luminosities are compatible with central optical depths of the diffuse component $\tau_V(0) \lesssim 0.7$, with a typical value $\tau_V(0) \sim 0.2$–$0.3$ (see, however, the somewhat larger values predicted by the models of Wise & Silva 1996). The corresponding effective extinction is $A_B \lesssim 0.05$–$0.10$ mag and $A_I \lesssim 0.02$–$0.04$ mag.

The giant elliptical galaxies found at the centers of cooling flow clusters are often surrounded by extended, ≈10–100 kpc, filamentary, and dusty emission-line nebulae, with a higher frequency in those clusters with cooling times shorter than a Hubble time (Heckman et al. 1989; Sparks, Macchetto, & Golombek 1989; Hu 1992; Voit & Donahue 1997; Donahue et al. 2000). Dust lanes in the central galaxies have, indeed, been directly observed (Pinkney et al. 1996). Optical and UV emission-line studies give extinction values in the range $A_V \sim 0.3$–$2$ mag for the dust associated with the nebula (Sparks et al. 1989; Hu 1992; Allen 1995; Voit & Donahue 1997; Donahue et al. 2000); infrared and submillimeter measurements give dust masses of the order of $10^7$–$10^8$ $M_\odot$, or $M_{\rm dust}/L_B \approx 10^{-4}$–$10^{-3}$ $M_\odot$ $L_\odot^{-1}$, for these systems (Cox, Bregman, & Schombert 1995; Edge et al. 1999). The existing controversy on the origin of the dust associated with the central galaxies of cooling flow clusters will be briefly reviewed in § 6. Such galaxies are, however, not a statistically significant component of elliptical galaxies in general; thus, their contribution to the dust mass budget of early-type galaxies is small.

### 3.5. Infrared-bright Galaxies

The galaxies discussed so far tend to be mostly "quiescent"—i.e., their bolometric output is *not dominated* by a single

TABLE 3
AVERAGE DUST ATTENUATION IN LOCAL GALAXIES

| Galaxy Type | $L_{dust}/L_{bol}$[a] | $A_{0.15,f}$[b] (mag) | $A_{0.15}$[c] (mag) | $A_{B,f}$[b] (mag) | $A_B$[c] (mag) | $A_{I,f}$[b] (mag) | $A_I$[c] (mag) | $A_{K,f}$[b] (mag) | $A_K$[c] (mag) |
|---|---|---|---|---|---|---|---|---|---|
| E/S0 ..... | 0.05–0.15 | 0.10–0.20 | ... | 0.05–0.10 | ... | 0.02–0.04 | ... | <0.02 | ... |
| Sa–Sab ..... | ... | 0.40–0.65 | 0.90–1.25 | 0.20–0.40 | 0.50–0.75 | 0.10–0.15 | 0.30–0.40 | $\lesssim$0.05 | $\lesssim$0.15 |
| Sb–Scd ..... | 0.45–0.65 | 0.60–0.80 | 1.20–1.45 | 0.30–0.50 | 0.65–0.95 | 0.15–0.20 | 0.40–0.45 | 0.05–0.10 | 0.15–0.20 |
| Irr ..... | 0.25–0.40 | 0.30–0.45 | 0.60–0.75 | 0.10–0.15 | 0.30–0.40 | $\sim$0.05 | $\sim$0.15 | $\lesssim$0.02 | $\lesssim$0.06 |

[a] Fraction of the bolometric radiation absorbed and/or scattered by dust.
[b] Face-on attenuation at the specified wavelength/band. The *B*-band and *I*-band values are derived from various authors (see text). The other wavelengths are from model 4 for E/S0s and from model 5 of § 2.2 for disks and irregulars.
[c] Inclination-averaged attenuation for the disk and irregular galaxies, from model 5 of § 2.2. For observational data at 0.15 $\mu$m, see Bell & Kennicutt 2001.

region of active star formation or by nuclear nonthermal activity—
and have modest infrared outputs. Their infrared luminosities in the 3–1000 $\mu$m band are typically $\approx 10^9\ L_\odot$ and less than $\sim(4–6) \times 10^{10}\ L_\odot$, with infrared-to-blue luminosity ratios $L_{IR}/L_B \sim 0.4–0.5$ (de Jong et al. 1984; Soifer et al. 1987; Devereux & Young 1991; Soifer & Neugebauer 1991; Hunter & Thronson 1996), and $\approx\frac{1}{2}$ or less of the stellar bolometric luminosity converted into infrared emission via dust reprocessing[7] (see Table 3).

Galaxies with $L_{IR} > 6 \times 10^{10}\ L_\odot$ and $L_{IR}/L_B > 1$ are progressively associated with dustier and more active systems for increasing values of the infrared luminosity (Rieke & Lebofsky 1986). The brightest infrared sources are not necessarily associated with the most massive galaxies, despite the existence of a relation between a galaxy's luminosity (mass) and its dust content (Wang & Heckman 1996). Infrared luminosity is a combination of dust content and activity: brighter sources have larger amounts of star formation and/or nonthermal activity embedded in dust. Most of the luminosity from galaxies with $L_{IR} \approx L_{bol} \gtrsim 10^{11}\ L_\odot \sim (3–4)L^*$ seems to be associated with sources heavily obscured by dust (Sanders & Mirabel 1996). At the bright end of the infrared luminosity function (Soifer et al. 1987; Soifer & Neugebauer 1991; Kim & Sanders 1998) are the ultraluminous infrared galaxies (ULIRGs), with luminosities from $L_{IR} \sim 10^{12}\ L_\odot$ up to $\sim 8 \times 10^{12}\ L_\odot$ (Soifer et al. 1987; Kim & Sanders 1998), infrared-to-blue ratios around 30–400 (Sanders & Mirabel 1996; Clements et al. 1996), and optical extinctions in excess of 10–40 mag (Genzel et al. 1998; Murphy et al. 2001). These sources show a continuum of properties as a function of increasing luminosity, with the fraction of starburst-dominated ULIRGs ranging from ~80%–85% at the low-luminosity end to ~50% for $L_{IR} > 2 \times 10^{12}\ L_\odot$ and the remaining fraction being AGN dominated (Genzel et al. 1998; Lutz et al. 1998; Veilleux, Kim, & Sanders 1999). Comprehensive reviews of the properties of ULIRGs are given in Sanders & Mirabel (1996) and Genzel & Cesarsky (2000).

Despite their large luminosities, bright infrared sources do not represent a major contributor to the energy budget of galaxies in the present-day universe. Such objects are relatively rare within the local 100–200 Mpc: galaxies with $L_{IR} \geq 10^{11}\ L_\odot$ and with $L_{IR} \geq 10^{12}\ L_\odot$ represent ~6% and less than 1%, respectively, of the total infrared emission in the local universe (Soifer et al. 1987; Sanders & Mirabel 1996; Kim & Sanders 1998; Yun, Reddy, & Condon 2001). However, the contribution of infrared-bright sources to the galaxy energy budget increases with redshift (see § 5.2), as does their relevance in the framework of galaxy evolution.

### 3.6. Summary

Although the issue of dust opacity of galaxies is far from settled, an overall picture is apparent: galaxies in the local universe are only moderately opaque, and extreme values of the opacity are found only in the statistically nondominant, more active systems.

Table 3 summarizes the main conclusions of this section by listing the effective extinction values for local galaxies according to morphological type. For disk and irregular galaxies, both the face-on and the inclination-averaged extinctions are given. For instance, in Sb–Scd galaxies, the typical inclination-averaged extinctions are 0.6–0.65 mag larger than face-on at 0.15 $\mu$m, ~0.4 mag at *B*, ~0.25 mag at *I*, and 0.1 mag at *K* for a stellar-to-dust scale height ratio that varies between 1 in the UV and 2 in the *I* and *K* bands (model 5 of § 2.2).

Among the nonactive galaxies, luminous Sb–Scd galaxies contain the largest amounts of dust, which absorb $\approx\frac{1}{2}$ of their bolometric light. For comparison, dust emission represents between 35% and 40% of the bolometric luminosity of the Milky Way (Cox, Krügel, & Mezger 1986; Sodroski et al. 1994). The dust content generally decreases in less luminous galaxies and for earlier and later type galaxies; dust absorbs less than ~15%

[7] The total infrared output $L_{IR}$ of the dust emission is derived from the infrared luminosity measured in the 8–120 or 40–120 $\mu$m *IRAS* window (Helou et al. 1988; Sanders & Mirabel 1996) multiplied by ~1.4 or ~2.2, respectively, to account for bolometric correction factors as modeled by Dale et al. (2001) from *ISO* data. The blue luminosity is $L_B \propto \lambda f(\lambda)$ (0.44 $\mu$m).

of the bolometric light in E/S0 galaxies, and the fraction rises to ≈30% in irregulars (Table 3).

Interpolating from Table 3, the inclination-averaged effective extinction of the stellar emission in late spiral galaxies at the rest-frame wavelength of H$\alpha$ is $A_{0.6563} \lesssim 0.60$ mag. This value should be compared with the effective extinction measured for the H$\alpha$ line emission, $A_{\rm H\alpha} \sim 0.8$–1.1 mag, from the ratio of the line to the reddening-free thermal radio emission (Kennicutt 1983, 1998; Niklas, Klein, & Wielebinski 1997; Bell & Kennicutt 2001). Although there are relatively large uncertainties associated with both numbers, the two extinction values suggest that the nebular emission is more reddened than the stellar continuum, with $A_{\rm H\alpha} \approx 1.5 A_{0.6563}$. Studies of controlled samples indicate a value of 2 as more typical for the ratio between the dust attenuation of the ionized gas and that of the stellar continuum, both in the case of spirals and irregulars (E. F. Bell 2001, private communication) and in the case of moderate-intensity starbursts (§ 4).

## 4. A CASE STUDY IN THE LOCAL UNIVERSE: STARBURST GALAXIES

Among local galaxies, starbursts occupy a special niche. The average UV and infrared luminosities (both proxies for SFR) per unit comoving volume increase with redshift by roughly an order of magnitude up to $z \sim 1$–2 (Lilly et al. 1996; Cowie, Songaila, & Barger 1999). Active star formation played a larger role in the past than today and may have been a fundamental ingredient in the shaping of galaxy populations.

Nuclear and circumnuclear starbursts occur in galaxies spanning a wide range of properties, from almost dust-free, infrared-faint, low-mass irregulars (e.g., Tol 1924−416 and NGC 1569) to dust-rich, massive spirals (e.g., NGC 5236) to infrared-bright interacting galaxies (e.g., NGC 7714 and NGC 6090) to mergers and ULIRGs (e.g., NGC 4194 and NGC 1614; Arp 220; Scoville et al. 1998). Nuclear and circumnuclear bursts of star formation can be triggered by a variety of mechanisms, including secular evolution of bars (Friedli & Benz 1995; Norman, Sellwood, & Hasan 1996) and galaxy interactions and mergers (Larson & Tinsley 1978; Keel et al. 1985; Sanders et al. 1988; Mihos & Hernquist 1996; Hibbard 1997). The latter produce the most luminous starbursts (ULIRGs), which rapidly deplete the molecular gas content of the galaxy as merging progresses. Less extreme starbursts, hosted in galaxies with $L_{\rm bol} \lesssim 5 \times 10^{11}\ L_\odot$, obey a positive correlation between the luminosity of the starburst and the luminosity and mass of the host galaxy (Heckman et al. 1998):

$$L_{B,\,\rm host}(L_\odot) \sim 10^{9.9} {\rm SFR}_{\rm starb}^{0.94}, \tag{5}$$

where $\rm SFR_{starb}$ is in $M_\odot\ {\rm yr}^{-1}$ for a Salpeter IMF in the mass range 0.1–100 $M_\odot$ (from the formulae of Kennicutt 1998). Equation (5) is probably a consequence of the fact that large SFRs are sustained by the massive gas inflows that only a deep potential well can support (Heckman et al. 1998). Indeed, from causality arguments, the maximum luminosity of a starburst scales as $\approx \sigma v^2$, with $\sigma$ the dispersion velocity of the gas and $v$ the rotation velocity of the host galaxy (Heckman 1994; Lehnert & Heckman 1996; Meurer et al. 1997). There are notable exceptions to this average trend: M82 is an example of a dwarf, $M \sim 10^{10}\ M_\odot$ (Sofue et al. 1992) and $L_{B,\,\rm host} \sim 5 \times 10^9\ L_\odot$, galaxy hosting a relatively powerful starburst, with ${\rm SFR} \sim 6\ M_\odot\ {\rm yr}^{-1}$ and $L_{\rm IR} \sim 3 \times 10^{10}\ L_\odot$. A secondary effect of both the $\rm SFR_{starb}$–host galaxy mass correlation and the mass-metallicity correlation is that the more powerful starbursts are hosted in the more metal-rich and dustier host galaxies (Heckman et al. 1998; also Fig. 7*c*):

$$10^{A_{0.15}} \sim 250\ {\rm SFR}_{\rm starb}^{2.2} \tag{6}$$

(see also Hopkins et al. 2001). Although equation (6) is not applicable to ULIRGs, still in the local universe there are no examples of "naked" Arp 220–like galaxies, emitting most of the luminosity produced by their ${\rm SFR} \sim 100$–$200\ M_\odot\ {\rm yr}^{-1}$ directly in the UV. Objects like Arp 220 tend to be heavily extincted, with $A_V \sim 15$–45 mag for Arp 220 itself (Scoville et al. 1998; Genzel et al. 1998; Shioya, Trentham, & Taniguchi 2001), and to be bright infrared sources (§ 3.5).

The rest of § 4 discusses the dust reddening and obscuration properties of the local starburst galaxies with $L_{\rm bol} \lesssim 5 \times 10^{11}\ L_\odot$. The specific sample contains starbursts that are UV luminous enough to have been detected by *IUE* (Kinney et al. 1993); it will be termed "UV selected" in what follows. The sample is not statistically complete or rigorously defined; however, it is representative of the broad range of properties of local UV-bright starbursts (Heckman et al. 1998). These galaxies are not as extreme in dust extinction and activity level as ULIRGs. They have SFRs per unit area in the range $\sim$0.3–20 $M_\odot\ {\rm yr}^{-1}\ {\rm kpc}^{-2}$ and cover a limited range in the parameter space of optical attenuation, $A_{\rm H\alpha} \sim 0$–2.5 mag. The attenuation refers to the integrated value across the starburst site; individual regions or clumps can have effective extinctions as high as $A_{\rm H\alpha} \sim 30$ mag (Beck et al. 1996; Calzetti et al. 1997). The host galaxies cover a wide variety of late-type morphologies, from grand-design spirals to irregular and amorphous to disturbed morphologies that result from interactions or merging processes. The starbursts mostly occupy the inner region of solid-body rotation of the host galaxy, with sizes of $\sim$0.5–4 kpc (Lehnert & Heckman 1996). The UV selection (Kinney et al. 1993; Calzetti et al. 1994) aids the discrimination from their more opaque and infrared-brighter counterparts. Although the UV selection results in some limitations to the applicability of the obscuration properties discussed below (see end of § 4.2), it does not entirely exclude dusty systems; the sample contains objects in which up to 90%–95% of the bolometric energy is reprocessed by dust. Table 4 gives three representative examples each for both the high-luminosity, dust-rich end and

TABLE 4
LOCAL UV-SELECTED STARBURSTS

| Name (1) | $D$ (Mpc) (2) | Morphology (3) | $L_{bol}$ ($L_\odot$) (4) | SFR ($M_\odot$ yr$^{-1}$) (5) | $L_{dust}/L_{bol}$ (6) | $A_{0.15}$ (mag) (7) | $A_B$ (mag) (8) | $A_I$ (mag) (9) | $A_{H\alpha}$ (mag) (10) |
|---|---|---|---|---|---|---|---|---|---|
| Dust-rich Starbursts[a] | | | | | | | | | |
| NGC 1614 ..... | 74 | SBc, merger | 4.8E+11 | 54.9 | 0.91 | 5.67 | 2.78 | 1.20 | 3.08 |
| NGC 4194 ..... | 40 | IBm, merger | 1.1E+11 | 9.9 | 0.86 | 3.20 | 1.57 | 0.68 | 1.74 |
| NGC 6090 ..... | 135 | Sd, merger | 4.1E+11 | 52.4 | 0.88 | 3.41 | 1.67 | 0.72 | 1.85 |
| Dust-poor Starbursts[a] | | | | | | | | | |
| NGC 1140 ..... | 23 | IBm | 9.1E+09 | 1.1 | 0.59 | 0.83 | 0.40 | 0.17 | 0.45 |
| NGC 1510 ..... | 12 | SA0 | 8.1E+08 | 0.06 | 0.42 | 0.52 | 0.25 | 0.11 | 0.28 |
| Tol 1924−416 ..... | 44 | Irr | 1.9E+10 | 2.8 | 0.42 | 0.52 | 0.25 | 0.11 | 0.28 |
| Average UV-selected Starburst[a] | | | | | | | | | |
| | | | | | | 1.60 | 0.78 | 0.34 | 0.86 |

NOTES.—Col. (1): galaxy name; col. (2): its distance for $H_0 = 65$ km s$^{-1}$ Mpc$^{-1}$; col. (3): galaxy morphology; col. (4): bolometric luminosity; col. (5): star formation rate, calculated from the obscuration-corrected Br$\gamma$ or H$\alpha$ line emission; Calzetti 1997a; using the conversion SFR $= 8.2 \times 10^{-40} L_{Br\gamma} = 7.9 \times 10^{-42} L_{H\alpha}$; Kennicutt 1998; col. (6): fraction of bolometric luminosity reprocessed by dust in the infrared; cols. (7)–(10): obscuration of the 0.15 $\mu$m, $B$ and $I$ stellar continuum, and H$\alpha$ emission line; Calzetti et al. 1994, 2000; Calzetti 1997a. For UV-selected starbursts, $A_{H\beta} = 1.47 A_{H\alpha}$.

[a] Examples of three dust-rich and three dust-poor starbursts in the UV-selected sample of Calzetti et al. 1994. The obscuration properties of these two extremes can be compared with those of an average UV-selected starburst (last line of table). Dustier systems are associated with more luminous host galaxies; Heckman et al. 1998.

the low-luminosity, dust-poor end of the UV-selected starbursts, together with the average of the sample.

### 4.1. Dust Obscuration Characteristics of Starbursts

Although the UV-selected starbursts form a heterogeneous set, their dust reddening and obscuration properties are remarkably uniform. Higher dust optical depths produce redder UV–to–near-IR SEDs and nebular emission-line ratios (Fig. 6), almost independent of the details of the dust distribution and of the intrinsic stellar population (Calzetti et al. 1994; Calzetti 1997a).

The geometry of the dust that best describes the reddening of the ionized gas emission in these systems, in the wavelength range 0.48–2.2 $\mu$m, is that of a foreground-like distribution. Figure 6*b* shows the comparison between observations and the models of § 2.2 for the attenuated-to-intrinsic hydrogen line ratios H$\alpha$/H$\beta$ and H$\beta$/Br$\gamma$. Internal dust does not appear to be a major component in the starburst region(s), and the little present is likely to be in compact clumps (Calzetti et al. 1995b). The main source of opacity appears to be given by dust that is external, or mostly external, to the starburst region (although still internal to the host galaxy), similar to a (clumpy) dust shell surrounding a central starburst. This is, of course, verified only in the *B*–*K* wavelength range where the reddening of the nebular emission lines has been measured; measurements at longer wavelengths could easily reveal more complex geometries. From a practical point of view, the data in Figure 6*b* are well described by a simple foreground, nonscattering dust distribution, with Milky Way (MW) diffuse ISM extinction curve and $R(V) = 3.1$; the reddening of the ionized gas is thus parameterized by the color excess $E(B-V)_{gas}$ (eq. [4]).

The stellar continuum colors show the trend to become redder for increasing reddening of the hydrogen emission line ratios (Figs. 6*a*, 6*c*, and 6*d*). The implications are twofold: (1) variations of the intrinsic SED from galaxy to galaxy are secondary relative to the trend induced by dust obscuration, and (2) within each starburst, the same foreground-like dust geometry holds for both the ionized gas and the nonionizing stellar continuum.

The first implication is not surprising, at least at UV wavelengths. Since we are observing the Rayleigh-Jeans part of the massive stars spectrum, the intrinsic UV spectral slope[8] $\beta_{26,0}$ is relatively constant over a fairly large range of ages, with values $-2.7 \gtrsim \beta_{26,0} \gtrsim -2.2$ for constant star formation over $10^6$ yr $\lesssim$ age $\lesssim 10^9$ yr (see Leitherer & Heckman 1995 and Table 6 in Appendix B). In the same conditions, the production of ionizing photons is also constant. In an instantaneous burst of star formation, the ionizing photons are more age sensitive than the nonionizing photons that produce the stellar continuum and disappear before appreciable changes in the UV spectral shape can be observed. The observed UV spectral slope $\beta_{26}$ of the UV-selected starbursts spans the range $-2.5 \lesssim \beta_{26} \lesssim +0.4$, much larger than what is expected from stellar population variations alone, and increases for increasing

[8] $\beta_{26,0}$ and $\beta_{26}$ refer to the intrinsic and observed, respectively, UV spectral slope measured between 0.125 and 0.26 $\mu$m as defined in Calzetti et al. (1994); see Appendix B for more details.

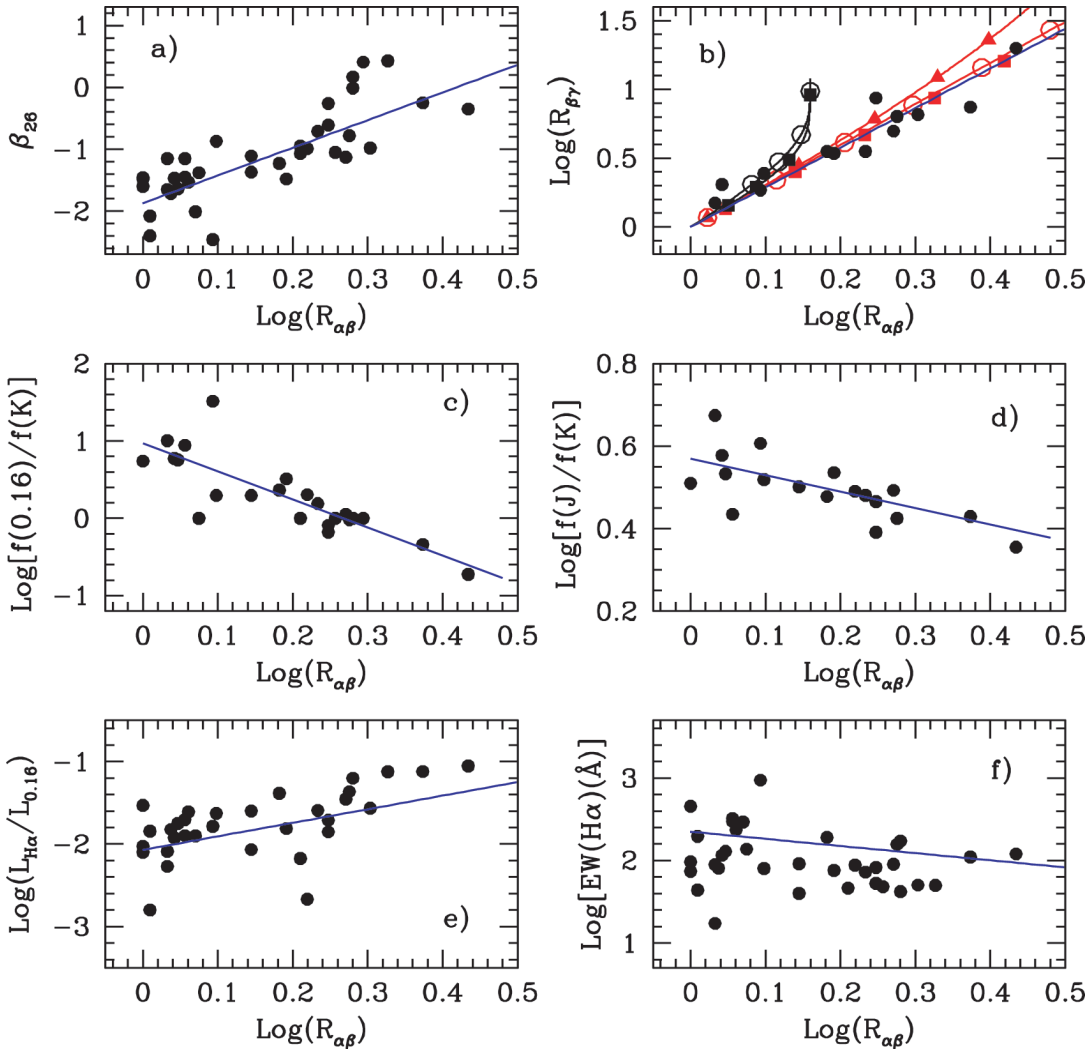


FIG. 6.—(*a*, *c*, *d*) UV–to–near-IR colors of ~50 UV-selected starbursts as a function of the attenuated-to-intrinsic hydrogen emission line ratio H$\alpha$/H$\beta$ ( *filled circles*). The relation between $R_{\alpha\beta}$ and the color excess of the ionized gas $E(B-V)_{gas}$ (§ 4.1) is given by eq. (4). The starburst obscuration curve (*blue line*) is derived from these data. Increasing values of $R_{\alpha\beta}$, i.e., larger amount of dust intercepted by the gas, correspond to redder colors of the stellar continuum (adapted from Calzetti et al. 1994; Calzetti 1997a). For the definition of $\beta_{26}$ see Appendix B; *f*(0.16), *f*(*J*), and *f*(*K*) are flux densities at the indicated wavelengths. (*b*) Correlation between the attenuated-to-intrinsic ratios of the hydrogen line pairs H$\alpha$/H$\beta$ and H$\beta$/Br$\gamma$; plotted with the data points are trends of the dust models of § 2.2 (with the same coding as Fig. 3). Homogeneous mixtures of gas and dust, either face-on or inclination-averaged, are excluded by the data, indicating that there is little internal dust in the starburst site (adapted from Calzetti et al. 1996). Panels (*e*) and ( *f* ) give for both the luminosity ratio $L_{H\alpha}/L_{0.16}$ and the equivalent width of H$\alpha$ the comparison between data points and expected trend of the starburst obscuration curve.

values of the attenuated-to-intrinsic hydrogen line ratios (i.e., color excess; Fig. 6).

In addition to correlating with the reddening of the ionized gas, the reddening of the UV stellar continuum, as measured by $\beta_{26}$, correlates with the infrared-to-blue and the infrared-to-UV luminosity ratios, $L_{IR}/L_B$ and $L_{IR}/L_{0.16}$ (Fig. 7 and Calzetti et al. 1995b; Meurer, Heckman, & Calzetti 1999). These ratios are a measure of the total dust opacity in the starburst region because the bulk of the starburst's energy is coming out in the UV-*B*. In addition, dust *absorption* is the main process that removes light from the line of sight (Calzetti et al. 1995b); when large galactic regions are observed, light scattered by dust out of the line of sight compensates, on average, that scattered into the line of sight. The opacity-reddening correlation means that measurements of reddening can be used to infer the total dust absorption in UV-selected starbursts (Meurer et al. 1999) with an uncertainty, $\Delta A_{0.16} \sim 0.6$ mag for individual objects and ~20% when averaged over large samples (Calzetti et al. 2000), that is dominated by variations in the starburst populations and in the details of the dust geometry from galaxy

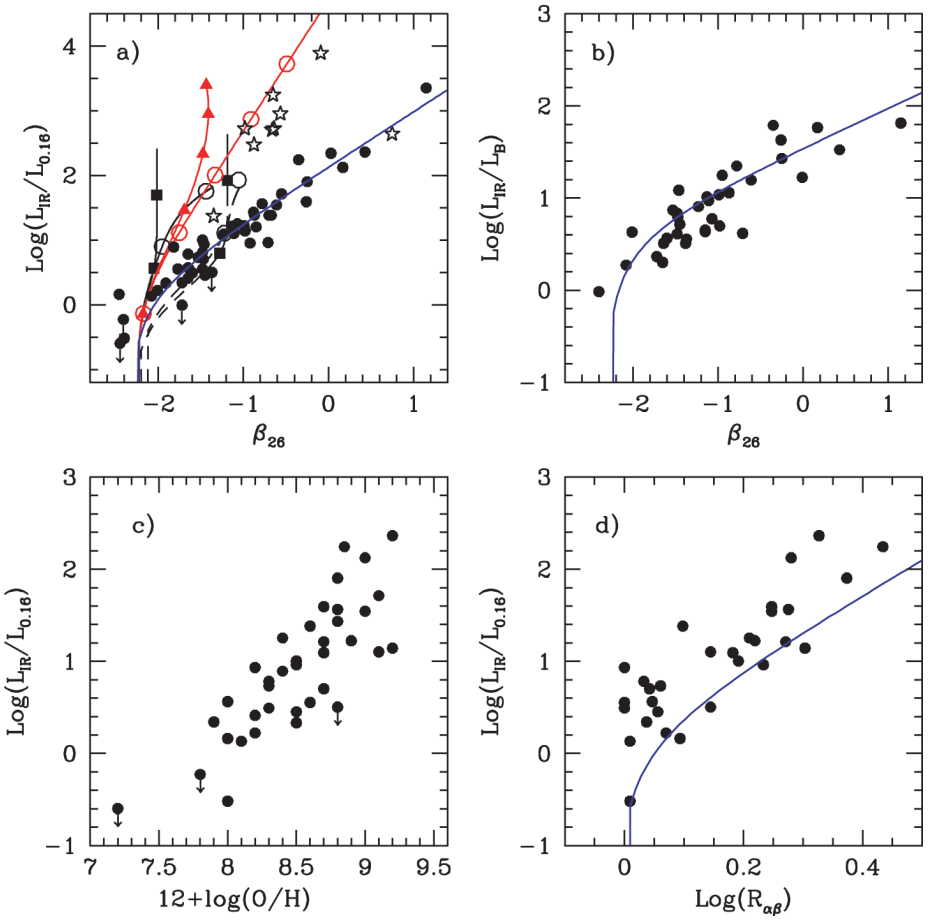


FIG. 7.—Dust bolometric luminosity, $L_{IR}$, normalized to the UV and $B$ stellar luminosities ($L_{0.16}$ in [$a$] and $L_B$ in [$b$], respectively) as a function of the UV spectral slope $\beta_{26}$ for the same starburst sample as in Fig. 6 (*circles*) and for nine ULIRGs (*stars* in [$a$]; Trentham, Kormendy, & Sanders 1999; Goldader et al. 2001). For most galaxies, where only *IRAS* measurements are available, the infrared luminosity in the 40–120 $\mu$m window is transformed into a dust bolometric luminosity using the correction $L_{IR} = 1.75L_{(40-120)}$ (Calzetti et al. 2000). The blue luminosity is that of the starburst region, from the data of McQuade, Calzetti, & Kinney (1995) and Storchi-Bergmann, Kinney, & Challis (1995). The luminosity ratios measure the starburst total dust opacity, while the UV slope is a measure of the UV reddening. The correlations imply that measuring the reddening in a UV-bright starburst gives a good handle on its global obscuration (adapted from Calzetti et al. 1995b; Meurer et al. 1999). In (*a*) the predicted trends from some of the models of § 2.2 (coded in the same fashion as in Fig. 3) are reported; in *b*, only the starburst obscuration curve is shown. ULIRGs deviate from the behavior of UV-selected starbursts, and combinations of clumpy distributions and homogeneous mixtures of dust and stars seem to better account for the data. (*c*, *d*) same data as in (*b*), as a function of the galaxy metallicity and of the attenuated-to-intrinsic H$\alpha$/H$\beta$ ratio, respectively. Dust opacity correlates with the metal content in starbursts (Heckman et al. 1998).

to galaxy. Such a correlation is expected for a foreground-like dust geometry (Fig. 3*d*; see discussion in Gordon et al. 2000).

The slopes of the correlations in Figure 6 identify the reddening suffered by the stellar continuum, $A_{\lambda 1,\,star} - A_{\lambda 2,\,star} = [k^e(\lambda_1) - k^e(\lambda_2)]E(B-V)_{gas}$, with $k^e(\lambda)$ the obscuration curve, while the total obscuration measurements of Figure 7 provide the zero point for $k^e(\lambda)$ (see also Calzetti et al. 2000). The intrinsic starburst flux density $f_i(\lambda)$ is thus recovered from the observed flux density $f_o(\lambda)$ via

$$f_i(\lambda) = f_o(\lambda)10^{0.4E(B-V)_{gas}k^e(\lambda)}, \qquad (7)$$

where the obscuration curve for the stellar continuum, $k^e(\lambda)$, is given by Calzetti et al. (2000):

$$k^e(\lambda) = 1.17(-1.857 + 1.040/\lambda) + 1.78 \quad \text{for} \quad 0.63\ \mu\text{m} \le \lambda \le 2.20\ \mu\text{m}; \qquad (8a)$$

$$k^e(\lambda) = 1.17(-2.156 + 1.509/\lambda - 0.198/\lambda^2 + 0.011/\lambda^3) + 1.78 \quad \text{for} \quad 0.12\ \mu\text{m} \le \lambda < 0.63\ \mu\text{m}. \qquad (8b)$$

Equations (8a) and (8b) fold into a single functional form a

variety of effects: extinction proper, scattering, and the geometrical distribution of the dust relative to the emitters. It is derived from the spatially integrated colors of the entire stellar population in the starburst and represents the "net" obscuration of the population itself. As mentioned above, the obscuration curve has mainly an absorption component because the effects of scattering are averaged out. Thus, it should not be confused with the extinction curve $k(\lambda)$ defined in § 2.1. Equations (8a) and (8b) imply that 1 mag of reddening between $B$ and $V$ for the ionized gas, $A_{B,\,\rm gas} - A_{V,\,\rm gas} = 1$ mag, corresponds to $A_{B,\,\rm star} - A_{V,\,\rm star} = 0.44$ mag of reddening for the stellar continuum. This fact can be alternatively expressed as

$$E(B-V)_{\rm star} = 0.44E(B-V)_{\rm gas}. \quad (9)$$

In other words, the stellar continuum suffers roughly one-half of the reddening suffered by the ionized gas (Calzetti et al. 1994; Fanelli, O'Connell & Thuan 1988; Mas-Hesse, Arnault, & Kunth 1989; see also Figs. 3*e* and 3*f*). Although $E(B-V)_{\rm star}$ parameterizes the amount of reddening of the stellar continuum, it is not a color excess proper as in the case of individual stars, because of the dust geometry effects folded in the expression of $k^e(\lambda)$. One obvious characteristic of the obscuration curve is the absence of the 0.2175 $\mu$m bump, which is a prominent feature of the MW extinction curve (Fig. 1). Dust/emitter geometries that can dilute the bump include mixed distributions with large optical depths (Natta & Panagia 1984; Granato et al. 2000; Gordon et al. 2000). However, mixed geometries do not account for the full range of observational data (Fig. 3) because the sources that contribute to the emerging SED are located at progressively lower optical depths $\tau_V$ for decreasing wavelength. In particular, the reddest UV slope produced by mixed geometries is $\beta_{26} \sim -0.7$ (Charlot & Fall 2000), to be compared with $\beta_{26} \sim 0$ observed in starburst galaxies (Fig. 6*a*). Thus, the lack of the feature is probably intrinsic to the *extinction curve* of the starbursts (Gordon, Calzetti, & Witt 1997) and may be due to the high UV energy densities that characterize these regions (§§ 2.1 and 4.2).

### 4.2. The Physical Origin of the Dust Geometry in "UV-bright" Starbursts

This section describes a dust model that attempts to reconcile two apparently contradictory facts: (1) stars in starbursts are on average a factor of ≈2 less reddened than the ionized gas (eq. [9]), and (2) both stars and ionized gas are affected by the same foreground-like dust distribution (Fig. 6). A schematic representation of a dust/star/gas configuration that can at the same time account for both effects is shown in Figure 8. Stars are born within optically thick molecular clouds, and the short-lived, most massive stars remain closely associated with their parental cloud and the gas they ionize for their entire lifetime (e.g., Walborn et al. 1999). These stars and their surrounding gas will be generally highly attenuated. As the starburst population evolves, the inside of the region of star formation becomes depleted of dust (Calzetti, Kinney, & Storchi-Bergmann 1996). With energy densities ≫100 times higher than in the local ISM, starburst environments are rather inhospitable to dust. Shocks from supernovae destroy dust grains, via grain-grain collisions and sputtering (Draine & Salpeter 1979; Jones et al. 1994). The average lifetime of a refractory grain is $\sim 8 \times 10^6$ yr, for a supernova rate of 0.05 yr$^{-1}$ and an ISM mass of $5 \times 10^8\ M_\odot$ (e.g., McKee 1989), about 1 order of magnitude or more shorter than the typical lifetimes of starbursts (Calzetti 1997a; Calzetti et al. 1997; Greggio et al. 1998; Aloisi, Tosi, & Greggio 1999). In addition, hot star wind– and supernova-driven outflows evacuate both interstellar gas and dust from the region (Heckman, Armus, & Miley 1990; De Young & Heckman 1994; Mac Low & Ferrara 1999; Ferrara & Tolstoy 2000; Heckman et al. 2000). R136, the central cluster in 30 Doradus, is an example of a few million years old cluster surrounded by an evacuating region (Scowen et al. 1998). Ionized gas separated, in projection, from the hot stars has also been observed in nearby starbursts (Hunter & Gallagher 1997; Wang, Heckman, & Lehnert 1998; Calzetti et al. 1999; Maíz-Apellániz & Walborn 2000).

The evacuated (clumpy) dust will act as a foreground-like distribution for both the gas (also at the edges of the region) and the central stars (Fig. 8; Calzetti et al. 1996; Witt & Gordon 2000; Gordon et al. 2000); however, the ionized gas will be more obscured than the stars, because of its spatial location and closer association with the dust (Calzetti 1997a). This gas is more likely to contribute to the nebular emission observed at UV-optical wavelengths than the gas in molecular clouds, because of its milder obscuration. In the presence of multiple generations of starburst populations, the long-lived, nonionizing stars have time to "diffuse" into regions of lower dust density (Calzetti et al. 1994; Charlot & Fall 2000; Granato et al. 2000), as their native clusters are disrupted by evaporation or by the host galaxy's gravitational field (Leisawitz & Hauser 1988; Kim, Morris, & Lee 1999; Tremonti et al. 2001). Cool stellar populations in the LMC have, for instance, been observed to be less embedded in dust than hotter stellar populations (Zaritsky 1999). A similar trend is observed in the young (<20 Myr) open clusters of the MW (Yadav & Sagar 2001). Massive, nonionizing stars can still produce significant UV emission. Hence, the integrated UV-optical stellar continuum from the combination of the aging, diffusing populations and the starburst-embedded young populations will be less obscured than the emission from the nebular gas (Calzetti et al. 1994; Gasda & Leitherer 1996). For the stellar continuum and the ionized gas to have correlated obscuration values (eq. [9]), multiple starburst generations or long-lasting star formation events (rather than "instantaneous" events) are needed to attain an equilibrium between the number of stars drifting out of molecular clouds/starburst regions and the number of newly born, dusty stars. Starbursts hosted in dwarf galaxies are observed to have ongoing star formation over ≳200 Myr (Calzetti

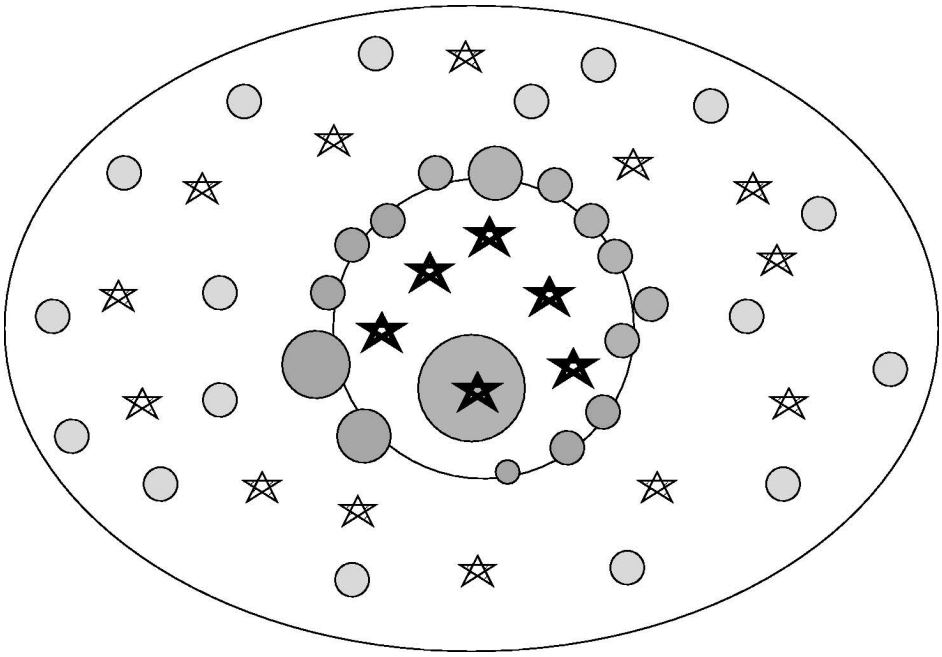

FIG. 8.—Schematic representation of the dust/star distribution in starburst galaxies that can account for most observational constraints. The starburst region (*center of figure*) contains the newly formed stellar population, including the short-lived, massive stars (*heavy stars*), some still embedded in the parental clouds. Gas outflows induced by hot star winds and supernova explosions from previous stellar generations have displaced dust and gas (*dark gray circles*) to the edges of the region. The ionized gas, located at the boundaries of the site, "sees" the surrounding dust as a "foreground distribution." The galaxy's diffuse ISM (*light gray circles*) is also surrounding the starburst. Both the galactic and the starburst-associated dust are clumpy (Gordon et al. 1997; Charlot & Fall 2000). Thus, the stellar continuum light will often emerge from regions that are not necessarily spatially coincident (in projection) with those of the dust and ionized gas (Calzetti 1997a). If star formation has been ongoing for longer than the lifetime of massive stars ($>10^7$ yr), the surroundings of the current starburst site become populated by the less massive, long-lived stars from previous starburst generations (*light stars*) that are diffusing into the less opaque general ISM or have dispersed their parental clouds (Calzetti et al. 1994; Charlot & Fall 2000). This model should be regarded as a simple approximation of the more realistic distribution of emitters and absorbers in starburst galaxies.

et al. 1997; Greggio et al. 1998; Aloisi, Tosi, & Greggio 1999), and durations could be as long in more massive starburst galaxies (Calzetti 1997a).

Although the obscuration curve can be widely applied to UV-selected starbursts, it is not necessarily applicable to systems with different stellar population or ISM characteristics. In the case of nonstarburst galaxies there is no obvious mechanism for creating a foreground-dust–like geometry. In extreme starbursts such as the ULIRGs, the nonapplicability of the obscuration curve has been demonstrated observationally (Goldader et al. 2001 and Fig. 7*a*). In these galaxies, the high central concentration of gas and dust is likely to induce more extreme geometries than in UV-selected galaxies and to produce combinations of clumpy mixed and foreground distributions. Galaxies whose infrared properties are intermediate between the ULIRGs and the UV-selected galaxies will progressively deviate from the dust geometry of the latter (Alonso-Herrero et al. 2001; Förster Schreiber et al. 2001). Dust in subsonic H II regions is likely to be mixed with the stars rather than having been pushed away or destroyed as in starbursts, and scattering of stellar light into the line of sight may be an important component in the attenuation budget (Caplan & Deharveng 1986; Bell et al. 2001). Because of the differences in the physical environment between the two types of objects, the foreground-dust–like approximation no longer holds for subsonic H II regions and equations (8a) and (8b) do not apply. Differences in the star formation history can also contribute to the difference between subsonic H II regions and starbursts, with instantaneous bursts being a better description for the former and extended star formation for the latter; thus, differential attenuation between ionized gas and stars is not necessarily expected in the H II regions. Supersonic H II regions could be at the boundary between the two extremes just discussed; one example is 30 Doradus, which has evolved to the point of resembling a ministarburst (Walborn 1991).

To conclude, the starburst obscuration curve is a purely empirical result, and its derivation is independent of any assumption about the starburst's population, the dust geometry, or the details of the extinction curve. It provides statistical estimates of the reddening and obscuration of local UV-selected starbursts, and deviations as large as ~0.6 mag from the mean obscuration at 0.16 $\mu$m are to be expected on an case-by-case basis. The physics of the starburst environment provides an explanation of the "foreground-dust–like" behavior of the

curve, of the correlation between the reddening of the ionized gas and that of the stellar continuum, and of the correlation between reddening and total obscuration. As a sample, local UV-selected starbursts are characterized by modest amounts of reddening and obscuration, which are correlated with the star formation activity (eq. [6]). The median color excess is $E(B-V)_{\rm gas} \sim 0.35$ (Calzetti 1997b), corresponding to UV continuum attenuations of $A_{\rm UV,\,star} \sim 1.6$, 1.4, and 1.1 mag at 0.15, 0.20, and 0.30 $\mu$m, respectively (Table 4 and Buat & Burgarella 1998; Meurer et al. 1999).

### 4.3. Useful Expressions

Observables such as the UV slope, the colors, and the luminosities and equivalent widths of the hydrogen lines can be readily related to the dust-induced color excess of the ionized gas and, through equation (9), of the stellar continuum. The UV slope is correlated with $E(B-V)_{\rm gas}$ (Fig. 6*a*), and equations (8a) and (8b) give

$$\beta_{26} = 2.08E(B-V)_{\rm gas} + \beta_{26,\,0}, \quad (10)$$

where a list of $\beta_{26,\,0}$ values is given in Table 6 in Appendix B. The slope of the correlation between $\beta_{26}$ and $E(B-V)_{\rm gas}$ is somewhat steeper than that measured by Calzetti et al. (1994) directly from the data ($1.88 \pm 0.28$), but the two are within 1 $\sigma$ of each other. It should also be noted that equation (10) becomes a lower envelope to the data points in Figure 6*a*, for $\beta_{26,\,0} < -2.25$, a value appropriate for dust-free, star-forming populations. This indicates that variations of the dust/stars/gas geometry from the schematic model of Figure 8 and/or of the stellar population from the theoretical extreme $\beta_{26,\,0} \leq -2.25$ have the effect of reddening the UV slope even for $E(B-V)_{\rm gas} \sim 0$. The vertical scatter in Figure 6*a* should thus be interpreted as due to such variations from galaxy to galaxy.

Reddening expressions for optical colors can be directly derived from equations (8a) and (8b) (see also Figs. 6*c* and 6*d*). A mixed UV-optical color, $0.28-V$, could be useful to infer the reddening of intermediate-redshift ($\langle z \rangle \sim 0.6$) starburst galaxies observed in *B* and *I*, and the reddening of one relative to the other is given by

$$A_{0.28,\,\rm star} = 1.80A_{V,\,\rm star}. \quad (11)$$

Under the assumption that the rest-frame UV emission and the nebular lines are both due to massive stars, the reddening of the UV continuum relative to the nebular hydrogen emission is given by

$$A_{0.16,\,\rm star} = 1.21A_{\rm H\beta,\,gas}, \quad (12)$$

$$A_{0.16,\,\rm star} = 1.78A_{\rm H\alpha,\,gas}, \quad (13)$$

$$A_{0.28,\,\rm star} = 1.29A_{\rm H\alpha,\,gas}. \quad (14)$$

Figure 6*e* shows the comparison between data of local galaxies and equation (13) (Calzetti 1997b). While the agreement between the data in the first four panels of Figure 6 and equations (8a) and (8b) is a direct consequence of the fact that those data were used to derive the starburst obscuration curve, the match between data and expected trend in the bottom two panels of the figure is a consistency check, since it was not imposed a priori.

One immediate consequence of the differential reddening between gas and stars is that the equivalent widths of the nebular lines depend on the amount of gas obscuration; for the H$\alpha$ and H$\beta$ emission lines the relations are (Calzetti et al. 1994)

$$\log\,[{\rm EW(H\beta)}_a/{\rm EW(H\beta)}_o] = -0.64E(B-V)_{\rm gas}, \quad (15)$$

$$\log\,[{\rm EW(H\alpha)}_a/{\rm EW(H\alpha)}_o] = -0.40E(B-V)_{\rm gas}, \quad (16)$$

where the attenuated and intrinsic EWs are directly compared. Comparison of these trends with the data points is shown in Figure 6*f*; the trend given by the obscuration curve marks an upper envelope to the ensemble of observed EWs because the presence of older stellar populations underlying the starbursts dilutes the contrast between the emission lines and the stellar continuum in the data.

Statistically speaking, the UV slope is a good estimator of the total obscuration affecting the starburst (Meurer et al. 1999 and Fig. 7); in particular, the ratio of the dust infrared luminosity, $L_{\rm IR}$, to the stellar UV or blue luminosity, $L_{0.16}$ or $L_B$, is related to $\beta_{26}$ via

$$\log\left[\frac{1}{1.68}\left(\frac{L_{\rm IR}}{L_{0.16}}\right)_{\rm star} + 1\right] \simeq \frac{A_{0.16,\,\rm star}}{2.5} = 0.84(\beta_{26} - \beta_{26,\,0}), \quad (17)$$

$$\log\left[\frac{1}{3.85}\left(\frac{L_{\rm IR}}{L_B}\right)_{\rm star} + 1\right] \simeq \frac{A_{B,\,\rm star}}{2.5} = 0.43(\beta_{26} - \beta_{26,\,0}). \quad (18)$$

The two constant values on the left-hand side of equations (17) and (18), 1.68 and 3.85, represent the bolometric corrections of the stellar emission relative to the UV or *B*. The correction for the *B* band is larger and subject to more uncertainties than that for the UV, hence the larger scatter in the data point of Figure 7*b*. Equation (17) can be rewritten as

$$\log\left[\frac{1}{1.68}\left(\frac{L_{\rm IR}}{L_{0.16}}\right)_{\rm star} + 1\right] = 1.76E(B-V)_{\rm gas}, \quad (19)$$

where the equation above represents a lower envelope to the data (Fig. 7 *d* and Calzetti et al. 2000) and has a scatter comparable to that of Figure 6*a*. The nature of the scatter in the $\beta_{26}$ versus $E(B-V)_{\rm gas}$ and in the $L_{\rm IR}/L_{0.16}$ versus $E(B-V)_{\rm gas}$ relations is the same: it is due to variations from galaxy to galaxy of the starburst populations and of the dust/star/gas geometry.

## 5. MEASUREMENTS OF DUST OPACITY IN HIGH-REDSHIFT GALAXIES

As discussed in the introduction, the energy balance between UV-optical and infrared cosmic background suggests that there have been infrared-luminous galaxies at all epochs. The number density of quasars was more than 100 times higher at $z \sim 2.5$ than today (e.g., Shaver et al. 1999), and star formation activity was ~3–10 times higher at $z \gtrsim 1$ than at $z \sim 0$ (Lilly et al. 1996; Cowie et al. 1999), flattening or decreasing only beyond $z \sim 1$–2 (Madau et al. 1996; Steidel et al. 1999). If the association between activity and dust opacity observed in the local universe (eq. [6]) holds at high redshift as well, galaxies in the past may have been as dusty as or dustier than today (§ 5.2).

Among the methods described in § 3, the multiwavelength comparison is the only practical approach for measuring the dust opacity of galaxies beyond the local few hundred megaparsecs. However, because of observational difficulties, the wavelength coverage of the typical sample is limited to a few windows, often with little overlap from sample to sample. Measures of the content, nature, and opacity effects of the dust in distant galaxies are therefore still at a very early stage, and the picture is vastly incomplete and controversial.

### 5.1. Dust in Damped Ly$\alpha$ Systems

The very first evidence for the presence of dust in high-redshift systems came from studies of damped Ly$\alpha$ systems (DLAs; Meyer & York 1987; Fall, Pei, & McMahon 1989; Meyer & Roth 1990; Pettini, Boksenberg, & Hunstead 1990; Pei, Fall, & Bechtold 1991; Pettini et al. 1994, 1997a, 2000a; Zuo et al. 1997; Vladilo 1998; Ge, Bechtold, & Kulkarni 2001). DLAs are the largest H I column density absorption systems seen in the spectra of background quasars, with $N(\mathrm{H\ I}) \geq 10^{20.3}$ cm$^{-2}$. Their metallicities cover the range ~1/100–1/10 solar for $z \sim 0.5$–4, with a mean value of ~1/13 solar at $z \sim 0.5$–3 and little evidence for evolution with redshift (Prochaska & Wolfe 2000; Pettini et al. 1999, 1997b; Lu et al. 1996). Selection biases against the dustiest and most metal-rich DLAs and problems with dust depletion corrections have been advocated as possible reasons for the observed weak metallicity evolution (Fall & Pei 1993; Boissé et al. 1998; Savaglio, Panagia, & Stiavelli 2000; see, however, Ellison et al. 2001). The dust fraction in DLAs is measured by comparing the abundance of dust-depleted metals such as Cr II, Fe II, and Si II against that of a metallicity tracer such as Zn II, all of them producing rest-frame UV absorption lines (Meyer & York 1987). The dust-to-metals ratio in DLAs is in the range 50%–60% of the MW value; this, combined with the generally low metallicities, indicates that DLAs are relatively transparent systems, with dust-to-gas ratios between 2% and 25% of the MW value (Fall, Pei, & McMahon 1989; Pei, Fall, & Bechtold 1991; Pettini et al. 1997a; Vladilo 1998). The absence of the 0.2175 $\mu$m dust absorption associated with DLAs led Pei et al. (1991) to conclude that the extinction curve in these systems is probably similar to the one observed in the Magellanic Clouds. More recently, though, Malhotra (1997) reported a ~3 $\sigma$ detection of the dust absorption feature in the composite spectra of Mg II absorbers. Although the presence of modest quantities of dust is well established in DLAs, the weak or absent evolution of the metal content and of the cosmological mass density with redshift (Rao & Turnshek 2000) questions their relationship to luminous galaxies and favors the interpretation that DLAs preferentially trace galaxies with extended gas distributions and low metal and dust contents (Le Brun et al. 1997; Turnshek, Rao, & Nestor 2001) and the unevolved outskirts of galaxies (Ferguson, Gallagher, & Wyse 1998).

### 5.2. Dust Emission from Distant Star-forming Galaxies

In recent years, facilities/instruments such as *ISO* and SCUBA at the James Clerk Maxwell Telescope have achieved high enough sensitivities in the mid- and far-infrared to detect *dust emission* beyond a few microns from statistically significant samples of galaxies at cosmological distances. Studies on the *ISO* and SCUBA surveys, especially the identification of the optical/near-IR counterparts to the infrared sources and the redshift measurements, are still ongoing, and the results described below should be considered in many instances preliminary.

*ISO* surveys have yielded ≈1500 sources in the redshift range $0 \lesssim z \lesssim 1.5$, down to a sensitivity limit of ≈0.1 mJy in the mid-IR (6.75, 12, and 15 $\mu$m) and ≈0.1 Jy in the far-IR (90 and 175 $\mu$m; Rowan-Robinson et al. 1997; Oliver et al. 1997; Taniguchi et al. 1997; Kawara et al. 1998; Clements et al. 1999; Altieri et al. 1999; Aussel et al. 1999; Flores et al. 1999a, 1999b; Puget et al. 1999; Serjeant et al. 2000; Scott et al. 2000; Efstathiou et al. 2000; Dole et al. 2001). Full lists of all surveys are given in Rowan-Robinson et al. (1999) and Elbaz (1999). The number counts at 175 $\mu$m account for ~10% of the CIB (Puget et al. 1999; Dole et al. 2001), showing that the bulk of the background has not been resolved yet at these wavelengths. Nevertheless, the number counts at mid- and far-IR wavelengths are about 3–10 times above the no-evolution extrapolation of the local *IRAS* counts (Elbaz et al. 1999; Aussel et al. 1999; Puget et al. 1999; Serjeant et al. 2000; Efstathiou, Rowan-Robinson, & Siebenmorgen 2000). The implication is a strong luminosity evolution, $L_{\mathrm{IR}} \propto (1+z)^{4.5}$, or a combination of luminosity and density evolution of the infrared sources out to $z \sim 1$ (Clements et al. 1999; Xu 2000; Chary & Elbaz 2001; Franceschini et al. 1994; Guiderdoni et al. 1998) that is comparable to or stronger than the luminosity evolution observed at rest-frame UV wavelengths out to the same redshift (Lilly et al. 1996; Cowie et al. 1999; Sullivan et al. 2000). The *ISO* counts are thus dominated by luminous infrared galaxies at $z \lesssim 1$, with $L_{\mathrm{bol}} \sim L_{\mathrm{IR}} \gtrsim 10^{11}\ h_{65}^{-2}\ L_{\odot}$ (Rowan-Robinson et al. 1997; Elbaz 1999; Xu 2000). Although this conclusion is based on the highly uncertain conversion of the 15 $\mu$m emission[9] to a total infrared

[9] At $z \sim 1$ the flux density at 15 $\mu$m is centered on the rest-frame emission of the aromatic features that dominate the region between 6 and 12 $\mu$m; the relation between the intensity of the features and the total infrared emission is still unsettled (Boselli et al. 1998; Dale et al. 2001).

luminosity, it is qualitatively supported by the optical counterparts of the *ISO* sources. Close to 100 mid-IR sources, with median redshift $\langle z \rangle \sim 0.7$–$0.8$, have so far been identified at optical/near-IR wavelengths (Aussel et al. 1999; Flores et al. 1999b; Rigopoulou et al. 2000) ($\langle z \rangle \sim 0.1$–$0.2$ for the 12 $\mu$m sample; Clements, Désert, & Franceschini 2001). Many of the rest-frame optical spectra show characteristics of dusty luminous starbursts, with current bursts of star formation superposed on a prominent population of A stars and with attenuation values $A_V \gtrsim 0.5$–$1.8$ mag (Flores et al. 1999b; Rigopoulou et al. 2000; Poggianti & Wu 2000).

At the time of writing, SCUBA surveys at 850 $\mu$m of "blank" fields and targeted lensed objects have detected a total of ≈100 sources with flux densities in the range ∼0.5–≳10 mJy and redshifts between $z \sim 1$ and 3, although sources as far away as $z \approx 5$ may be present (Smail, Ivison, & Blain 1997; Hughes et al. 1998; Barger et al. 1998, 1999b, 2000; Smail et al. 1998, 1999, 2000; Eales et al. 1999, 2000; Lilly et al. 1999; Chapman et al. 2001; Fox et al. 2001; Scott et al. 2001). The number counts down to 2 mJy and to 0.5 mJy account for ∼20%–30% and more than 90%, respectively, of the CIB (Hughes et al. 1998; Barger et al. 1998; Eales et al. 1999, 2000; Barger, Cowie, & Sanders 1999a; Blain et al. 1999c). However, the latter fraction is potentially affected by small number statistics: so far only a few sources have flux densities below 2 mJy, the SCUBA confusion limit in blank fields, all of them from the survey of lensed galaxies (Blain et al. 1999a). Observations at 850 $\mu$m probe the Rayleigh-Jeans tail of the thermal dust emission of galaxies at least to redshift ≈5–7. A source at $z \geq 1$ and with an 850 $\mu$m flux density of 2 mJy corresponds to a luminosity $L_{\rm IR} \sim 2 \times 10^{12}\ h_{65}^{-2}\ L_\odot$, for typical SEDs of local infrared-selected galaxies (Lisenfeld, Isaak, & Hills 2000; Dunne et al. 2000; Dunne & Eales 2001); this is roughly the luminosity of a ULIRG like Arp 220. The few optical/near-IR counterparts that have been identified are faint, often with $I > 24$ and $K \gtrsim 20$–$21$ (Smail et al. 1998, 1999; Barger et al. 1999b; Lilly et al. 1999; Ivison et al. 2000); in most cases the ratio $L_{\rm IR}/L_R < 0.05$, where $L_R$ is the luminosity in the observer-frame $R$ band, and the infrared emission accounts for more than 95%–99% of the bolometric luminosity. It is indeed widely accepted, also on the basis of the few available multiwavelength SEDs, that the SCUBA sources are "cosmological ULIRGs" (Hughes et al. 1998; Barger et al. 1998; Lilly et al. 1999; Smail et al. 1998; Ivison et al. 2000), although this generalization has been recently questioned (Eales et al. 2000). The median redshift of the surveys is $\langle z \rangle \simeq 2.5$ (Lilly et al. 1999; Smail et al. 1999, 2000; Barger et al. 1999b, 2000; Eales et al. 2000; Chapman et al. 2001; Fox et al. 2001); however, less than 10% of all the sources have reliable redshift determinations from optical/near-IR counterparts, and a total of ≈50% of the sample have photometric redshifts, most often derived from the radio/submillimeter spectral index relation of Carilli & Yun (1999). The comoving number density of SCUBA sources in the redshift range $z = 1$–$3$ brighter than 6 mJy is $\sim(3$–$5) \times 10^{-5}\ h_{65}^3$ Mpc$^{-3}$ in our cosmology (Barger et al. 2000; Scott et al. 2001), about 2 orders of magnitude larger than the corresponding number density of local ULIRGs brighter than $10^{12}\ L_\odot$ (Kim & Sanders 1998). A strong luminosity evolution, possibly as strong as $L_{\rm IR} \propto (1+z)^3$ to $z \sim 2$, is also implied by the number counts (e.g., Scott et al. 2001). Although the statistical properties of the sources are often inferred using the star-forming Arp 220 as a template, a fraction of AGNs is present in the sample (Ivison et al. 1998; Barger et al. 1999b). Current best estimates, based on the X-ray luminosity of the sources, favor an AGN fraction of ∼20% (Severgnini et al. 2000; Hornschemeier et al. 2000; Fabian et al. 2000; Barger et al. 2001); this value will generally depend on the source luminosity range, as it does in the local universe (Genzel et al. 1998; Lutz et al. 1998; Veilleux et al. 1999).

### 5.3. Dust Reddening and Obscuration in Distant Star-forming Galaxies

Multiwavelength observations of optically selected samples of intermediate- and high-redshift galaxies are generally limited to the rest-frame UV and optical windows, with few exceptions (e.g., Flores et al. 1999b; Chapman et al. 2000). Such surveys suffer the same limitations of local UV-optical samples, with the added complication of the often incomplete wavelength coverage. By probing only the *differential attenuation*, the UV-optical data provide, in principle, lower limits to the actual dust opacity of the galaxy (§ 2.2, but see also § 4). In order to differentiate an aging stellar population from dust as the cause of the SED reddening, a variety of approaches have been adopted by different authors. Common diagnostics include the Balmer line decrement H$\alpha$/H$\beta$, line-to-continuum ratios, e.g., H$\alpha$/UV and H$\beta$/UV, and multicolor SED fitting. Limitations to each of these diagnostics are discussed in § 2.2 and in the sections below, as appropriate.

#### *5.3.1. Galaxies at Redshift $z \lesssim 2$*

For a UV-selected sample of star-forming galaxies at $z \approx 0.2$, Sullivan et al. (2000, 2001) derive an average attenuation $A_{\rm H\alpha} \sim 0.8$ mag and find tentative evidence that those systems follow an obscuration-SFR correlation similar to that observed in more local galaxies (Wang & Heckman 1996; Heckman et al. 1998; Hopkins et al. 2001). The authors use a combination of UV (0.20 $\mu$m), optical (H$\alpha$ and H$\beta$), and radio (1.4 GHz) data to analyze their sample, although their reddening estimates are mostly based on the subsample for which they can measure H$\alpha$/H$\beta$ ratios. If the starburst obscuration curve (§ 4) applies to $z \approx 0.2$ star-forming galaxies, an attenuation $A_{\rm H\alpha} \sim 0.8$ mag for the nebular line corresponds to $A_{0.20} \sim 1.3$ and $A_{0.16} \sim 1.4$ for the UV stellar continuum. Although these figures agree with local measurements of the extinction at UV and H$\alpha$ in star-forming galaxies (§ 3.6 and Table 3), the UV selection of the sample potentially biases the

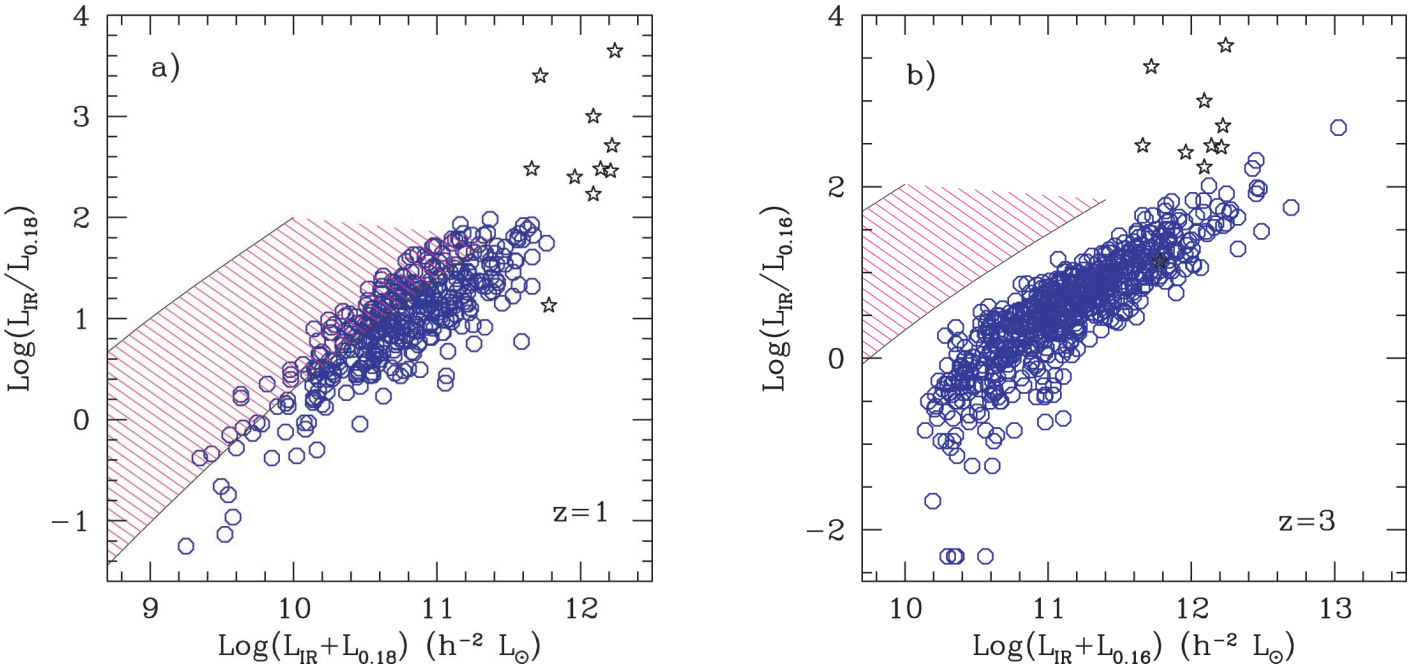


FIG. 9.—UV-to-IR luminosity ratio as a function of the total UV plus IR luminosity for star-forming galaxies at (*a*) $z \sim 1$ and (*b*) $z \sim 3$ from Fig. 11 of Adelberger & Steidel (2000), with data kindly provided by K. Adelberger (2001, private communication) and modified to our selected cosmology, $\Omega_M = 1$, $\Omega_\Lambda = 0$, and $H_0 = 65$ km s$^{-1}$ Mpc$^{-1}$. The blue circles are the high-redshift data; the shaded region shows the locus occupied by the local star-forming and starburst galaxies (Wang & Heckman 1996; Heckman et al. 1998); the black stars are the ULIRGs from Goldader et al. (2001) and Trentham et al. (1999). The infrared luminosity of the high-redshift galaxies is derived using UV data and the $\beta$ vs. $L_{IR}/L_{UV}$ correlation (eq. [17] and Adelberger & Steidel 2000). For fixed UV/IR ratio, the faint luminosity end of the high-redshift galaxy distributions is determined by selection effects, while the bright luminosity end is free from such effects. Thus, if the UV/IR vs. $\beta$ relationship holds for the distant star-forming galaxies, more actively star-forming galaxies are on average more opaque, similar to the trend observed in local galaxies (Wang & Heckman 1996; Heckman et al. 1998; see also Fig. 5). It also highlights that at fixed UV/IR ratio (fixed opacity), higher redshift galaxies tend to be brighter at the high-luminosity end than local galaxies. Since the sum of the UV and IR luminosities measures the SFR, high-redshift galaxies tend to be more actively star forming than local galaxies for fixed dust opacity (Adelberger & Steidel 2000).

reddening measures toward low values by excluding more heavily extincted galaxies.

The $z \sim 1$ Balmer break sample of Adelberger & Steidel (2000) is also a rest-frame–UV/blue-selected one. Exploiting the presence of the Balmer discontinuity at ~0.365 $\mu$m in galaxy SEDs to select $z \sim 1$ candidates (a derivative of the Lyman break technique; see next section), these authors have obtained spectroscopic confirmation for ≈700 galaxies. The sample contains a large variety of galaxies, from active starbursts to quiescent star forming to poststarbursts. If the $z \sim 1$ galaxies with blue ($\beta_{26} \lesssim -0.3$) SEDs are analogs of local starbursts and follow the same IR/UV versus $\beta$ relation, they also follow an obscuration-SFR relation similar to the local one, with a comparable range of attenuations (Fig. 9*a*). However, for fixed opacity, the $z \sim 1$ galaxies tend to have on average brighter UV + IR luminosities (larger SFRs) than the $z \sim 0$ galaxies. Thus, even taking selection effects into account, the distant galaxies are, on average, more actively star forming for the same amount of obscuration than the local starbursts (Adelberger & Steidel 2000).

Glazebrook et al. (1999), Yan et al. (1999), and Moorwood et al. (2000) use rest-frame H$\alpha$ observations and H$\alpha$/UV comparisons to infer dust reddening in star-forming galaxies at redshift $z \sim 1$–2.2. The *I*-band–selected sample of Glazebrook et al. (1999) corresponds to rest frame ~*V* for a $z = 1$ galaxy: the longer wavelength selection of the samples mitigates, although does not remove completely, the bias against dust-obscured galaxies introduced by UV selections (for the Canada-France Redshift Survey employed by Glazebrook et al. 1999, see Lilly et al. 1995, and for the sample used by Yan et al. 1999, see McCarthy et al. 1999). The presence of dust reddening in the $z \sim 1$–2.2 samples is derived from the discrepancy between the measured $L_{H\alpha}/L_{0.28}$ luminosity ratio and the ratio predicted by dust-free models.[10] Figure 10 compares the range of attenuated-to-intrinsic values $(L_{H\alpha}/L_{0.28})_a/(L_{H\alpha}/L_{0.28})_o$ derived from data by the three groups of authors[11] with predictions from the dust models of § 2.2. Geometries where dust and stars are homogeneously

[10] Moorwood et al. (2000) measure the rest-frame $L_{H\alpha}/L_{0.25}$ ratio; the small extrapolation to $L_{H\alpha}/L_{0.28}$ is done here assuming a constant star formation population.

[11] The intrinsic ratio $(L_{H\alpha}/L_{0.28})_o$ is an average of H$\alpha$ and UV luminosities for a variety of IMFs, star formation histories, and metallicities of stellar populations; see Table 3 in Glazebrook et al. (1999).

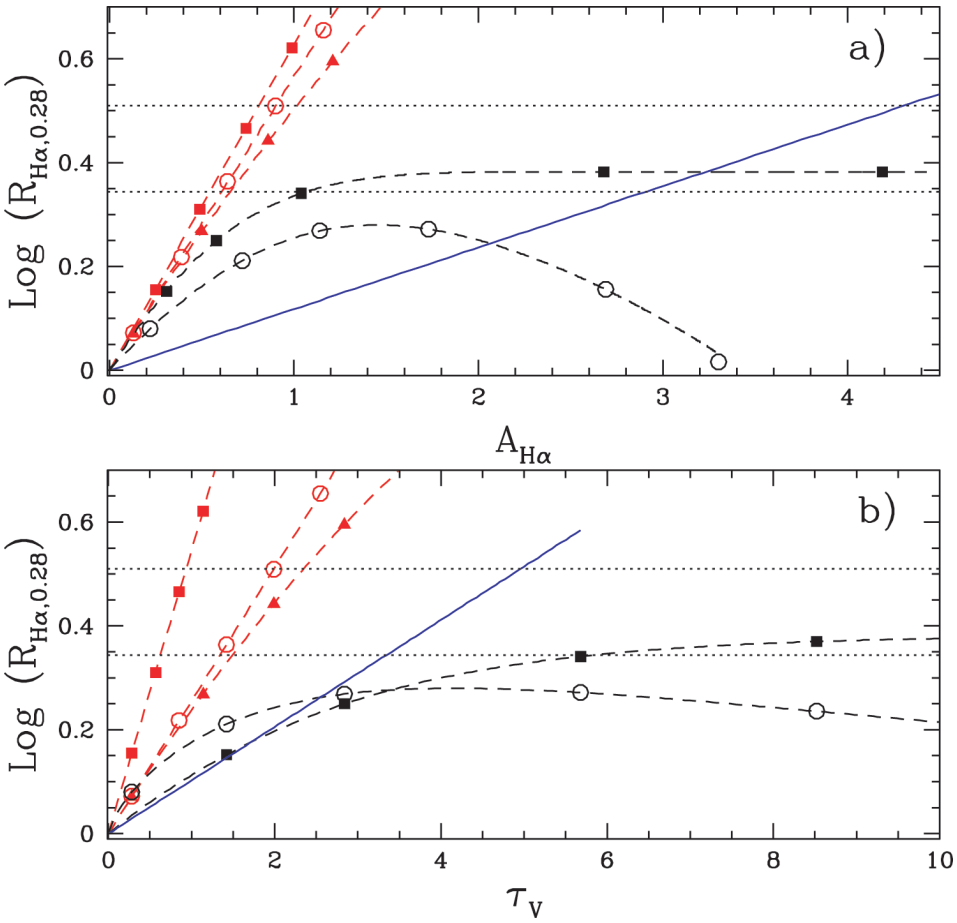


FIG. 10.—Attenuated-to-intrinsic $L_{H\alpha}/L_{0.28}$ ratio in $z \sim 1$–2 galaxies, $R_{H\alpha,\,0.28} = (L_{H\alpha}/L_{0.28})_o/(L_{H\alpha}/L_{0.28})_o$, as a function (*a*) of the obscuration at H$\alpha$ and (*b*) of the dust optical depth $\tau_V$. The range of observational values is marked by the two horizontal lines. The models of dust/emitter distribution are coded as in Fig. 3, but only the cases of the SMC extinction curve and of the starburst obscuration curve are shown.

mixed, in either spheroidal or flattened distributions, appear less effective in reproducing the observed H$\alpha$/UV ratios than foreground geometries (Fig. 10). If the foreground and starburst distributions bracket the possible range of dust/emitter morphologies for the $z \sim 1$–2 H$\alpha$ galaxies, the front-to-back optical depths are $\tau_V \sim 0.6$–4.9 mag (Fig. 10, *bottom panel*), and the effective attenuations are $A_{H\alpha} \sim 0.6$–4.3 mag, $A_{0.28} \sim 1.5$–5 mag, and $A_{0.16} \sim 3$–7 mag for SMC extinction. MW-like and SMC-like extinction curves give results that are less than 0.1 mag apart at $\lambda \geq 0.28$ $\mu$m but ~1.2 mag different at $\lambda = 0.16$ $\mu$m, with larger obscurations given by the SMC extinction curve. Uncertainties in the metallicity, IMF, and star formation history of the galaxy stellar populations introduce a factor $\gtrsim 2$ additional scatter on the inferred opacities (Table 3 in Glazebrook et al. 1999). The major limitation is, however, that dust opacities measured from the current H$\alpha$ surveys of galaxies are probably not representative of the $z \sim 1$–2 population as a whole. By number, the samples of Glazebrook et al. (1999) and Moorwood et al. (2000) are small (13 galaxies and five galaxies, respectively); the sample of Yan et al. (1999), albeit 2.5 times larger than that of Glazebrook et al. (1999), does not measure the H$\alpha$ emission on the same galaxies for which UV is available. For such small samples, sensitivity limits induce a strong selection effect: the observed galaxies will be among the brightest in H$\alpha$, and, in addition, contamination from AGN/Seyfert nuclei is not excluded (Whittle 1992). Therefore, such surveys sample the high end of the activity and dust obscuration ranges for optically detectable systems at $z \sim 1$–2 (Glazebrook et al. 1999; Sullivan et al. 2000; and eq. [6]).

In summary, the limited information available on galaxies at $z \approx 1$ suggests that dust opacities cover a range similar to that of local star-forming and starburst galaxies; they may follow a similar relation $A_\lambda \propto \log(\mathrm{SFR})^\alpha$ (see eq. [6]), with the proportionality constant revised downward relative to the local sample.

### 5.3.2. *Galaxies at Redshift $z > 2$*

To date, the surveys that have most efficiently secured large populations of galaxies beyond $z \sim 2$ are those that exploit the Lyman discontinuity at rest frame 0.0912 $\mu$m to identify high-redshift candidates; these are the so-called Lyman break galaxies

(LBGs; Guhathakurta, Tyson, & Majewski 1990; Steidel & Hamilton 1992; Steidel et al. 1996a, 1996b, 1999; Giavalisco, Steidel, & Macchetto 1996b; Lowenthal et al. 1997; Giavalisco et al. 1998; Adelberger et al. 1998; Adelberger & Steidel 2000). So far, there are ~1000 spectroscopically confirmed LBGs at $z \sim 3$ and ~70 at $z \sim 4$. The LBG population is a substantial component of the high-redshift "zoo": their comoving number density at $z = 3$ is $n(z = 3) \sim 3 \times 10^{-2}\ h_{65}^3$ Mpc$^{-3}$ (Steidel et al. 1999), comparable to the density of local galaxies (Marzke, Huchra, & Geller 1994). By selection, i.e., because of the need of presenting a relatively blue continuum longward of Ly$\alpha$, this high-redshift population tends to be biased against systems with predominantly old populations, or systems with large amounts of dust extinction. Indeed, most LBGs show evidence for ongoing or recent star formation activity (Steidel et al. 1996b; Pettini et al. 2000b, 2001; Papovich et al. 2001). From a purely phenomenological point of view, LBGs resemble local UV-selected starburst galaxies (§ 4). The obscuration-corrected SFRs per unit galactic area are ~0.2–25 $M_\odot$ yr$^{-1}$ kpc$^{-2}$, for a 0.1–100 $M_\odot$ Salpeter IMF (Steidel et al. 1996b, 1999; Papovich et al. 2001; Shapley et al. 2001), corresponding to ~0.5%–50% the maximum SFR per unit galactic area measured in the local universe (Lehnert & Heckman 1996; Meurer et al. 1997); this is similar to the observed range in nearby UV-selected starbursts. Rest-frame UV spectra show a wealth of absorption features, and often P Cygni profiles in the C IV (1550 Å) line (Steidel et al. 1996b), which indicates the predominance of young, massive stars. Nebular emission lines observed in the brightest LBGs (Pettini et al. 1998, 2001; Teplitz et al. 2000a) have intensities comparable to those of local starbursts (Meurer et al. 1999). The observed blueshifts in the UV interstellar absorption lines relative to the systemic redshifts of LBGs have been interpreted as bulk gas outflows with velocities $v \sim 200$–$500$ km s$^{-1}$ (Pettini et al. 1998, 2000b), again very similar to what is observed in nearby starbursts (Heckman et al. 2000). Finally, more luminous LBGs tend to be dustier (Fig. 9*b* and eq. [6]; Adelberger & Steidel 2000; Shapley et al. 2001). However, dissimilarities also exist between the two classes of galaxies. Star formation extends over a large fraction of the galactic body in LBGs, typically 5–30 $h_{65}^{-2}$ kpc$^2$ (Giavalisco et al. 1996b, 1998), while it is confined within the inner ~1 kpc$^2$ in local starbursts. As a result, LBGs are, on average, more rapidly star forming than either $z \sim 0$ or $z \sim 1$ galaxies (Fig. 9; Adelberger & Steidel 2000; Shapley et al. 2001). The bulk outflows in LBGs have velocities that are similar to those of local infrared-bright starbursts like NGC 6240 and a few times larger than those of H II galaxies (Heckman et al. 2000; Heckman & Leitherer 1997; Kunth et al. 1998; Gonzalez Delgado et al. 1998). The implications of such differences are not fully understood yet.

Establishing how much dust LBGs contain is the subject of ongoing debate. Metals are definitely present in these systems. Although the exact value of the metallicity has not been constrained, it most likely lies between 0.1 and 0.7 $Z_\odot$ (Pettini et al. 2000b, 2001; Leitherer et al. 2001). The UV spectral slopes of LBGs have median value $\beta_{26} \sim -1.5$ (Adelberger & Steidel 2000), significantly redder than the value $\beta_{26,0} \sim -2.2$ to $-2.7$ expected for a dust-free star-forming population (Appendix B). If interpreted in the same fashion as the UV slope of nearby UV-selected starbursts, LBGs suffer from dust obscuration at the level of $A_{0.16} \sim 1$–2 mag (Calzetti 1997b; Pettini et al. 1998; Dickinson 1998; Meurer et al. 1999; Steidel et al. 1999; Adelberger & Steidel 2000) and, possibly, more (Meurer et al. 1997; Sawicki & Yee 1998). However, a number of uncertainties and systematics limit the usefulness of UV data alone to derive obscuration estimates. First and foremost, the high-redshift galaxy for which reddening corrections are sought needs to possess active, ongoing star formation (i.e., not to be a poststarburst); this appears to be true for the LBGs as a population but may not be true on a individual basis (Papovich et al. 2001). Second, for most LBGs the UV slope is derived from photometry alone; the conversion of $G-\mathcal{R}$ colors[12] to $\beta_{26}$ suffers from uncertainties due to the presence of both intrinsic (stellar lines and Lyman break) and intervening (Ly$\alpha$ forest) absorption in the photometric filters (Adelberger & Steidel 2000; Pettini et al. 2001). Finally, because of the age-dust degeneracy, the intrinsic UV slope is a free parameter that can lead to greater than 1 mag difference in the derived obscuration value at 0.16 $\mu$m (cf. Sawicki & Yee 1998; Steidel et al. 1999).

Supplementing the UV with rest-frame optical data provides further leverage for determining the level of dust reddening in LBGs. The negligible correlation between $L_{H\beta}/L_{0.16}$ and the UV slope found for a sample of $\lesssim$15 luminous LBGs[13] supports the notion that LBGs are subject to modest reddening (Pettini et al. 1998, 2001; Teplitz et al. 2000a). Although this result is still dominated by the large scatter induced by both observational and model uncertainties (Pettini et al. 2001), it is consistent with what is observed in local UV-selected starbursts,[14] for which an obscuration of 1–2 mag at 0.16 $\mu$m corresponds to the modest reddening $A_{0.16} - A_{H\beta} \sim 0.15$–0.3 (§ 4.3).

Although the age-dust degeneracy cannot be easily broken even with the addition of long-wavelength data, extending the wavelength coverage of LBGs to the rest-frame optical has helped delimit the locus of allowed combinations in the age-dust plane (Papovich et al. 2001; Shapley et al. 2001). Using complementary data sets of LBGs in terms of luminosity range,

[12] The $G$ and $\mathcal{R}$ filters have central wavelengths 0.483 and 0.693 $\mu$m, respectively (Steidel & Hamilton 1992).

[13] Measures of dust reddening obtained by comparing the UV continuum with the [O III] (0.5007 $\mu$m) emission line (Teplitz et al. 2000a) are not discussed because of the strong dependence of the nebular line intensity, up to 1 order of magnitude variation, on the chemical and physical conditions of the gas (Jansen 2000; Charlot & Longhetti 2001).

[14] All considerations are based on the assumption that the dust in LBGs is distributed like that of local UV-selected starbursts. If, instead, the most appropriate dust geometry is a homogeneous spheroid or a face-on flattened disk, the average UV slope $\beta_{26} \sim -1.5$ corresponds to obscurations $A_{0.16} \sim 1.2$ mag and '$A_{H\beta} \sim 0.50$ mag and a differential obscuration between the two of ~0.7 mag; the latter is probably too large to be reconciled with observational data. Highly inclined disks are not considered in the obscuration budget because they would probably be too dim in the UV to be selected as LBGs.

TABLE 5
REDDENING AND OBSCURATION OF $z \sim 3$ GALAXIES

| Parameter | SMM J14011+0252 | MS 1512-cB58 | West MMD 11 | $L^*$ LBG |
|---|---|---|---|---|
| $z$ ..... | 2.565 | 2.729 | 2.982 | ~3 |
| $AB_{\mathcal{R}}$ (mag) ..... | 21.25[a] | 20.41[a] | 24.05 | ~24.5 |
| $G-\mathcal{R}$ ..... | 0.69[b] | 0.72 | 0.80 | 0.6 |
| $\beta_{26}$ ..... | −0.74[c] | −1.34[d] | −0.90[e] | −1.5[f] |
| $A_{0.16,\,star}$ ..... | 3.1 | 1.8 | 2.7 | 1.5 |
| $E(B-V)_{star}$ (UV) ..... | 0.31 | 0.18 | 0.27 | 0.15 |
| $E(B-V)_{star}$ (H$\beta$) ..... | ... | 0.1 ± 0.1[g] | 0 ± 0.2 | ... |
| $F_{pred}$ (IR) (ergs s$^{-1}$ cm$^{-2}$) ..... | 3.7E−13 | 2.3E−13 | 1.9E−14 | 3.2E−15 |
| $f_{obs}$ (450 $\mu$m) (mJy) ..... | 42 ± 7 | ... | 22 ± 23 | <10 |
| $f_{pred}$ (450 $\mu$m) (mJy)[h] ..... | 25.9, 71.6 | 19.5, 51.9 | 2.1, 5.3 | 0.36, 0.89 |
| $f_{obs}$ (850 $\mu$m) (mJy) ..... | 15 ± 2 | <4 | 5.5 ± 1.4 | <1 |
| $f_{pred}$ (850 $\mu$m) (mJy)[h] ..... | 4.0, 19.0 | 3.2, 14.6 | 0.4, 1.6 | 0.06, 0.27 |

NOTES.—Predicted and observed values for three highly reddened $z \sim 3$ galaxies, the two lensed galaxies SMM J14011+0252 and MS 1512-cB58, and West MMD 11, compared with the average $z \sim 3L^*$ LBG. SMM J14011+0252 is a SCUBA-discovered star-forming galaxy; Ivison et al. 2000; Adelberger & Steidel 2000. The quantity $z$ is the redshift; $AB_{\mathcal{R}}$ is the AB magnitude at the observer's frame 0.693 $\mu$m (see note for MS 1512-cB58); $G-\mathcal{R}$ is the $G-\mathcal{R}$ color (corresponding to a 0.12−0.17 color for a $z = 3$ galaxy) corrected for the opacity of the intervening Ly$\alpha$ forest (Pettini et al. 2001); $\beta_{26}$ is the UV slope (Appendix B); $A_{0.16,\,star}$ and $E(B-V)_{star}$ (UV) are the stellar obscuration at 0.16 $\mu$m and the color excess derived from the UV slope $\beta_{26}$ (§ 4.3), assuming an intrinsic UV slope $\beta_{26,\,0} = -2.2$, which is equivalent to a ~1 Gyr continuous star formation population; $E(B-V)_{star}$ (H$\beta$) is the stellar color excess derived from the $L_{0.16}/L_{H\beta}$ luminosity ratio; for a discussion of the uncertainties due to model assumptions, see Pettini et al. 2001; $F_{pred}$ (IR) is the predicted infrared flux of the dust emission, using the IR/UV vs. $\beta$ correlation (eq. [17]); $f_{obs}$ (450 $\mu$m) and $f_{obs}$ (850 $\mu$m) are the observed flux densities at 450 and 850 $\mu$m from Ivison et al. 2000 for SMM J14011+0252, Sawicki 2001 and van der Werf et al. 2001 for MS 1512-cB58, and Chapman et al. 2000 for West MMD 11; $f_{pred}$ (450 $\mu$m) and $f_{pred}$ (850 $\mu$m) are the predicted flux densities at 450 and 850 $\mu$m for a single-temperature modified blackbody (eq. [20]) and two choices of the dust temperature and emissivity; for reference, the predicted 1.2 mm flux densities are 1.0 mJy ($T = 50$ K and $\epsilon = 2$) and 5.7 mJy ($T = 40$ K and $\epsilon = 1.5$) for MS 1512-cB58, to be compared with the observed value 1.06 ± 0.35 mJy; Baker et al. 2001.

[a] The AB magnitudes of SMM J14011 and MS 1512-cB58 are not corrected for the lens magnification factor. $AB_{\mathcal{R}}$ of MS 1512-cB58 is at the observer's wavelength 0.654 $\mu$m (Ellingson et al. 1996) and has intrinsic value $AB_{\mathcal{R}} \simeq 24.5$.

[b] The $G-\mathcal{R}$ color of SMM J14011+0252 has not been corrected for the opacity of the intervening Ly$\alpha$ forest; Adelberger & Steidel 2000.

[c] As derived by Adelberger & Steidel 2000.

[d] Derived from $\beta_{18} = -1.10$ using eq. (B2); $\beta_{18}$ was directly measured from the UV spectrum kindly provided by M. Pettini & C. Steidel 2000, private communication.

[e] Derived by convolving a 1 Gyr constant star formation synthetic SED reddened by Ly$\alpha$ forest and dust absorption with the $G$ and $\mathcal{R}$ bandpasses (moved to the galaxy's rest frame) until the observed color is reproduced and then fitting a power law through the UV windows of Calzetti et al. 1994.

[f] From Fig. 12 of Adelberger & Steidel 2000.

[g] The measured H$\alpha$/H$\beta$ emission line ratio of MS 1512-cB58 (Teplitz et al. 2000b) yields $E(B-V)_{star} = 0.03^{+0.10}_{-0.03}$.

[h] Derived for dust temperature $T = 50$ K and emissivity $\epsilon = 2$ (first value) and for $T = 40$ K and $\epsilon = 1.5$ (second value).

Papovich et al. (2001) and Shapley et al. (2001) have established that there is an inverse correlation between the age of the stellar populations in a galaxy and the amount of dust reddening it suffers: the older the galaxy, the lower its reddening. In agreement with previous results (Sawicki & Yee 1998), LBGs whose SEDs are compatible with young ($\lesssim 10^8$ yr) stellar populations are also dusty. Whatever dust is present, it is not preferentially obscuring selected regions of the galaxies, because of the similarity between the rest-frame UV and optical morphologies (Bunker 1999; Dickinson 2000). A typical LBG obscuration of $A_{0.16} \sim 1$–2 mag, with a median of ~1.5 mag and a high-end tail around 4.5–5 mag (Steidel et al. 1999; Papovich et al. 2001; Shapley et al. 2001), is currently the most broadly accepted value.

Despite all the uncertainties in estimating dust obscuration in LBGs, the inferred opacity values are modest enough that the high-redshift galaxies are expected to be faint submillimeter emitters, with 850 $\mu$m flux densities at or below the SCUBA detection limit of ~1–2 mJy (Adelberger & Steidel 2000; Peacock et al. 2000). Out of $\gtrsim 10$ LBGs targeted with SCUBA, only a couple have been detected (Chapman et al. 2000; van der Werf et al. 2001). Table 5 gives three examples (two LBGs and one

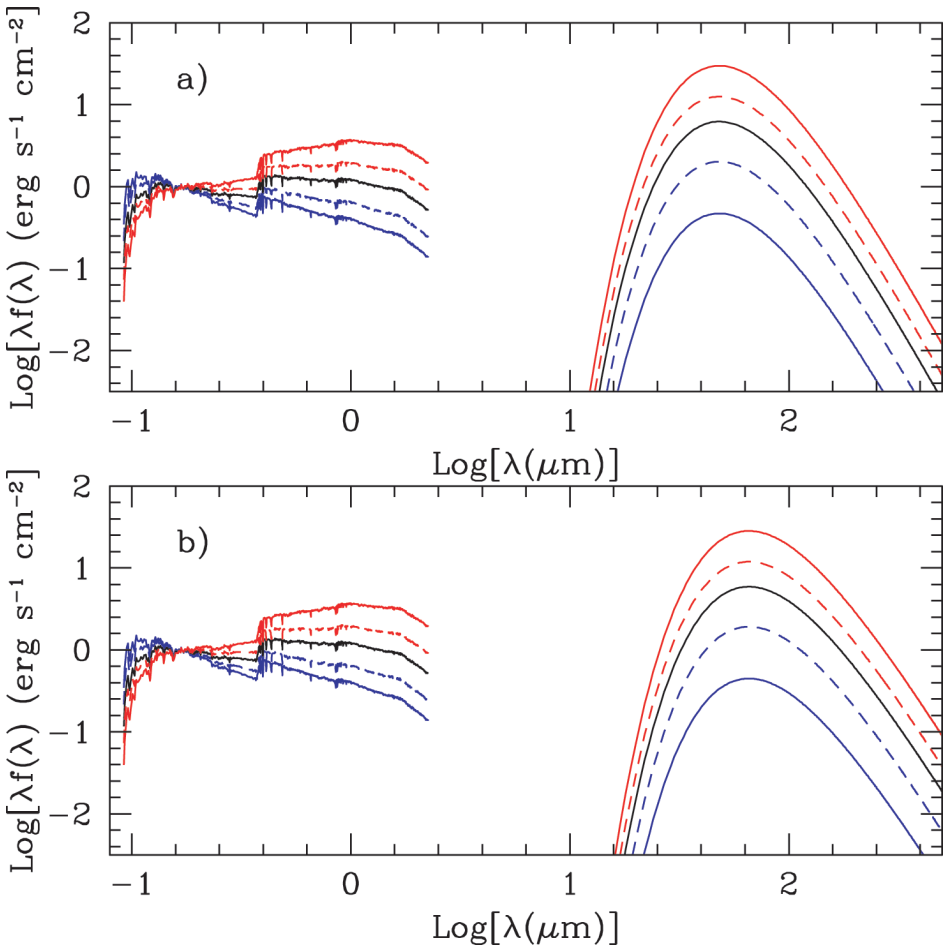


FIG. 11.—UV-to-IR SED of a 1 Gyr constant star formation population, attenuated by the starburst obscuration curve (eq. [8]), is shown for increasing amounts of dust: $E(B-V)_{\rm gas} = 0.05$ (*blue solid line*), 0.20 (*blue dashed line*), 0.40 (*black line*), 0.55 (*red dashed line*), and 0.75 (*red solid line*). All SEDs are arbitrarily normalized to the flux density at 0.17 $\mu$m. The infrared SED is schematically represented by a single-temperature dust component with (*a*) $T = 50$ K and $\epsilon = 2$ and (*b*) $T = 40$ K and $\epsilon = 1.5$ to highlight differences in the long-wavelength regime.

SCUBA source) of highly reddened $z \sim 3$ galaxies, plus the average values of a typical LBG. The three examples are meant to show some of the most attenuated cases that are also detected at rest-frame UV. Table 5 demonstrates that the exact prediction of the flux density at rest frame $\approx$200 $\mu$m is heavily dependent on the adopted dust temperature(s) and emissivity, because long infrared wavelengths probe only the Rayleigh-Jeans tail of the thermal dust emission in galaxies (Fig. 11). Local galaxies, although extensively used as analogs of high-redshift galaxies, are of limited help in this respect, given the wide range of properties they show. If the flux density of a local galaxy beyond 60–70 $\mu$m is parameterized by a modified blackbody with dust emissivity $\propto \nu^{\epsilon}$,

$$f_{\rm IR} \propto \nu^{\epsilon} B(\nu, T), \tag{20}$$

ULIRGs and bright IR-selected galaxies tend to be well described either by a single-temperature component with $T \sim 40$ K and $\epsilon \sim 1.5$ (Lisenfeld et al. 2000; Blain et al. 1999a) or by a warm/cool two-temperature model with $\epsilon = 2$ (Dunne & Eales 2001); however, there is tentative indication that UV-bright, metal-poor starbursts have hotter dust SEDs, with $T \sim 50$ K and $\epsilon = 2$ (Tol 1924−416; Calzetti et al. 2000). Equation (20), which is used for purely illustrative purposes, is clearly an oversimplification of the dust SED in local galaxies, which is characterized by a range of temperatures and, at rest frame $\lambda \lesssim 40$–70 $\mu$m, by the emission from nonequilibrium dust grains (Sellgren 1984; Draine & Anderson 1985; Li & Draine 2001; see also § 2.1). In starbursts, the latter component represents ~25% of the total infrared emission. Given the uncertainty of the submillimeter measures and the current poor understanding of the detailed physics of dust emission in both local and high-redshift galaxies, the opacity of LBGs is still relatively unconstrained by submillimeter observations (Ouchi et al. 1999; Sawicki 2001; and Table 5). Further complications (and uncertainties) arise when the comparison between predictions and observations of infrared flux densities is made for individual objects (van der Werf et al. 2001; Sawicki

2001; Baker et al. 2001); reddening/obscuration corrections at UV-optical wavelengths are accurate only in a statistical sense and, generally, do not apply on a one-to-one basis to individual objects. For instance, if the dust geometry in a particular system is such that the scattering out of the line of sight is larger than that into the line of sight, the infrared energy, which is due to the absorption part of the extinction only, will be overestimated when derived from UV data.

### 5.4. Summary

There is so far limited overlap between infrared and optical surveys at intermediate and high redshift (e.g., Aussel et al. 1999; Flores et al. 1999b; Barger et al. 1999b; Rigopoulou et al. 2000; Chapman et al. 2000). Consequently, multiwavelength coverage from the rest-frame ~UV-optical to the infrared is available only for a small number of galaxies. To make matters worse, observational limitations lead to vastly different selection criteria for the optical surveys in different redshift bins (Glazebrook et al. 1999; Yan et al. 1999; Moorwood et al. 2000; Steidel et al. 1996b). Thus, conclusions about the dust opacity of galaxy populations as a whole and as a function of redshift are at the moment based on "reasonable" extrapolations of existing data rather than hard evidence.

Available infrared and optical data support the scenario that $z \approx 1$ star-forming galaxies cover at least the same range of dust opacities as local galaxies. The luminosity (or combined luminosity and density) evolution implied by the *ISO* counts suggests that luminous infrared galaxies, with $L_{\rm bol} \sim L_{\rm IR} \gtrsim 10^{11}\ h_{65}^{-2}\ L_{\odot}$, were common at $z \lesssim 1$. The range of dust attenuation values at UV wavelengths inferred for optically selected $z \sim 1$ galaxies is comparable to those of local disk galaxies and UV-selected starbursts (Fig. 9), although the distant galaxies tend to be more luminous (more active) on average. Larger samples with more extended wavelength coverage are needed before a more complete picture can be drawn in this redshift range.

The ISM of $z \sim 3$ galaxies has been observed to be metal polluted to at least $\approx 0.1\ Z_{\odot}$, implying that nonnegligible amounts of dust must be present in the galaxy population at large by $z = 3$ and, in many cases, earlier (Shapley et al. 2001). The observed properties of the $z > 1$ SCUBA sources and of the LBGs suggest that both objects are the high-redshift analogs of local actively star-forming galaxies, where dust content and level of activity determines a continuum of characteristics. The SCUBA sources are at the high end of such a continuum, with powerful activity, both thermal and nonthermal, and large dust contents that make them similar to local ULIRGs; more than 95% of their bolometric light is absorbed by dust. LBGs appear to span a larger range of the continuum of dust content and activity level, although they tend to have, on average, lower values than the SCUBA sources. Typical UV attenuations are $A_{0.16} \sim 1$–2 mag, corresponding to 35%–95% of the bolometric light being absorbed by dust.

Assuming that the local infrared luminosity function can be applied to high-redshift sources as well, the comoving number density of $z \approx 3$ SCUBA galaxies with 850 $\mu$m flux densities brighter than 2 and 0.5 mJy (corresponding to $\sim 2 \times 10^{12}$ and $\sim 5 \times 10^{11}\ L_{\odot}$ for an Arp 220–like SED) would be $\approx 4 \times 10^{-4}\ h_{65}^{3}$ Mpc$^{-3}$ and $\approx 10^{-2}\ h_{65}^{3}$ Mpc$^{-3}$, respectively. High-redshift infrared galaxies as bright as Arp 220 are almost 100 times less numerous than LBGs; for comparison, in the local universe ULIRGs are more than 4 orders of magnitude less numerous than optically selected galaxies. At lower 850 $\mu$m luminosities, $z \sim 3$ SCUBA sources are about as numerous as LBGs at the same redshift, but there could be large overlap between the two samples at the millijansky level. LBGs are, in fact, predicted to occupy the faint end of the SCUBA 850 $\mu$m source counts, with flux densities of a few millijanskys or less (Adelberger & Steidel 2000). Thus, although SCUBA sources down to 0.5 mJy at all redshifts already account for more than 90% of the CIB, a nonnegligible fraction of this, at least 25%, could be due to LBGs (Peacock et al. 2000; Adelberger & Steidel 2000; van der Werf et al. 2001).

## 6. INTRACLUSTER AND INTERGALACTIC DUST

Intracluster and intergalactic dust are briefly discussed in view of their potential importance in the interpretation of the intermediate- and high-redshift universe. The amount, nature, and sources of the dust in the intracluster and intergalactic media are still a controversial matter, despite the large number of independent researches tackling the issue.

The metallicity of the present-day intracluster medium (ICM) is fairly high, about $\frac{1}{3}$–$\frac{1}{2}$ solar, implying that a nonnegligible fraction of the gas in the ICM has been ejected from the cluster's galaxies (Mushotzky et al. 1996; Mushotzky & Loewenstein 1997; Voit & Donahue 1997). The high metallicity is not automatically accompanied, however, by a high dust content of the ICM. The ICM hot gas effectively destroys dust through sputtering. The typical timescale for sputtering in a $\gtrsim 10^7$ K hot ambient gas is $t_{\rm sput} \approx 10^6 a/n$, where $t_{\rm sput}$ is measured in years, $a$ is the size of the dust grain in microns, and $n$ is the density of the ICM in cm$^{-3}$ (Draine & Salpeter 1979; Dwek, Rephaeli, & Mather 1990). In the high-density cores of clusters ($n \gtrsim 10^{-3}$ cm$^{-3}$), a 0.1 $\mu$m dust grain survives a few times $10^8$ yr, with smaller grains being destroyed on shorter timescales than the large grains (Dwek et al. 1990). Small grains can survive only outside the cores of clusters, i.e., beyond the central $\approx 1$ Mpc. Dust needs to be constantly replenished in the ICM, and the likely sources are enriched winds from the cluster's galaxies, intracluster stars, and, in dynamically young clusters, winds from infalling spiral galaxies (Dwek et al. 1990; Popescu et al. 2000). The timescales for the dust injection in the ICM are of order $10^9$ yr or longer, implying that the grain size distribution, and therefore the shape of the extinction curve, depends mainly on the sputtering efficiency at the selected cluster location (Dwek et al. 1990).

Various direct and indirect methods have been employed to

detect dust in the ICM. Deficits in background counts of galaxies, quasars, and clusters behind galaxy clusters of various richness have been interpreted as extinction in the range $A_B^o \sim 0.2$–$0.5$, with patches that can exceed $A_B^o \approx 1$ mag (Zwicky 1957; Karachentsev & Lipovetskii 1969; Bogart & Wagoner 1973; Boyle, Fong, & Shanks 1988; Szalay, Hollósi, & Tóth 1989; Romani & Maoz 1992). Conversely, reddening measurements of cluster members (Ferguson 1993) or background galaxies (Maoz 1995) give upper limits of $A_B^o \sim 0.2$ mag. The two methods thus give contradictory results, and neither is completely bias free: deficits in background counts can be due not only to dust but also to confusion; low reddening values can be attributed to a gray extinction curve, grayer than an MW-like curve, because of the selective destruction of small grains in the ICM. Tentative infrared detections of ICM dust emission, using *IRAS* and *ISO* data (Wise et al. 1993; Stickel et al. 1998), either are at low significance level or have been argued to be due to emission from cluster members (Quillen et al. 1999).

The presence of dust is well established in the centers of cooling flow clusters (see discussion in § 3.4), but the issue of its origin is still controversial. In particular, it is not clear whether this is an extended component, such as condensates from the cooled cluster gas or a by-product of star formation triggered by the cooling flow (Hu et al. 1983; Hu 1992; Fabian, Johnstone, & Daines 1994; Allen 1995; Hansen, Jörgensen, & Nörgaard-Nielsen 1995; Crawford et al. 1999; Edge 2001), or is directly associated with the central galaxy, possibly from a merging event that the galaxy underwent (Sparks et al. 1989; Sparks, Ford, & Kinney 1993; Donahue et al. 2000). The MW-like form of the extinction curve in the central galaxies has been extensively used as an argument to support the galactic origin of the dust in cooling flow clusters; as remarked above, ICM-processed dust would tend to be depleted in small grains and therefore produce a gray extinction (Sparks et al. 1989, 1993; Donahue et al. 2000). However, if soft X-ray absorption is present in the centers of the clusters, dust absorption in the cooling flow would appear to be the direct physical explanation (Voit & Donahue 1995). The tentative detection of the neutral oxygen edge, and thus of dust, in the Perseus cluster (Arnaud & Mushotzky 1998) and the widespread presence of CO emission in low-radio–emitting cooling flow clusters (Edge 2001) are countered by *XMM* data that do not support the presence of large amounts of cool gas in the center of some of the clusters and, therefore, do not require a large amount of dust to explain the soft X-ray spectral shape (Tamura et al. 2001; Kaastra et al. 2001; Peterson et al. 2001).

At present, the presence and nature of dust in the intergalactic medium (IGM) is even more uncertain than that in the ICM, although it is widely accepted that the IGM is metal enriched. Hydrodynamical cold dark matter simulations identify the Ly$\alpha$ forest as the IGM, i.e., modest baryon density fluctuations in a ionizing background (Cen et al. 1994; Petitjean, Muecket, & Kates 1995; Zhang, Anninos, & Norman 1995; Hernquist et al. 1996; Theuns et al. 1998). The Ly$\alpha$ forest accounts for a significant fraction, greater than 50%, of the baryons at $z \approx 3$ (Rauch et al. 1997); its metallicity at $z \sim 2.5$–$3$ is $\sim$0.2%–1% $Z_\odot$ down to column densities $N(\mathrm{H\ I}) \sim 10^{14.5}$ cm$^{-2}$ (Tytler et al. 1995; Songaila & Cowie 1996; Ellison et al. 1999), while metallicity values at lower column densities remain uncertain (Ellison et al. 2000). These values could be lower limits to the IGM metallicity if there is a "missing metals" problem as pointed out by Renzini (1999) and Pettini (1999) on the basis of the metals produced by star formation by $z \sim 2.5$. The metallicity of the Ly$\alpha$ forest increases for decreasing redshift, being $\sim$10 times more metal rich at $z \sim 0.5$ than at $z \sim 2.5$–$3$ (Barlow & Tytler 1998). In the local universe, the Ly$\alpha$ forest accounts for only $\approx$20% of the baryons (Penton, Shull, & Stocke 2000) and matter associated with galaxies and clusters for another $\approx$25%–30% (Fukugita, Hogan, & Peebles 1998; Cen & Ostriker 1999); thus, $\sim$50% of the baryons at $z = 0$, and possibly of the metals, are contained in a yet undetected phase of the IGM, proposed to be hot gas (Cen & Ostriker 1999). Various mechanisms have been considered for the metal, and possibly dust, pollution of the IGM; they include supernova ejecta from galaxies and/or subgalactic structures, dynamical encounters between galaxies, ram-pressure stripping, and Population III stars (Ostriker & Gnedin 1996; Nath & Trentham 1997; Gnedin 1998; Ferrara, Pettini, & Shchekinov 2000; Cen & Bryan 2001; Madau, Ferrara, & Rees 2001; Aguirre et al. 2001). The different mechanisms are nonexclusive, although each one could be dominant relative to the other at specific cosmological epochs.

Early attempts to detect diffuse dust in the IGM investigated the evolution of the mean quasar spectral index with redshift (Wright 1981; Cheng, Gaskell, & Koratkar 1991), with the basic result that the presence of IGM dust is negligible for MW-like extinction, up to at least $z \approx 2$ (Cheng et al. 1991). MW-like IGM dust should also leave an imprint on the cosmic microwave background because it would reemit in the submillimeter per millimeter regime the absorbed background radiation (Rowan-Robinson, Negroponte, & Silk 1979; Wright 1981; Bond, Carr, & Hogan 1991). The tight *COBE* upper limit to deviations from blackbody emission (Fixsen et al. 1996) limits the IGM dust to $A_V \lesssim 0.3$ mag to $z = 5$, with negligible value to $z = 3$ (Loeb & Haiman 1997; Ferrara et al. 1999b). However, if sputtering is efficient in the hot IGM, dust has a grayer extinction than MW-like (for a challenge to the sputtering argument, see Simonsen & Hannestad 1999; Aguirre 1999). Gray IGM dust can be present in larger quantities than MW-like dust without violating the *COBE* limits, but its emission would represent $\gtrsim$75% of the CIB at 850 $\mu$m (Aguirre & Haiman 2000). Source counts with SCUBA account already for more than 90% of the CIB (§ 5.2), which challenges the case for large amounts of gray dust. So far, the strongest limits have come from observations of cosmological supernovae. For gray dust with minimum grain size $\sim$0.1 $\mu$m, the model of Aguirre (1999) gives $A_B - A_V \lesssim 0.01$ and $A_B - A_I \sim 0.2$ for $A_V \sim 0.2$–$0.3$ to $z = 0.5$; at $z = 2$, $A_V \sim 0.6$–$0.7$ mag. Using observations of Type Ia supernovae at $z \sim 0.5$ and $z \sim 1.7$, Riess et al. (2000, 2001) have placed a limit of $A_V \sim 0.1$–

0.15 to the amount of diffuse, gray IGM dust to $z = 0.5$. In summary, although the actual numbers are still not settled, IGM dust is likely to produce small attenuations at most redshifts.

## 7. CONCLUSIONS AND FUTURE DEVELOPMENTS

Current observational data indicate that the population of local galaxies is characterized by modest values of the dust opacity. Typically, 50% or less of the total stellar energy is absorbed by dust. The same evidence points out that the definition of "modest opacity" is wavelength dependent; for example, in the UV, at 0.15 $\mu$m, a nonactive galaxy can lose up to 80% of its energy to dust. Luminous, intermediate- to late-type spirals are dustier than both elliptical galaxies, by ~1.0–1.4 mag in the UV, and irregulars, by 0.5–0.8 mag. Luminous galaxies are on average more metal rich and dust rich than their faint counterparts. Dust opacity also increases with thermal and nonthermal activity, with the high end of the distribution given by the ULIRGs.

Although the wealth of data and wavelength coverage for local galaxies has started to uncover the dust opacity of these systems, we are still missing a few crucial pieces of the puzzle. The largest among these is the one-to-one relation between absorbed stellar SEDs and dust emission SEDs. At first order, hotter stars are expected to heat the dust to higher temperatures than cooler stars (Helou 1986), but we do not have yet the direct link between individual dust emission and heating components; we do not know the dependence of the dust SED on parameters such as metallicity, radiation field, gas density, galactic environment, etc.; and questions still surround the relation between radiation intensity and PAH emission, despite the progress made with *ISO* (Cesarsky et al. 1996; Genzel & Cesarsky 2000; Dale et al. 2001; Hunter et al. 2001). The main reason for these limitations to our comprehension of the dust absorption-emission relationship is the large mismatch in angular resolution between UV–to–near-IR observations and current mid/far-infrared data. While observations probing the direct stellar light can easily reach subarcsecond resolution, existing data on dust emission are at the arcminute-resolution level, especially at wavelengths above ~40 $\mu$m, where the bulk of the energy from dust emerges. Upcoming infrared missions such as the *Space Infrared Telescope Facility* (*SIRTF*), the Stratospheric Observatory for Infrared Astronomy (SOFIA), and *FIRST* (now the *Herschel Space Observatory*) promise to bridge this gap. They will also push the wavelength coverage all the way to 600–700 $\mu$m, thus probing the cold dust emission in local galaxies, which is the repository of most of the dust mass.

UV- and optical-selected, intermediate- and high-redshift galaxy surveys carry the inherent limitation that physical parameters directly derived from the observations are affected by dust in a way that is not easily quantifiable. This is further complicated by the fact that instrumental sensitivity limits favor detection of the luminous representatives of any galaxy class, that may tend to have relatively high dust content. Estimates of the SFRs in intermediate- and high-redshift galaxies using Balmer lines (Glazebrook et al. 1999; Yan et al. 1999; Moorwood et al. 2000) and infrared emission (Flores et al. 1999b; Blain et al. 1999d; Barger et al. 2000) are generally a few times higher than the analogous estimates using the rest-frame UV emission (Lilly et al. 1996; Madau et al. 1996; Steidel et al. 1999). As discussed in § 5, the presence of dust in galaxies at cosmological distances is reasonably established, but the quantification of its effects as a function of redshift is still an ongoing process. Linked to this is the puzzle of the nature of the UV-selected and IR-selected sources, and of their relationship: whether they represent overlapping populations or the two ends of a continuum of properties possibly parameterized by activity and dust content is still an open question.

The absence of full characterization of the dust emission and absorption in distant galaxies is mostly due to the scant overlap between optically selected and infrared-selected surveys. This is due to sensitivity limitations at both ends of the spectrum, to angular resolution limitations at long wavelengths, to the small number of objects in some of the samples, and to the sparse wavelength coverage of the dust emission SED by current submillimeter/radio instrumentation. *SIRTF* and *FIRST* initially and then the Atacama Large Millimeter Array and the *Next Generation Space Telescope* will be able to fill the gaps. In particular, the last two instruments, with their subarcsecond resolution and high sensitivities, should mark a breakthrough in our understanding of the high-redshift universe and of its stellar, gas, and dust content up to $z \sim 20$.

The author is grateful to Mark Dickinson, Megan Donahue, Paul Goudfrooij, Claus Leitherer, and Mark Voit for insightful comments on specific sections of this review. She thanks Kurt Adelberger for data on the Lyman break and Balmer break galaxies and Max Pettini and Chuck Steidel for the UV spectrum of MS 1512-cB58. She is also indebted with Veronique Buat, Bruce Draine, Tim Heckman, Nino Panagia, Marcia Rieke, and Max Pettini for a critical reading of the manuscript, which has greatly improved its content and presentation.

## APPENDIX A

## ADOPTED NOMENCLATURE FOR EXTINCTION AND OBSCURATION

The dimming effects of light are generally termed "extinction" only in the simple geometrical case of a point

source behind a dust screen (§ 2.1), where the attenuation suffered by the source can be directly related to the optical depth of the dust screen. In this review, the extinction at wavelength λ is indicated as

$$A_\lambda^o = 1.086\tau_\lambda \quad \text{(A1)}$$

(eq. [2]). The dimming of background galaxies due to the dust in a foreground galaxy can generally be considered extinction because the foreground galaxy can be modeled in a first approximation as a homogeneous screen in front of point sources (§ 3.1).

For more general distributions of dust and emitters, the dimming and reddening of the light is no longer directly related to the extinction or the optical depth of the dust layer and is called indiscriminately "effective extinction," "obscuration," or "attenuation." The effective extinction $A_\lambda$ is defined as

$$A_\lambda = m_{\lambda,a} - m_{\lambda,o}, \quad \text{(A2)}$$

where $m_{\lambda,o}$ is the magnitude of the dust-free source and $m_{\lambda,a}$ is the measured (attenuated) magnitude; $A_\lambda$ measures the magnitudes of attenuation suffered by an extended source at the specified wavelength/band. By definition, $A_\lambda \equiv A_\lambda^o$ for a foreground, homogeneous, nonscattering dust screen.

For dust/emitter distributions that do not have spherical symmetry, such as spiral galaxies, the face-on effective extinction is termed $A_{\lambda,f}$, while $A_\lambda$ indicates the effective extinction averaged over all inclinations.

## APPENDIX B

## THE DEFINITION OF THE UV SPECTRAL SLOPE $\beta$

Throughout this review, two different definitions of the UV spectral slope, $\beta$ and $\beta_{26}$, have been used. In this context, the spectral slope is derived from the fit $f(\lambda) \propto \lambda^\beta$ within a specified wavelength range, with $f(\lambda)$ the flux density of the source. The various definitions reflect historical reasons driven mostly by observational constraints.

The default $\beta$ adopted in this review (§ 2.2) is measured between 0.125 and 0.30 $\mu$m, using a set of wavelength windows that avoid the strong stellar and interstellar absorption features. An example of such windows is given in Calzetti et al. (1994), although the ones used to derive $\beta$ here are better tuned for use with model spectra rather than with observed spectra and extend all the way to 0.3 $\mu$m. This definition of $\beta$ has been adopted to ensure an appropriate comparison between different extinction curves and dust models, as in Figures 2 and 3, because the fitting windows are selected to avoid the strong and wide dust feature at 0.2175 $\mu$m.

The UV slope $\beta_{26}$ used in § 4 is a fit through the 10 windows of Calzetti et al. (1994) and corresponds to deriving the slope in the wavelength range 0.125–0.26 $\mu$m, using spectral regions mostly devoid of strong absorption lines. This definition of the UV slope is observation driven, as it was used to obtain measurements from *IUE* spectra of a local UV-selected starburst sample. The wavelength range is bluer than that of $\beta$ above and was chosen by Calzetti et al. (1994) to avoid including in the fits the older stellar populations underlying the starbursts. These older populations can contribute to the spectra starting around 0.27–0.28 $\mu$m, when the fluxes of F stars become nonnegligible. For reference, a list of $\beta_{26}$ values for dust-free stellar populations, both for instantaneous burst and for constant star formation, is given in Table 6.

A convenient definition of the UV slope for studies of high-redshift galaxies is $\beta_{18}$, measured roughly between ~0.12 and ~0.18 $\mu$m. At $z \sim 3$, the optical window gives information shortward of ~0.2 $\mu$m, thus forcing the UV slope fitting to a much shorter range than possible with local galaxies. The details of the actual wavelength range vary with redshift and with the observing technique (whether spectroscopy or imaging, and depending on the filters used).

The relation between the three quantities, as given by models of stellar populations reddened by the starburst obscuration curve of § 4, is

$$\beta_{26} = (1.020 \pm 0.018)\beta - (0.018 \pm 0.065), \quad \text{(B1)}$$

$$\beta_{18} = (1.156 \pm 0.013)\beta_{26} + (0.454 \pm 0.075). \quad \text{(B2)}$$

The uncertainty following each coefficient refers to the maximum variance observed by varying a number of parameters in the models and fits: (1) stellar populations from both Leitherer et al. (1999) and G. Bruzual & S. Charlot (2001, in preparation) models; (2) stellar populations with constant star formation in the range 5–1000 Myr and instantaneous bursts in the age range 5–12 Myr; (3) both 0.2 and 1 $Z_\odot$ metallicities; and (4) fitting windows that progressively include or exclude weak absorption lines in the spectra. The latter turns out to be the main driver of the variance, while changes in the characteristics of the stellar populations have only a small impact. The relations between the three slopes would, however, change from equations (B1) and (B2) if more extreme cases of stellar population mix, such as the addition of an old (age > 1 Gyr) component, were considered; in this case, $\beta$ and $\beta_{26}$ would be strongly affected, because of the long-wavelength baseline.

TABLE 6
ULTRAVIOLET SPECTRAL SLOPES

| Age (Myr) | $\beta_{26,0}^{\rm inst}$ | $\beta_{26,0}^{\rm const}$ |
|---|---|---|
| 2 ..... | −2.70 | −2.68 |
| 5 ..... | −2.50 | −2.61 |
| 10 ..... | −2.45 | −2.57 |
| 15 ..... | −2.30 | −2.55 |
| 30 ..... | −2.09 | −2.50 |
| 50 ..... | −1.93 | −2.45 |
| 100 ..... | −1.61 | −2.38 |
| 300 ..... | −0.20 | −2.28 |
| 500 ..... | ... | −2.26 |
| 900 ..... | ... | −2.23 |

NOTES.—The UV spectral slope $\beta_{26}$, as defined in Appendix B, is given for both instantaneous burst (second column) and constant star formation (third column) populations at selected ages, for the dust-free case. The model populations are from Leitherer et al. 1999, for solar metallicity.

noise in the *IUE* data may have prevented the detection of such

Of interest for high-redshift studies is the consideration that while $\beta_{26}$ and $\beta$ follow each other closely, $\beta_{18}$ is always redder (more positive) than the other two, and the discrepancy increases for increasing value of the slopes. The reason for this counterintuitive behavior is the presence of the well-known "iron curtain" at long UV wavelengths: this is a wide dip in the 0.23–0.28 $\mu$m range of the UV spectra due to the presence of a large number of closely spaced Fe absorption lines (Leitherer et al. 1999). The UV slopes fitted with the longer wavelength baseline have windows in this continuum-depressed region, hence their more negative values. Increasing dust obscuration affects the short-wavelength slope more than the long-wavelength ones, hence the trend for $\beta_{18}$ to become progressively redder than $\beta_{26}$ as their values increase (i.e., as the UV spectra become more dust reddened).

Meurer et al. (1999) derive an empirical relation between $\beta_{26}$ and a short-wavelength UV slope $\beta_{\rm SW}$ (close, but not identical, to $\beta_{18}$) from *IUE* spectra of the UV-selected starbursts. Their findings, that $\beta_{26} = \beta_{\rm SW} - 0.16$, are consistent with the long-wavelength slope being bluer than the short-wavelength one. However, they do not measure an increasingly redder $\beta_{\rm SW}$ for increasing values of both slopes. A possible reason is that an effect. In this review, it is assumed that equations (B1) and (B2) are valid for UV-selected starbursts.

## REFERENCES


Adelberger, K. L., & Steidel, C. C. 2000, ApJ, 544, 218
Adelberger, K. L., Steidel, C. C., Giavalisco, M., Dickinson, M. E., Pettini, M., & Kellogg, M. 1998, ApJ, 505, 18
Aguirre, A. 1999, ApJ, 525, 583
Aguirre, A., & Haiman, Z. 2000, ApJ, 532, 28
Aguirre, A., Hernquist, L., Schaye, J., Katz, N., Weinberg, D. H., & Gardner, J. 2001, ApJ, 561, 521
Allen, S. W. 1995, MNRAS, 276, 947
Aloisi, A., Tosi, M., & Greggio, L. 1999, AJ, 118, 302
Alonso-Herrero, A., Engelbracht, C. W., Rieke, M. J., Rieke, G. H., & Quillen, A. C. 2001, ApJ, 546, 952
Altieri, B., et al. 1999, A&A, 343, L65
Alton, P. B., et al. 1998, A&A, 335, 807
Arimoto, N., Sofue, Y., & Tsujimoto, T. 1996, PASJ, 48, 275
Arnaud, K. A., & Mushotzky, R. F. 1998, ApJ, 501, 119
Aussel, H., Cesarsky, C. J., Elbaz, D., & Starck, J. L. 1999, A&A, 342, 313
Baker, A. J., Lutz, D., Genzel, R., Tacconi, L. J., & Lehnert, M. D. 2001, A&A, 372, L27
Barger, A. J., Cowie, L. L., Mushotzky, R. F., & Richards, E. A. 2001, AJ, 121, 662
Barger, A. J., Cowie, L. L., & Richards, E. A. 2000, AJ, 119, 2092
Barger, A. J., Cowie, L. L., & Sanders, D. B. 1999a, ApJ, 518, L5
Barger, A. J., Cowie, L. L., Sanders, D. B., Fulton, E., Taniguchi, Y., Sato, Y., Kawara, K., & Okuda, H. 1998, Nature, 394, 248
Barger, A. J., Cowie, L. L., Smail, I., Ivison, R. J., Blain, A. W., & Kneib, J.-P. 1999b, AJ, 117, 2656
Barlow, T. A., & Tytler, D. 1998, AJ, 115, 1725
Baugh, C. M., Cole, S., Frenk, C. S., & Lacey, C. G. 1998, ApJ, 498, 504
Beck, S. C., Turner, J. L., Ho, P. T., Lacy, J. H., & Kelly, D. M. 1996, ApJ, 457, 610
Beckman, J. E., Peletier, R. F., Knapen, J. H., Corradi, R. L. M., & Gentet, L. J. 1996, ApJ, 467, 175
Bell, E. F., Gordon, K. D., Kennicutt, R. C., Jr., & Zaritsky, D. 2001, ApJ, in press
Bell, E. F., & Kennicutt, R. C., Jr. 2001, ApJ, 548, 681
Berlind, A. A., Quillen, A. C., Pogge, R. W., & Sellgren, K. 1997, AJ, 114, 107
Bianchi, L., Clayton, G. C., Bohlin, R. C., Hutchings, J. B., & Massey, P. 1996, ApJ, 471, 203
Bianchi, S., Ferrara, A., Davies, J. I., & Alton, P. B. 2000, MNRAS, 311, 601
Blain, A. W., Ivison, R. J., Kneib, J.-P., & Smail, I. 1999a, in ASP Conf. Ser. 193, The Hy-Redshift Universe, ed. A. J. Bunker & W. J. M. van Breugel (San Francisco: ASP), 246
Blain, A. W., Jameson, A., Smail, I., Longair, M. S., Kneib, J.-P., & Ivison, R. J. 1999b, MNRAS, 309, 715
Blain, A. W., Kneib, J.-P., Ivison, R. J., & Smail, I. 1999c, ApJ, 512, L87
Blain, A. W., Smail, I., Ivison, R. J., & Kneib, J.-P. 1999d, MNRAS, 302, 632
Block, D. L., & Greenberg, J. M. 1996, New Extragalactic Perspectives in the New South Africa (Dordrecht: Kluwer)
Block, D. L., Witt, A. N., Grosbol, P., Stockton, A., & Moneti, A. 1994, A&A, 288, 383
Bogart, R., & Wagoner, R. 1973, ApJ, 181, 609
Boissé, P., Le Brun, V., Bergeron, J., & Deharveng, J.-M. 1998, A&A, 333, 841
Bond, J. R., Carr, B. J., & Hogan, C. J. 1991, ApJ, 367, 420
Boselli, A., et al. 1998, A&A, 335, 53
Bosma, A., Byun, Y., Freeman, K. C., & Athanassoula, E. 1992, ApJ, 400, L21

Bouchet, P., Lequeux, J., Maurice, E., Prevot, L., & Prevot-Burnichon, M. L. 1985, A&A, 149, 330
Boulanger, F., Beichman, C., Désert, F. X., Helou, G., Pérault, M., & Ryter, C. 1988, ApJ, 332, 328
Boyle, B. J., Fong, R., & Shanks, T. 1988, MNRAS, 231, 897
Bregman, J. N., Snider, B. A., Grego, L., & Cox, C. V. 1998, ApJ, 499, 670
Brodie, J. P., & Huchra, J. P. 1991, ApJ, 379, 157
Bruzual, G. A., Magris, G. C., & Calvet, N. 1988, ApJ, 333, 673
Buat, V., & Burgarella, D. 1998, A&A, 334, 772
Buat, V., & Xu, C. 1996, A&A, 306, 61
Bunker, A. J. 1999, in ASP Conf. Ser. 191, Photometric Redshifts and High Redshift Galaxies, ed. R. J. Weymann, L. J. Storrie-Lombardi, M. Sawicki, & R. J. Brunner (San Francisco: ASP), 317
Burgh, E. B. 2001, Ph.D. thesis, Johns Hopkins Univ.
Burstein, D., Haynes, M. P., & Faber, S. M. 1991, Nature, 353, 515
Byun, Y. I. 1993, PASP, 105, 993
Byun, Y. I., Freeman, K. C., & Kylafis, N. D. 1994, ApJ, 432, 114
Calzetti, D. 1997a, AJ, 113, 162
———. 1997b, in AIP Conf. Proc. 408, The Ultaviolet Universe at Low and High Redshift, ed. W. H. Waller, M. N. Fanelli, J. E. Hollis, & A. C. Danks (Woodbury: AIP), 403
Calzetti, D., Armus, L., Bohlin, R. C., Kinney, A. L., Koornneef, J., & Storchi-Bergmann, T. 2000, ApJ, 533, 682
Calzetti, D., Bohlin, R. C., Gordon, K. D., Witt, A. N., & Bianchi, L. 1995a, ApJ, 446, L97
Calzetti, D., Bohlin, R. C., Kinney, A. L., Storchi-Bergmann, T., & Heckman, T. M. 1995b, ApJ, 443, 136
Calzetti, D., Conselice, C. J., Gallagher, J. S., & Kinney, A. L. 1999, AJ, 118, 797
Calzetti, D., & Heckman, T. M. 1999, ApJ, 519, 27
Calzetti, D., Kinney, A. L., & Storchi-Bergmann, T. 1994, ApJ, 429, 582
———. 1996, ApJ, 458, 132
Calzetti, D., Meurer, G. R., Bohlin, R. C., Garnett, D. R., Kinney, A. L., Leitherer, C., & Storchi-Bergmann, T. 1997, AJ, 114, 1834
Caplan, J., & Deharveng, L. 1986, A&A, 155, 297
Cardelli, J. A., Clayton, G. C., & Mathis, J. S. 1989, ApJ, 345, 245
Carilli, C. L., & Yun, M. S. 1999, ApJ, 513, L13
Carollo, C. M., Franx, M., Illingworth, G. D., & Forbes, D. A. 1997, ApJ, 481, 710
Cen, R., & Bryan, G. L. 2001, ApJ, 546, L81
Cen, R., Miralda-Escudé, J., Ostriker, J. P., & Rauch, M. 1994, ApJ, 437, L9
Cen, R., & Ostriker, J. P. 1999, ApJ, 514, 1
Cesarsky, D., Lequeux, J., Abergel, A., Perault, M., Palazzi, E., & Tran, D. 1996, A&A, 315, L305
Chandrasekhar, S. 1960, Radiative Transfer (New York: Dover)
Chapman, S. C., Richards, E. A., Lewis, G. F., Wilson, G., & Barger, A. J. 2001, ApJ, 548, L147
Chapman, S. C., et al. 2000, MNRAS, 319, 318
Charlot, S., & Fall, S. M. 2000, ApJ, 539, 718
Charlot, S., & Longhetti, M. 2001, MNRAS, 323, 887
Chary, R., & Elbaz, D. 2001, ApJ, 556, 562
Cheng, F. H., Gaskell, C. M., & Koratkar, A. P. 1991, ApJ, 370, 487
Chini, R., Krügel, E., & Kreysa, E. 1986, A&A, 167, 315
Choloniewski, J. 1991, MNRAS, 250, 486
Clements, D. L., Désert, F.-X., & Franceschini, A. 2001, MNRAS, 325, 665
Clements, D. L., Désert, F.-X., Franceschini, A., Reach, W. T., Baker, A. C., Davies, J. K., & Cesarsky, C. 1999, A&A, 346, 383
Clements, D. L., et al. 1996, MNRAS, 279, 459
Corradi, R. L. M., Beckman, J. E., & Simonneau, E. 1996, MNRAS, 282, 1005
Cowie, L. L., Songaila, A., & Barger, A. J. 1999, AJ, 118, 603
Cox, C. V., Bregman, J. N., & Schombert, J. M. 1995, ApJS, 99, 405
Cox, P., & Kessler, M. F. 1999, The Universe as Seen by *ISO* (ESA-SP 427; Noordwijk: ESA)
Cox, P., Krügel, E., & Mezger, P. G. 1986, A&A, 155, 380
Crawford, C. S., Allen, S. W., Ebeling, H., Edge, A. C., & Fabian, A. C. 1999, MNRAS, 306, 857
Dale, D. A., Helou, G., Contursi, A., Silbermann, N. A., & Kolhatkar, S. 2001, ApJ, 549, 215
Davies, J. I., Alton, P. B., Trewhella, M., Evans, R., & Bianchi, S. 1999, MNRAS, 304, 495
Davies, J. I., & Burstein, D. 1995, The Opacity of Spiral Disks (Dordrecht: Kluwer)
Davies, J. I., Phillips, S., Boyce, P. J., & Disney, M. J. 1993, MNRAS, 260, 491
de Jong, T., Clegg, P. E., Soifer, B. T., Rowan-Robinson, M., Habing, H. J., Houck, J. R., Aumann, H. H., & Raimond, E. 1984, ApJ, 278, L67
Désert, F.-X., Boulanger, F., & Puget, J.-L. 1990, A&A, 237, 215
de Vaucouleurs, G. 1959a, AJ, 64, 397
Devereux, N. A., & Young, J. S. 1991, ApJ, 371, 515
De Young, D. S., & Heckman, T. M. 1994, ApJ, 431, 598
Di Bartolomeo, A., Barbaro, G., & Perinotto, M. 1995, MNRAS, 277, 1279
Dickinson, M. E. 1998, in The Hubble Deep Field, STScI May Symp., ed. M. Livio, S. M. Fall, & P. Madau (Cambridge: Cambridge Univ. Press), 219
———. 2000, Philos. Trans. R. Soc. London, A, 358, 2001
Disney, M., Davies, J., & Phillips, S. 1989, MNRAS, 239, 939
Dole, H., et al. 2001, A&A, 372, 364
Domingue, D. L., Keel, W. C., Ryder, S. D., & White, R. E. 1999, AJ, 118, 1542
Donahue, M., Mack, J., Voit, G. M., Sparks, W., Elston, R., & Maloney, P. R. 2000, ApJ, 545, 670
Draine, B. T., & Anderson, N. 1985, ApJ, 292, 494
Draine, B. T., & Lee, H. M. 1984, ApJ, 285, 89
Draine, B. T., & Salpeter, E. E. 1979, ApJ, 231, 77
Duley, W. W., Jones, A. P., & Williams, D. A. 1989, MNRAS, 236, 709
Dunne, L., & Eales, S. A. 2001, MNRAS, 327, 697
Dunne, L., Eales, S. A., Edmunds, M., Ivison, R., Alexander, P., & Clements, D. L. 2000, MNRAS, 315, 115
Dutra, C. M., Bica, E., Clariá, J. J., Piatti, A. E., & Ahumada, A. V. 2001, A&A, 371, 895
Dwek, E., Rephaeli, Y., & Mather, J. C. 1990, ApJ, 350, 104
Eales, S. A., Lilly, S., Gear, W., Dunne, L., Bond, J. R., Hammer, F., Le Fevre, O., & Crampton, D. 1999, ApJ, 515, 518
Eales, S. A., Lilly, S., Webb, T., Dunne, L., Gear, W., Clements, D., & Yun, M. 2000, AJ, 120, 2244
Ebneter, K., & Balick, B. 1985, AJ, 90, 183
Ebneter, K., Djorgovski, S., & Davis, M. 1988, AJ, 95, 422
Edge, A. C. 2001, MNRAS, in press (astro-ph/0106225)
Edge, A. C., Ivison, R. J., Smail, I., Blain, A. W., & Kneib, J.-P. 1999, MNRAS, 306, 599
Edmunds, M. G., & Phillips, S. 1997, MNRAS, 292, 733
Efstathiou, A., Rowan-Robinson, M., & Siebenmorgen, R. 2000, MNRAS, 313, 734
Efstathiou, A., et al. 2000, MNRAS, 319, 1169
Elbaz, D. 1999, in Building Galaxies: From the Primordial Universe to the Present, ed. F. Hammer, T. X. Thuan, V. Cayatte, B. Guiderdoni, & J. Tran Thanh Van (Singapore: World Scientific), 195
Elbaz, D., et al. 1999, A&A, 351, L37
Ellingson, E., Yee, H. K. C., Bechtold, J., & Elston, R. 1996, ApJ, 466, L71

Ellison, S. L., Lewis, G. F., Pettini, M., Chaffee, F. H., & Irwin, M. J. 1999, ApJ, 520, 456
Ellison, S. L., Songaila, A., Schaye, J., & Pettini, M. 2000, AJ, 120, 1175
Ellison, S. L., Yan, L., Hook, I. M., Pettini, M., Wall, J. V., & Schaver, P. 2001, A&A, submitted
Elmegreen, D. M. 1980, ApJS, 43, 37
Emsellem, E. 1995, A&A, 303, 673
Fabian, A. C., Johnstone, R. M., & Daines, S. J. 1994, MNRAS, 271, 737
Fabian, A. C., et al. 2000, MNRAS, 315, L8
Fall, S. M., & Pei, Y. C. 1993, ApJ, 402, 479
Fall, S. M., Pei, Y. C., & McMahon, R. G. 1989, ApJ, 341, L5
Fanelli, M. N., O'Connell, R. W., & Thuan, T. X. 1988, ApJ, 334, 665
Ferguson, A. M. N., Gallagher, J. S., & Wyse, R. F. G. 1998, AJ, 116, 673
Ferguson, H. C. 1993, MNRAS, 263, 343
Ferrara, A., Bianchi, S., Cimatti, A., & Giovanardi, C. 1999a, ApJS, 123, 437
Ferrara, A., Nath, B., Sethi, S. K., & Shchekinov, Y. 1999b, MNRAS, 303, 301
Ferrara, A., Pettini, M., & Shchekinov, Y. 2000, MNRAS, 319, 539
Ferrara, A., & Tolstoy, E. 2000, MNRAS, 313, 291
Fitzpatrick, E. L. 1986, AJ, 92, 1068
———. 1999, PASP, 111, 63
Fixsen, D. J., Cheng, E. S., Gales, J. M., Mather, J. C., Shafer, R. A., & Wright, E. L. 1996, ApJ, 473, 576
Fixsen, D. J., Dwek, E., Mather, J. C., Bennett, C. L., & Shafer, R. A. 1998, ApJ, 508, 123
Flores, H., et al. 1999a, A&A, 343, 389
———. 1999b, ApJ, 517, 148
Forbes, D. A., Franx, M., & Illingworth, G. D. 1995, AJ, 109, 1988
Förster Schreiber, N. M., Genzel, R., Lutz, D., Kunze, D., & Sternberg, A. 2001, ApJ, 552, 544
Fox, M. J., et al. 2001, MNRAS, submitted (astro-ph/0107585)
Franceschini, A., Mazzei, P., deZotti, G., & Danese, L. 1994, ApJ, 427, 140
Friedli, D., & Benz, W. 1995, A&A, 301, 649
Fukugita, M., Hogan, C. J., & Peebles, P. J. E. 1998, ApJ, 503, 518
Furton, D. G., Laiho, J. W., & Witt, A. N. 1999, ApJ, 526, 752
Gasda, S., & Leitherer, C. 1996, in ASP Conf. Ser. 98, From Stars to Galaxies: The Impact of Stellar Physics on Galaxy Evolution, ed. C. Leitherer, U. Fritze-von Alvensleben, & J. Huchra (San Francisco: ASP), 451
Ge, J., Bechtold, J., & Kulkarni, V. P. 2001, ApJ, 547, L1
Genzel, R., & Cesarsky, C. J. 2000, ARA&A, 38, 761
Genzel, R., et al. 1998, ApJ, 498, 579
Giavalisco, M., Livio, M., Bohlin, R. C., Macchetto, F. D., & Stecher, T. P. 1996a, AJ, 112, 369
Giavalisco, M., Steidel, C. C., Adelberger, K. L., Dickinson, M. E., Pettini, M., & Kellogg, M. 1998, ApJ, 503, 543
Giavalisco, M., Steidel, C. C., & Macchetto, F. D. 1996b, ApJ, 470, 189
Giovanelli, R., Haynes, M. P., Salzer, J. J., Wegner, G., da Costa, L. N., & Freudling, W. 1994, AJ, 107, 2036
———. 1995, AJ, 110, 1059
Glazebrook, K., Blake, C., Economou, F., Lilly, S., & Colless, M. 1999, MNRAS, 306, 843
Gnedin, N. Y. 1998, MNRAS, 294, 407
Goad, J. W., & Roberts, M. S. 1981, ApJ, 250, 79
Goldader, J. D., Meurer, G. R., Heckman, T. M., Seibert, M., Sanders, D., Calzetti, D., & Steidel, C. C. 2001, ApJ, submitted
González, R. A., Allen, R. J., Dirsch, B., Ferguson, H. C., Calzetti, D., & Panagia, N. 1998, ApJ, 506, 152
Gonzalez Delgado, R. M., Leitherer, C., Heckman, T. M., Lowenthal, J. D., Ferguson, H. C., & Robert, C. 1998, ApJ, 495, 698
Gordon, K. D., Calzetti, D., & Witt, A. N. 1997, ApJ, 487, 625
Gordon, K. D., & Clayton, G. C. 1998, ApJ, 500, 816
Gordon, K. D., Clayton, G. C., Witt, A. N., & Misselt, K. A. 2000, ApJ, 533, 236
Gordon, K. D., Misselt, K. A., Witt, A. N., & Clayton, G. C. 2001, ApJ, 551, 269
Goudfrooij, P., & de Jong, T. 1995, A&A, 298,784
Goudfrooij, P., Hansen, L., Jorgensen, H. E., & Norgaard-Nielsen, H. U. 1994, A&AS, 105, 341
Granato, G. L., Lacey, C. G., Silva, L., Bressan, A., Baugh, C. M., Cole, S., & Frenk, C. S. 2000, ApJ, 542, 710
Greenberg, J. M. 1984, Sci. Am., 250, 124
———. 1989, in IAU Symp. 135, Interstellar Dust, ed. L. J. Allamandola & A. G. G. M. Tielens (Dordrecht: Kluwer), 239
Greenberg, J. M., et al. 2000, ApJ, 531, L71
Greggio, L., Tosi, M., Clampin, M., De Marchi, G., Leitherer, C., Nota, A., & Sirianni, M. 1998, ApJ, 504, 725
Guhathakurta, P., Tyson, J. A., & Majewski, S. R. 1990, ApJ, 357, L9
Guiderdoni, B., Hivon, E., Bouchet, F. R., & Maffei, B. 1998, MNRAS, 295, 877
Haas, M. 1998, A&A, 337, L1
Hansen, L., Jörgensen, H. E., & Nörgaard-Nielsen, H. U. 1995, A&A, 297, 13
Hauser, M. G., & Dwek, E. 2001, ARA&A, 39, 249
Hauser, M. G., et al. 1998, ApJ, 508, 25
Heckman, T. M. 1994, in Mass-Transfer Induced Activity in Galaxies, ed. I. Shlosman (Cambridge: Cambridge Univ. Press), 234
Heckman, T. M., Armus, L., & Miley, G. K. 1990, ApJS, 74, 833
Heckman, T. M., Baum, S. A., Van Breugel, W. J. M., & McCarthy, P. 1989, ApJ, 338, 48
Heckman, T. M., Lehnert, M. D., Strickland, D. K., & Armus, L. 2000, ApJS, 129, 493
Heckman, T. M., & Leitherer, C. 1997, AJ, 114, 69
Heckman, T. M., Robert, C., Leitherer, C., Garnett, D. R., & van der Rydt, F. 1998, ApJ, 503, 646
Helou, G. 1986, ApJ, 311, L33
Helou, G., Khan, I. R., Malek, L., & Boehmer, L. 1988, ApJS, 68, 151
Henyey, L. C., & Greenstein, J. L. 1941, ApJ, 93, 70
Hernquist, L., Katz, N., Weinberg, D. H., & Miralda-Escudé, J. 1996, ApJ, 457, L51
Hibbard, J. E. 1997, in AIP Conf. Proc. 393, Star Formation Near and Far, Seventh Astrophysics Conf., ed. S. S. Holt & L. G. Mundy (Woodbury: AIP), 259
Holmberg, E. 1958, Medd. Lunds Astron. Obs. Ser. II, 136, 1
Hopkins, A. M., Connolly, A. J., Haarsma, D. B., & Cram, L. E. 2001, AJ, 122, 288
Hornschemeier, A. E., et al. 2000, ApJ, 541, 49
Hu, E. M. 1992, ApJ, 391, 608
Hu, E. M., Cowie, L. L., Kaaret, P., Jenkins, E. B., York, D. G., & Roesler, F. L. 1983, ApJ, 275, L27
Hughes, D. H., et al. 1998, Nature, 394, 241
Huizinga, E., & van Albada, T. S. 1992, MNRAS, 254, 677
Hunter, D. A. 1997, PASP, 109, 937
Hunter, D. A., & Gallagher, J. S. 1997, ApJ, 475, 65
Hunter, D. A., Gallagher, J. S., Rice, W. L., & Gillett, F. C. 1989, ApJ, 336, 152
Hunter, D. A., Gillett, F. C., Gallagher, J. S., III, Rice, W. L., & Low, F. J. 1986, ApJ, 303, 171

Hunter, D. A., & Sage, L. 1993, PASP, 105, 374
Hunter, D. A., & Thronson, H. A. 1996, ApJ, 461, 202
Hunter, D. A., et al. 2001, ApJ, 553, 121
Ivison, R. J., Smail, I., Barger, A. J., Kneib, J.-P., Blain, A. W., Owen, F. N., Kerr, T. H., & Cowie, L. L. 2000, MNRAS, 315, 209
Ivison, R. J., Smail, I., Le Borgne, J.-F., Blain, A. W., Kneib, J.-P., Bezecourt, J., Kerr, T. H., & Davies, J. K. 1998, MNRAS, 298, 583
Jansen, R. A. 2000, Ph.D. thesis, Univ. Groningen
Jenniskens, P. 1993, A&A, 274, 653
Jones, A. P., Tielens, A. G. G. M., Hollenbach, D. J., & McKee, C. F. 1994, ApJ, 433, 797
Jones, H., Davies, J. I., & Trewhella, M. 1996, MNRAS, 283, 316
Jura, M. 1977, Nature, 266, 702
Jura, M., Kim, D. W., Knapp, G. R., & Guhathakurta, P. 1987, ApJ, 312, L11
Kaastra, J. S., Ferrigno, C., Tamura, T., Paerels, F. B. S., Peterson, J. R., & Mittaz, J. P. D. 2001, A&A, 365, L99
Karachentsev, I. D., & Lipovetskii, V. A. 1969, Soviet Astron., 12, 909
Kawara, K., et al. 1998, A&A, 336, L9
Keel, W. C. 1983, AJ, 88, 1579
Keel, W. C., Kennicutt, R. C., Jr., Hummel, E., & van der Hulst, J. M. 1985, AJ, 90, 708
Keel, W. C., & White, R. E., III. 2001a, AJ, 121, 1442
———. 2001b, AJ, 122, 1369
Kennicutt, R. C., Jr. 1983, ApJ, 272, 54
———. 1998, ARA&A, 36, 189
Kim, D. C., & Sanders, D. B. 1998, ApJS, 119, 41
Kim, S.-H., Martin, P. G., & Hendry, P. D. 1994, ApJ, 422, 164
Kim, S. S., Morris, M., & Lee, H. M. 1999, ApJ, 525, 228
Kinney, A. L., Bohlin, R. C., Calzetti, D., Panagia, N., & Wyse, R. F. G. 1993, ApJS, 86, 5
Knapp, G. R., Guhathakurta, P., Kim, D. W., & Jura, M. 1989, ApJS, 70, 329
Koornneef, J., & Code, A. D. 1981, ApJ, 247, 860
Kuchinski, L. E., Terndrup, D. M., Gordon, K. D., & Witt, A. N. 1998, AJ, 115, 1438
Kunth, D., Mas-Hesse, J. M., Terlevich, E., Terlevich, R., Lequeux, J., & Fall, S. M. 1998, A&A, 334, 11
Kylafis, N. D., & Bahcall, J. N. 1987, ApJ, 317, 637
Lanzetta, K. M., Chen, H.-W., Fernández-Soto, A., Pascarelle, S., Yahata, N., & Yahil, A. 1999, in ASP Conf. Ser. 193, The Hy-Redshift Universe, ed. A. J. Bunker & W. J. M. van Breugel (San Francisco: ASP), 544
Larson, R. B., & Tinsley, B. M. 1978, ApJ, 219, 46
Lauer, T. R., et al. 1995, AJ, 110, 2622
Le Brun, V., Bergeron, J., Boissé, P., & Deharveng, J.-M. 1997, A&A, 321, 733
Léger, A., & Puget, J.-L. 1984, A&A, 137, L5
Lehnert, M. D., & Heckman, T. M. 1996, ApJ, 472, 546
Leisawitz, D., & Hauser, M. G. 1988, ApJ, 332, 954
Leitherer, C., & Heckman, T. M. 1995, ApJS, 96, 9
Leitherer, C., Leão, J., Heckman, T. M., Lennon, D., Pettini, M., & Robert, C. 2001, ApJ, 550, 724
Leitherer, C., et al. 1999, ApJS, 123, 3
Lequeux, J., Maurice, E., Prevot, L., Prevot-Burnichon, M.-L., & Rocca-Volmerange, B. 1984, in IAU Symp. 108, Structure and Evolution of the Magellanic Clouds, ed. S. van den Bergh & K. S. de Boer (Dordrecht: Reidel), 405
Lequeux, J., Maurice, E., Prevot-Burnichon, M. L., Prevot, L., & Rocca-Volmerange, B. 1982, A&A, 113, L15
Li, A., & Draine, B. T. 2001, ApJ, 554, 778
Lilly, S. J., Eales, S. A., Gear, W. K. P., Hammer, F., Le Fevre, O., Crampton, D., Bond, J. R., & Dunne, L. 1999, ApJ, 518, 641
Lilly, S. J., LeFevre, O., Crampton, D., Hammer, F., & Tresse, L. 1995, ApJ, 455, 50
Lilly, S. J., LeFevre, O., Hammer, F., & Crampton, D. 1996, ApJ, 460, L1
Lisenfeld, U., Isaak, K. G., & Hills, R. 2000, MNRAS, 312, 433
Loeb, A., & Haiman, Z. 1997, ApJ, 490, 571
Londale-Persson, C. J., & Helou, G. 1987, ApJ, 314, 513
Lowenthal, J. D., et al. 1997, ApJ, 481, 673
Lu, L., Sargent, W. L. W., Barlow, T. A., Churchill, C. W., & Vogt, S. S. 1996, ApJS, 107, 475
Lutz, D., Spoon, H. W. W., Rigopoulou, D., Moorwood, A. F. M., & Genzel, R. 1998, ApJ, 505, L103
Lutz, D., et al. 1996, A&A, 315, L269
Mac Low, M.-M., & Ferrara, A. 1999, ApJ, 513, 142
Madau, P., Ferguson, H. C., Dickinson, M. E., Giavalisco, M., Steidel, C. C., & Fruchter, A. 1996, MNRAS, 283, 1388
Madau, P., Ferrara, A., & Rees, M. J. 2001, ApJ, 555, 92
Maíz-Apellániz, J., & Walborn, N. R. 2000, poster paper presented at the IAU 24th General Assembly
Malhotra, S. 1997, ApJ, 488, L101
Maoz, D. 1995, ApJ, 455, L115
Martin, M. C. 1998, A&AS, 131, 77
Marzke, R. O., Huchra, J. P., & Geller, M. J. 1994, ApJ, 428, 43
Mas-Hesse, J. M., Arnault, P., & Kunth, D. 1989, Ap&SS, 157, 131
Mathis, J. S. 1990, ARA&A, 28, 37
———. 1996, ApJ, 472, 643
Mathis, J. S., Mezger, P. G., & Panagia, N. 1983, A&A, 128, 212
Mathis, J. S., Rumpl, W., & Nordsieck, K. H. 1977, ApJ, 217, 425
Mathis, J. S., & Whiffen, G. 1989, ApJ, 341, 808
Matthews, L. D., & Wood, K. 2001, ApJ, 548, 150
McCarthy, P. J., et al. 1999, ApJ, 520, 548
McKee, C. F. 1989, in IAU Symp. 135, Interstellar Dust, ed. L. J. Allamandola & A. G. G. M. Tielens (Dordrecht: Kluwer), 431
McQuade, K., Calzetti, D., & Kinney, A. L. 1995, ApJS, 97, 331
Meier, D. S., Turner, J. L., Crosthwaite, L. P., & Beck, S. C. 2001, AJ, 121, 740
Merluzzi, P. 1998, A&A, 338, 807
Meurer, G. R., Heckman, T. M., & Calzetti, D. 1999, ApJ, 521, 64
Meurer, G. R., Heckman, T. M., Lehnert, M. D., Leitherer, C., & Lowenthal, J. 1997, AJ, 114, 54
Meyer, D. M., & Roth, K. C. 1990, ApJ, 363, 57
Meyer, D. M., & York, D. G. 1987, ApJ, 319, L45
Mezger, P. G., Mathis, J. S., & Panagia, N. 1982, A&A, 105, 372
Mihos, J. C., & Hernquist, L. 1996, ApJ, 464, 641
Misiriotis, A., Kylafis, N. D., Papamastorakis, J., & Xilouris, E. M. 2000, A&A, 353, 117
Misselt, K. A., Clayton, G. C., & Gordon, K. D. 1999, ApJ, 515, 128
Misselt, K. A., Gordon, K. D., Clayton, G. C., & Wolff, M. J. 2001, ApJ, 551, 277
Moorwood, A. F. M., van der Werf, P. P., Cuby, J. C., & Oliva, E. 2000, A&A, 362, 9
Moriondo, G., Giovanelli, R., & Haynes, M. P. 1998, A&A, 338, 795
Murphy, T. W., Soifer, B. T., Matthews, K., Armus, L., & Kiger, J. R. 2001, AJ, 121, 97
Mushotzky, R. F., & Loewenstein, M. 1997, ApJ, 481, L63
Mushotzky, R. F., Loewenstein, M., Arnaud, K. A., Tamura, T., Fukazawa, Y., Matsushita, K., Kikuchi, K., & Hatsukade, I. 1996, ApJ, 466, 686
Nandy, K., Morgan, D. H., Willis, A. J., Wilson, R., & Gondhalekar, P. M. 1981, MNRAS, 196, 955
Nath, B. B., & Trentham, N. 1997, MNRAS, 291, 505
Natta, A., & Panagia, N. 1976, A&A, 50, 191
———. 1984, ApJ, 287, 228
Nelson, A. E., Zaritsky, D., & Cutri, R. M. 1998, AJ, 115, 2273

Niklas, S., Klein, U., & Wielebinski, R. 1997, A&A, 322, 19
Norman, C. A., Sellwood, J. A., & Hasan, H. 1996, ApJ, 462, 114
Oliver, S. J., et al. 1997, MNRAS, 289, 471
Ortolani, S., Renzini, A., Gilmozzi, R., Marconi, G., Babuy, B., Bica, E., & Rich, M. R. 1995, Nature, 377, 701
Osterbrock, D. E. 1989, Astrophysics of Gaseous Nebulae and Active Galactic Nuclei (Mill Valley: University Science Books)
Ostriker, J. P., & Gnedin, N. Y. 1996, ApJ, 472, L63
Ouchi, M., Yamada, T., Kawai, H., & Ohta, K. 1999, ApJ, 517, L19
Pak, S., Jaffe, D. T., van Dishoeck, E. F., Johansson, L. E. B., & Booth, R. S. 1998, ApJ, 498, 735
Papovich, C., Dickinson, M., & Ferguson, H. C. 2001, ApJ, 559, 620
Peacock, J. A., et al. 2000, MNRAS, 318, 535
Pei, Y. C., Fall, S. M., & Bechtold, J. 1991, ApJ, 378, 6
Pei, Y. C., Fall, S. M., & Hauser, M. G. 1999, ApJ, 522, 604
Peletier, R. F., Valentijn, E. A., Moorwood, A. F. M., Freudling, W., Knapen, J. H., & Beckman, J. E. 1995, A&A, 300, L1
Peletier, R. F., & Willner, S. P. 1992, AJ, 103, 1761
Penton, S. V., Shull, J. M., & Stocke, J. T. 2000, ApJ, 544, 150
Peterson, J. R., et al. 2001, A&A, 365, L104
Petitjean, P., Muecket, J. P., & Kates, R. E. 1995, A&A, 295, L9
Pettini, M. 1999, in Chemical Evolution from Zero to High Redshift, ed. J. Walsh & M. Rosa (Berlin: Springer), 233
Pettini, M., Boksenberg, A., & Hunstead, R. W. 1990, ApJ, 348, 48
Pettini, M., Ellison, S. L., Steidel, C. C., & Bowen, D. V. 1999, ApJ, 510, 576
Pettini, M., Ellison, S. L., Steidel, C. C., Shapley, A. E., & Bowen, D. V. 2000a, ApJ, 532, 65
Pettini, M., Kellogg, M., Steidel, C. C., Dickinson, M. E., Adelberger, K. L., & Giavalisco, M. 1998, ApJ, 508, 539
Pettini, M., King, D. L., Smith, L. J., & Hunstead, R. W. 1997a, ApJ, 478, 536
Pettini, M., Shapley, A. E., Steidel, C. C., Cuby, J.-G., Dickinson, M., Moorwood, A. F. M., Adelberger, K. L., & Giavalisco, M. 2001, ApJ, 554, 981
Pettini, M., Smith, L. J., Hunstead, R. W., & King, D. L. 1994, ApJ, 426, 79
Pettini, M., Smith, L. J., King, D. L., & Hunstead, R. W., & King, D. L. 1997b, ApJ, 486, 665
Pettini, M., Steidel, C. C., Adelberger, K. L., Dickinson, M. E., & Giavalisco, M. 2000b, ApJ, 528, 96
Pinkney, J., et al. 1996, ApJ, 468, L13
Pizagno, J., & Rix, H.-W. 1998, AJ, 116, 2191
Poggianti, B. M., & Wu, H. 2000, ApJ, 529, 157
Popescu, C. C., Tuffs, R. J., Fischera, J., & Völk, H. 2000, A&A, 354, 480
Prochaska, J. X., & Wolfe, A. M. 2000, ApJ, 533, L5
Puget, J.-L., Abergel, A., Bernard, J.-P., Boulanger, F., Burton, W. B., Désert, F.-X., & Hartmann, D. 1996, A&A, 308, L5
Puget, J.-L., et al. 1999, A&A, 345, 29
Quillen, A. C., Rieke, G. H., Rieke, M. J., Caldwell, N., & Engelbracht, C. 1999, ApJ, 518, 632
Radovich, M., Kahanpää, J., & Lemke, D. 2001, A&A, 377, 73
Rao, S. M., & Turnshek, D. A. 2000, ApJS, 130, 1
Rauch, M., et al. 1997, ApJ, 489, 7
Reach, W. T., Boulanger, F., Contursi, A., & Lequeux, J. 2000, A&A, 361, 895
Renzini, A. 1999, in Chemical Evolution from Zero to High Redshift, ed. J. Walsh & M. Rosa (Berlin: Springer), 185
Rieke, G. H., & Lebofsky, M. J. 1985, ApJ, 288, 618
———. 1986, ApJ, 304, 326
Rieke, G. H., Lebofsky, M. J., Thompson, R. I., Low, F. J., & Tokunaga, A. T. 1980, ApJ, 238, 24
Rieke, G. H., Loken, K., Rieke, M. J., & Tamblyn, P. 1993, ApJ, 412, 99
Riess, A., et al. 2000, ApJ, 536, 62
———. 2001, ApJ, 560, 49
Rigopoulou, D., et al. 2000, ApJ, 537, L85
Rix, H.-W., & Rieke, M. J. 1993, ApJ, 418, 123
Roberts, M. S., & Haynes, M. P. 1994, ARA&A, 32, 115
Roberts, M. S., Hogg, D. E., Bregman, J. N., Forman, W. R., & Jones, C. 1991, ApJS, 75, 751
Romani, R. W., & Maoz, D. 1992, ApJ, 386, 36
Rowan-Robinson, M., & Crawford, J. 1989, MNRAS, 238, 523
Rowan-Robinson, M., & Efstathiou, A. 1993, MNRAS, 263, 675
Rowan-Robinson, M., Negroponte, J., & Silk, J. 1979, Nature, 281, 635
Rowan-Robinson, M., et al. 1997, MNRAS, 289, 490
———. 1999, in The Universe as Seen by *ISO*, ed. P. Cox & M. F. Kessler (Noordwijk: ESA), 1011
Sadler, E. M., & Gerhard, O. E. 1985, MNRAS, 214, 177
Sanders, D. B., & Mirabel, I. F. 1996, ARA&A, 34, 749
Sanders, D. B., Soifer, B. T., Elias, J. H., Madore, B. F., Matthews, K., Neugebauer, G., & Scoville, N. Z. 1988, ApJ, 325, 74
Savaglio, S., Panagia, N., & Stiavelli, M. 2000, in ASP Conf. Ser. 215, Cosmic Evolution and Galaxy Formation: Structure, Interactions, and Feedback, ed. J. Franco, E. Terlevich, O. López-Cruz, & I. Aretxaga (San Francisco: ASP), 65
Sawicki, M. 2001, AJ, 121, 2405
Sawicki, M., & Yee, H. K. C. 1998, AJ, 115, 1329
Schutte, W. A., et al. 1998, A&A, 337, 261
Scott, D., et al. 2000, A&A, 357, L5
Scott, S. E., et al. 2001, MNRAS, submitted (astro-ph/0107446)
Scoville, N. Z., et al. 1998, ApJ, 492, L107
Scowen, P. A., et al. 1998, AJ, 116, 163
Sellgren, K. 1984, ApJ, 277, 623
———. 1994, in ASP Conf. Ser. 58, The First Symposium on the Infrared Cirrus and Diffuse Interstellar Clouds, ed. R. M. Cutri & W. B. Latter (San Francisco: ASP), 243
———. 2001, Spectrochim. Acta A, 57, 627
Serjeant, S., et al. 2000, MNRAS, 316, 768
Severgnini, P., et al. 2000, A&A, 360, 457
Shapley, A. E., Steidel, C. C., Adelberger, K. L., Dickinson, M., Giavalisco, M., & Pettini, M. 2001, ApJ, in press
Shaver, P. A., Hook, I. M., Jackson, C. A., Wall, J. V., & Kellermann, K. I. 1999, in ASP Conf. Ser. 156, Highly Redshifted Radio Lines, ed. C. L. Carilli, S. J. E. Radford, K. M. Menten, & G. I. Langston (San Francisco: ASP), 163
Shioya, Y., Trentham, N., & Taniguchi, Y. 2001, ApJ, 548, L29
Silva, L., Granato, G. L., Bressan, A., & Danese, L. 1998, ApJ, 509, 103
Simonsen, J. T., & Hannestad, S. 1999, A&A, 351, 1
Skillman, E. D., Kennicutt, R. C., Jr., & Hodge, P. W. 1989, ApJ, 347, 875
Smail, I., Ivison, R. J., & Blain, A. W. 1997, ApJ, 490, L5
Smail, I., Ivison, R. J., Blain, A. W., & Kneib, J.-P. 1998, ApJ, 507, L21
Smail, I., Ivison, R. J., Kneib, J.-P., Blain, A. W., Barger, A. J., Owen, F. N., & Morrison, G. 1999, MNRAS, 308, 1061
Smail, I., Ivison, R. J., Owen, F. N., Blain, A. W., & Kneib, J.-P. 2000, ApJ, 528, 612
Sobolev, V. V. 1963, A Treatise on Radiative Transfer (Princeton: Van Nostrand)
Sodroski, T. J., et al. 1994, ApJ, 428, 638
Sofue, Y., Reuter, H.-P., Krause, M., Wielebinski, R., & Nakai, N. 1992, ApJ, 395, 126
Soifer, B. T., Houck, J. R., & Neugebauer, G. 1987, ARA&A, 25, 187
Soifer, B. T., & Neugebauer, G. 1991, AJ, 101, 354
Songaila, A., & Cowie, L. L. 1996, AJ, 112, 335
Sparks, W. B., Ford, H. C., & Kinney, A. L. 1993, ApJ, 413, 531
Sparks, W. B., Macchetto, F., & Golombek, D. 1989, ApJ, 345, 153
Sprayberry, D., & Foltz, C. B. 1992, ApJ, 390, 39

Steidel, C. C., Adelberger, K. L., Giavalisco, M., Dickinson, M. E., & Pettini, M. 1999, ApJ, 519, 1
Steidel, C. C., Giavalisco, M., Dickinson, M. E., & Adelberger, K. L. 1996a, AJ, 112, 352
Steidel, C. C., Giavalisco, M., Pettini, M., Dickinson, M., & Adelberger, K. 1996b, ApJ, 462, L17
Steidel, C. C., & Hamilton, D. 1992, AJ, 104, 941
Stickel, M., Lemke, D., Mattila, K., Haikala, L. K., & Haas, M. 1998, A&A, 329, 55
Storchi-Bergmann, T., Kinney, A. L., & Challis, P. 1995, ApJS, 98, 103
Sullivan, M., Mobasher, B., Chan, B., Cram, L., Ellis, R., Treyer, M., & Hopkins, A. 2001, ApJ, 558, 72
Sullivan, M., Treyer, M. A., Ellis, R. S., Bridges, T. J., Milliard, B., & Donas, J. 2000, MNRAS, 312, 442
Szalay, A. S., Hollósi, J., & Tóth, G. 1989, ApJ, 339, L5
Tamura, T., et al. 2001, A&A, 365, L87
Taniguchi, Y., et al. 1997, A&A, 328, L9
Teplitz, H. I., et al. 2000a, ApJ, 542, 18
———. 2000b, ApJ, 533, L65
Theuns, T., Leonard, A., Efstathiou, G., Pearce, F. R., & Thomas, P. A. 1998, MNRAS, 301, 478
Tielens, A. G. G. M. 1989, in IAU Symp. 135, Interstellar Dust, ed. L. J. Allamandola & A. G. G. M. Tielens (Dordrecht: Kluwer), 239
Tran, H., Tsvetanov, Z., Ford, H. C., Davies, J., Jaffe, W., van den Bosch, F. C., & Rest, A. 2001, AJ, 121, 2928
Tremonti, C. A., Calzetti, D., Leitherer, C., & Heckman, T. M. 2001, ApJ, 555, 322
Trentham, N., Kormendy, J. K., & Sanders, D. B. 1999, AJ, 117, 2152
Trewhella, M. 1998, MNRAS, 297, 807
Trewhella, M., Davies, J. I., Alton, P. B., Bianchi, S., & Madore, B. F. 2000, ApJ, 543, 153
Trewhella, M., Davies, J. I., Disney, M. J., & Jones, H. G. W. 1997, MNRAS, 288, 397
Trewhella, M., Madore, B., & Kuchinski, L. 1999, in ASP Conf. Ser. 176, Observational Cosmology: The Development of Galaxy Systems, ed. G. Giuricin, M. Mezzetti, & P. Salucci (San Francisco: ASP), 454
Turnshek, D. A., Rao, S. M., & Nestor, D. B. 2001, in ASP Conf. Ser., Extragalactic Gas at Low Redshift, ed. J. S. Mulchaey, J. Stocke, & J. Prochaska (San Francisco: ASP), in press (astro-ph/0108142)
Tytler, D., Fan, X. M., Burles, S., Cottrell, L., Davis, C., Kirkman, D., & Zuo, L. 1995, in QSO Absorption Lines, ed. G. Meylan (Garching: ESO), 289
Valentijn, E. A. 1990, Nature, 346, 153
van den Bergh, S. 1974, ApJ, 193, 63
Van der Werf, P. P., Kraiberg Knudsen, K., Labbé, I., & Franx, M. 2001, in The Far-Infrared and Submillimeter Spectral Energy Distributions of Active and Starburst Galaxies, ed. P. Barthel, B. Wilkes, & I. van Bemmel (Amsterdam: Elsevier), in press
van Dokkum, P. G., & Franx, M. 1995, AJ, 110, 2027
Városi, F., & Dwek, E. 1999, ApJ, 523, 265
Veilleux, S., Kim, D.-C., & Sanders, D. B. 1999, ApJ, 522, 113
Verter, F., & Hodge, P. 1995, ApJ, 446, 616
Vladilo, G. 1998, ApJ, 493, 583
Voit, G. M., & Donahue, M. 1995, ApJ, 452, 164
———. 1997, ApJ, 486, 242
Voshchinnikov, N. V., & Mathis, J. S. 1999, ApJ, 526, 257
Wainscoat, R. J., Hyland, A. R., & Freeman, K. C. 1990, ApJ, 348, 85
Walborn, N. R. 1991, in Massive Stars in Starbursts, ed. C. Leitherer, N. R. Walborn, T. M. Heckman, & C. A. Norman (Cambridge: Cambridge Univ. Press), 145
Walborn, N. R., Barbá, R. H., Brandner, W., Rubio, M., Grebel, E. K., & Probst, R. G. 1999, AJ, 117, 225
Wang, B. 1991, ApJ, 383, L37
Wang, B., & Heckman, T. M. 1996, ApJ, 457, 645
Wang, J., Heckman, T. M., & Lehnert, M. D. 1998, ApJ, 509, 93
Weingartner, J. C., & Draine, B. T. 2001, ApJ, 548, 296
White, R. E., & Keel, W. C. 1992, Nature, 359, 129
White, R. E., Keel, W. C., & Conselice, C. J. 2000, ApJ, 542, 761
White, S. D. M., & Frenk, C. S. 1991, ApJ, 379, 52
Whittle, M. 1992, ApJS, 79, 49
Wilson, C. D., Walker, C. E., & Thornely, M. D. 1997, ApJ, 483, 210
Wise, M. W., O'Connell, R. W., Bregman, J. N., & Roberts, M. S. 1993, ApJ, 405, 94
Wise, M. W., & Silva, D. R. 1996, ApJ, 461, 155
Witt, A. N., Friedmann, B. C., & Sasseen, T. P. 1997, ApJ, 481, 809
Witt, A. N., & Gordon, K. D. 1996, ApJ, 463, 681
———. 2000, ApJ, 528, 799
Witt, A. N., Thronson, H. A., & Capuano, J. M. 1992, ApJ, 393, 611
Wolff, M. J., Clayton, G. C., & Gibson, S. J. 1998, ApJ, 503, 815
Wright, E. L. 1981, ApJ, 250, 1
Xilouris, E. M., Byun, Y. I., Kylafis, N. D., Paleologou, E. V., & Papamastorakis, J. 1999, A&A, 344, 868
Xilouris, E. M., Kylafis, N. D., Papamastorakis, J., Paleologou, E. V., & Haerendel, G. 1997, A&A, 325, 135
Xu, C. 2000, ApJ, 541, 134
Xu, C., & Buat, V. 1995, A&A, 293, L65
Xu, C., & Helou, G. 1996, ApJ, 456, 163
Yadav, R. K. S., & Sagar, R. 2001, MNRAS, 328, 370
Yamamoto, T. M., & Vansevicius, V. 1999, PASJ, 51, 405
Yan, L., McCarthy, P. J., Freudling, W., Teplitz, H. J., Malumuth, E. M., Weymann, R. J., & Malkan, M. A. 1999, ApJ, 519, L47
Young, J. S., & Scoville, N. Z. 1991, ARA&A, 29, 581
Yun, M. S., Reddy, N. A., & Condon, J. J. 2001, ApJ, 554, 803
Zaritsky, D. 1994, AJ, 108, 1619
———. 1999, AJ, 118, 2824
Zaritsky, D., Kennicutt, R. C., Jr., & Huchra, J. P. 1994, ApJ, 420, 87
Zhang, Y., Anninos, P., & Norman, M. L. 1995, ApJ, 453, L57
Zuo, L., Beaver, E. A., Burbidge, E. M., Cohen, R. D., Junkkarinen, V. T., & Lyons, R. W. 1997, ApJ, 477, 568
Zwicky, F. 1957, in Morphological Astronomy (Berlin: Springer), 101